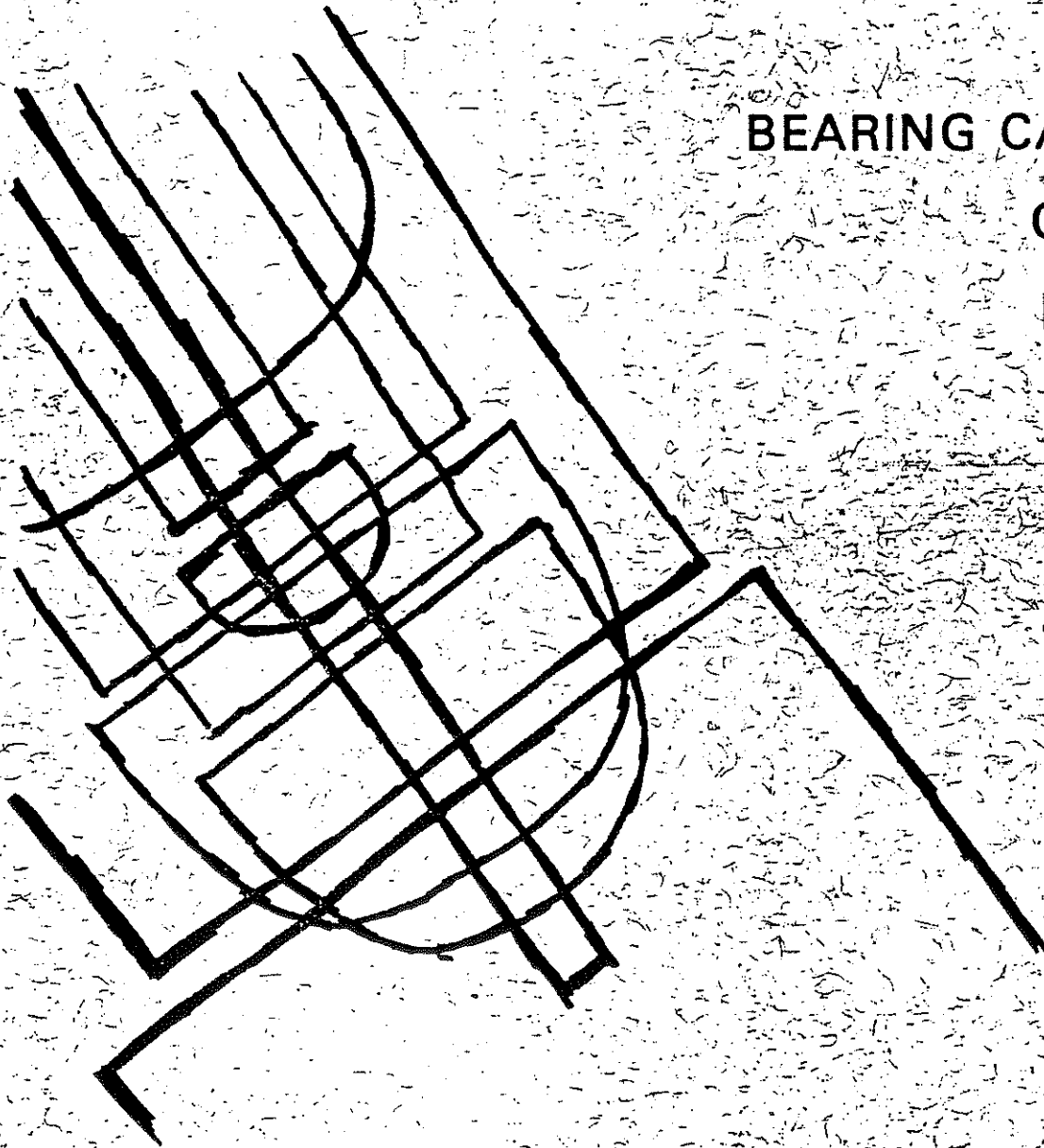


DIVISION OF  
SOLID MECHANICS  
STRUCTURES  
AND  
MECHANICAL DESIGN  
REPORT NO. 31

DYNAMIC STUDIES  
ON THE  
BEARING CAPACITY  
OF PILES  
PHASE II  
VOL. 1



SCHOOL OF ENGINEERING • CASE WESTERN RESERVE UNIVERSITY

1968

## ACKNOWLEDGEMENTS

The cooperation, assistance and advice on technical matters of P. Eckert, R. Dowalter, and R. Grover all of the Ohio Department of Highways contributed substantially to the success of this project phase. In administrative matters the assistance of C. R. Hanes, Ohio Department of Highways, was appreciated.

Many contractors on bridge construction projects provided assistance in obtaining dynamic records during driving. The assistance of the National Engineering and Contracting Company, Cleveland, Ohio, in many other aspects of the project is gratefully acknowledged.

Dr. R. H. Scanlan now of Princeton University but formerly associated with the project and Case Institute of Technology provided valuable advice on the analytical effort reported in Chapter IV.

DYNAMIC STUDIES ON THE BEARING CAPACITY OF PILES

Volume I

Final Project Report of Phase II

July 1, 1968

by

G. G. Goble

J. J. Tomko

F. Rausche

P. M. Green

This research was sponsored by the Ohio Department of Highways and the Bureau of Public Roads. The opinions, findings and conclusions expressed in this publication are those of the authors and not necessarily those of the State or the Bureau of Public Roads.

## ABSTRACT

The purpose of this report is to present the results of the past two years work on a research project, "Dynamic Studies on the Bearing Capacity of Piles", now completing its fourth year of activity. (August 1968) A previous project report (Ref. 1) presented the results of the first two-year phase, and it was assumed, in preparing this report that the reader is familiar with the previous work.

The general goals of the project during the past two years remained unchanged; that is, to find and prove a relationship between dynamic measurements made during impact pile driving and existing static capacity. The simplified, previously proposed, theory has been modified to increase its accuracy and reduce scatter in the results. This modification is supported by an examination of experimental results and by analysis of the pile as an elastic body.

Nineteen small scale piles were driven at three sites, each with different soil conditions, during the past two years. In addition, results were obtained from nine full scale load test piles driven on active highway construction projects. One pile was driven to three different depths by a contractor under control of research project personnel. Transducers were developed and tested to simplify the field measurement operations on full scale

piles.

Correlation between the static capacity and the dynamic prediction was good for small scale piles driven in sand but unsatisfactory for cohesive soils. For full scale piles this characteristic was not evident. Correlation was good for all types of soils.

A special purpose computer was designed and constructed to perform the computations for capacity predictions instantaneously in the field. This device has been tested but further experience is required. Based on present experience it seems likely that it will be possible to use a device of this type on a routine basis.

The static and dynamic results obtained to date are collected in Volume II of this report.

## TABLE OF CONTENTS

### Chapter

1	Introduction	1
2	Transducer Development	5
2.1	Introduction	5
2.2	Force Transducer	6
2.3	Clip-On Transducer	9
2.4	Model Pile Force Transducers	11
3	Test Results and Correlation	12
3.1	Modified Rigid Pile Mathematical Model	12
3.2	Small Scale Test Results	13
3.3	Full Scale Test Results	17
3.4	Akron Tests	19
3.5	Summary	22
4	Analytical Study	25
4.1	Elementary Theoretical Models of an Elastic Pile	25
4.2	Elastic Wave Equation Using Finite Fourier Transform	39
4.3	Comparison of Theoretical Predictions with Experimental Results	49
4.4	Elastic Wave Equation with Variable Static Resistance Law	56

4.5	Summary of Results	57
5	Special Purpose Computer	59
5.1	General Description	59
5.2	Computer Organization	59
5.3	Computer Calibration	63
6	Conclusions	66
	References	68
	Tables	69
	Figures	86

## CHAPTER I

### INTRODUCTION

The purpose of this report is to present the results of the past two years' work (July 1966-July 1968) on a research project, "Dynamic Studies on the Bearing Capacity of Piles", now completing its fourth year of activity. A previous project report (Reference 1) presented the work completed during the first two-year phase. The equipment developed was described in detail, static and dynamic measurements were reported, a practical and simple theory was presented, and correlation between theory and experiment was given. Also, the beginning of a more detailed theoretical analysis was presented. Familiarity with Reference 1 was assumed in preparing this report, particularly regarding the experimental equipment.

The general goals of the project during the past two years remained unchanged; that is, to find and prove a relationship between dynamic measurements made during driving and existing static capacity. In the previous phase of the project a simplified theory was proposed. This approach stated that the ultimate strength of the pile is given by

$$R_0 = F(t_0) - ma(t_0) \quad 1.1$$

where  $F(t_0)$  is the force acting at the top of the pile and  $a(t_0)$  is the acceleration at the top of the pile both measured at time



$t_0$  when the velocity of the top of the pile first reaches zero after the hammer blow. The mass of the pile is  $M$ . The above relationship is based on an assumed resistance force of the form

$$R(t) = R_0 + R_1 v + R_2 v^2 + \dots \quad 1.2$$

where  $v$  is the velocity of the pile, assumed to be a rigid body. Thus,  $R_0$  is the static resistance. It can be determined by a simple force balance at the time of zero velocity as indicated in equation 1.1.

Measurements of force and acceleration are made at the top of the pile and recorded on a high speed oscillograph. The acceleration record is then integrated to obtain velocity and the time of zero velocity. Predicted static resistance can then be obtained with force and acceleration using equation 1.1.

During the previous project phase a number of small scale piles were driven and tested in sand. Also, measurements were made on a limited number of full scale piles driven and load tested in connection with Ohio Department of Highways construction projects.

In the present phase a modification was made in the proposed simplified theory which improves the correlation and reduces the scatter of the prediction for successive hammer blows. The theory remains simple enough for routine application. This modification is described in Chapter III.

Additional small scale piles were studied in other soil types and measurements were made on further full scale piles. One full scale pile with special instrumentation was driven under research project control by special arrangement with the contractor on an active Ohio Department of Highways construction project. The results of all these efforts are discussed in Chapter III.

Force measurements have been obtained using resistance strain gages attached to the pile. While this method gives good results it is inconvenient for routine use. Two types of transducers for measuring force were developed for easier use. Their design, test, and calibration is reported in Chapter II.

An analytical study of the pile as an elastic rod subjected to an impact force has been made. The beginning of this work was reported in Reference 1. The total effort is reported in Chapter IV and correlation between theoretical and measured dynamic response is given.

The simplified mathematical model described in equation 1.1 has been applied by examining the oscillograph records manually. If this approach is to find routine application, the computations must be made during, or at least very shortly after, the driving operation. The necessary equipment must be such that it can be used under routine field conditions by operators having no extensive special training. A special purpose computer to

perform this function has been designed, built and partially tested. It provides a readout of predicted ultimate capacity within two milliseconds after the zero velocity time. A brief description of the device is given in Chapter V.

The test results in the form of tables and curves for all successful tests since the beginning of the project have been collected and are presented in Volume II.

## CHAPTER II

### TRANSDUCER DEVELOPMENT

#### 2.1 Introduction

The prediction of pile bearing capacity as proposed by this project requires the measurement of force and acceleration at the top of the pile. Acceleration measurements, while not trivial have become quite routine due to developments in electronic devices. Commercially available components can be assembled to perform this task. For this project a piezoelectric accelerometer was selected for its high natural frequency and ruggedness. The instrumentation system is described in detail in Reference 1. This system is a very sensitive one and has required considerable care in its use, but with all factors considered it offers advantages over other types of systems.

The force measurement on full scale piles has been accomplished by attaching resistance strain gages directly to the pile. Since the piles of interest were all of steel having a known area, it was possible to convert accurately from strain to force. However, this method does not represent a reasonable means of obtaining force measurements as the operation becomes more routine. The application of gages under all weather conditions is a difficult procedure. Even if it were simplified it would be much more desirable to have

a reusable transducer. This avoids the use of many strain gages and can reduce the cost of applying the technique. Transducers of this type can be constructed, calibrated, and tested by project personnel.

Two types of transducers were developed. One type uses the same approach as that used in the Michigan study (Reference 2) and introduces a force measuring device between the hammer and the pile. The device designed and reported here was quite inexpensive and avoids some of the difficulty experienced in the Michigan study. It has been used on three full scale tests and has performed satisfactorily.

The second device attaches directly to the pile and provides a calibrated strain measurement. This device which will be referred to as the strain transducer, is much lighter in weight than the force transducer and uses less space in the driving system, but like the strain gage it depends on a known value for pile area and modulus.

Additional force transducers were developed for use on the model piles. They will also be described.

## 2.2 Full Scale Pile Force Transducer

The requirements placed on the force transducer can be outlined as follows:

1. The output must be accurate and linear for a range of zero to 300 kips, static and dynamic compression forces.

2. The design must withstand the repeated application of large forces without distress, and the strain gage locations must stay in the linear range of the material.
3. The transducer should be as light as possible so that it can be handled manually.
4. The transducer must provide a stable element in the driving system with no tendency to rotate, or displace laterally.

A 12-3/4-inch outside diameter pipe with a 1/2-inch wall thickness and a 20-inch length was used. The large diameter provided stability, and the rather long length minimized local bending due to contact stresses. At the mid-length of the pipe, four one inch diameter holes were drilled at 90 degrees from each other. In each of these holes strain gages were placed parallel and transverse to the axis of the pipe. Due to the stress concentration at the holes the axial gage experienced about twice the applied strain and the transverse gage a strain approximately equal in magnitude to the applied axial strain but of opposite sign. Since the strain gages were placed in the center of the wall, local bending effects were further reduced. The choice of pipe and the stress concentration at the holes allows the device to be used up to a load of 320 kips with no evidence of yielding.

The strain gages used were Micro Measurement MA-06-062DF-120 attached with BR-600 cement. Other aspects of gage application

and protection were as reported in Reference 1. The holes were completely filled with W. T. Bean Company Gagecote #5. The strain gages were hooked up in a full bridge having 240 ohms in each leg. The effects of gross bending in the transducer were cancelled with this arrangement. One inch thick, 14-inch square steel plates were welded to the top and bottom of the pipe. An 11-inch diameter hole was drilled out to further minimize the introduction of local bending effects at the ends. In use, the transducer is then bolted to a heavy plate which has been tack welded to the end of the pile. The upper end of the transducer is bolted to a driving head made up of a short piece of pile welded to another heavy plate.

Experience with diesel hammers revealed that very high frequency accelerations were usually present. These motions were undesirable for application of the proposed method and equipment and were avoided by introducing an additional cushion assembly between the top of the transducer and the transducer driving head. The most successful cushion consisted of multiple alternating layers of plywood and rubber. A drawing of the transducer is shown in Figure 2.1 and a picture of it in Figure 2.2. It can be seen in a driving setup with the cushion in Figure 3.6.

The transducer was calibrated statically in a 200 kip universal testing machine. The calibration curve is shown in Figure 2.3. The linearity was excellent and hysteresis not noticeable. Static

and dynamic measurements on a full scale pile were also made. For comparison two strain gages were attached to the pile. Figure 2.4 shows the result of a static load test. Figure 2.5 shows the output from the two sources when the pile was struck. It should be noted that there was a distance of 28 inches between the gages on the pile and those on the transducer. The differences may be explained by this factor and the relatively crude conversion of strain to force for the pile gages. Some variation must be expected in the field, but the static calibration was repeated in the testing machine and found unchanged.

### 2.3 Clip-On Strain Transducer

A transducer was developed which can be easily attached to the pile and which gives a readout of strain at the point of attachment. Previous attempts were unsuccessful because of slippage at the attachment points. To avoid undesirable effects of inertia forces it had to be light and attach as flat as possible to the pile. A drawing of the design is shown in Figure 2.6. It was made of aluminum with gages placed at locations of tension and compression stress. A transducer is used on each side of the pile to cancel out the effect of gross bending. The gages used were Micro Measurement EA-13-062DF-120 with Eastman 910 cement. The gages were protected in the usual manner. The gages of the two transducers were connected so that those



experiencing strains of the same direction were in series. Thus, the two transducers form two 240 ohm arms of the bridge. The other two arms are contained in a termination box.

The transducers bolt directly to the pile with self-tapping bolts. A template holds the device during attachment and prevents damage.

The static calibration was performed by attaching the transducer pair to a pipe section which was equipped with strain gages attached directly to the pipe walls. A maximum of 900 microinches strain was applied, and after two cycles of loading and unloading the positions of the transducers were interchanged and the loading repeated. The result of the test is shown in Figure 2.7. The transducers show good linearity and hysteresis was less than 1%. Dynamic calibration was performed on both a model pile and a full scale pile. After more than 50 blows on the full scale pile the zero still held indicating no slip of the attachment. Correlation was made with a record obtained from the force transducer described in the previous section. A dynamic record is shown in Figure 2.8. Magnitude and time response agree well considering that the transducers are about three feet apart.

A photograph of the transducers attached to a piece of pipe is shown in Figure 2.9. A steel template is still attached to the one on the right.

## 2.4 Model Pile Force Transducers

Obtaining force records from model piles at points below grade has caused some difficulty. Due to the small diameter of the model piles it is very difficult to attach strain gages on the inside at sufficient distance from the ends of the pipe. Transducers were designed with a load carrying inner tube and thin outer protecting shell having the same outside diameter as the model pile itself. This shell is prevented from carrying load by use of a rubber ring at its end. The design is shown in Figure 2.10. Three of these transducers were built; one for the tip of the pile and two for intermediate stations along the pile. The wall thickness of the inner tube was different for each transducer so that the sensitivity increased with depth.

Eight active strain gages were attached to each transducer using techniques previously outlined. They were connected in a four arm bridge with 240 ohms in each arm. A photograph of the completed devices with the protective shells removed is shown in Figure 2.11.

All three transducers were calibrated, both with and without the covers in place. No difference in calibration could be detected. The calibration curves are shown in Figure 2.12.

The transducers have performed in a satisfactory fashion in field use. The results of force measurements at four stations along the pile are shown in Figure 2.13.

## CHAPTER III

### Test Results and Correlation

#### 3.1 Modified Rigid Pile Mathematical Model

The use of the rigid pile mathematical model yields equation 1.1. A detailed discussion of this equation is contained in Reference 1 and will not be repeated here. This approach has given quite good correlation with measured static strength for full scale piles. It is, however, disturbing to examine certain characteristics of the measured dynamic records. Consider Figure 3.1. In the neighborhood of the point of zero velocity the slope of the acceleration curve is large. Thus, a small shift in the point of zero velocity can cause a great change in the inertia force and a substantial change in the predicted capacity. The record of force at the top of the pile is always quite smooth, and a small change in the point of measurement does not greatly affect its value. Due to the unreliability of the inertia portion of the predicted capacity some scatter must be expected in the results for different hammer blows.

Consider now the velocity curve of Fig. 3.1. In the descending portion of the curve it might be decomposed into two parts. One is an approximately linear curve as indicated, and the second is an oscillation about the straight line. Physically this can be

interpreted as a rigid body motion with a constantly decreasing velocity. Superimposed on this motion is an oscillation due to the elastic deformation of the pile. It is assumed that the rigid body portion represents a satisfactory average of the pile motion. Thus, the slope of the linear portion of the velocity curve is proposed as the approximation of the acceleration. This value can be used with the force at the instant of zero velocity to give an improved prediction of the resistance. A qualitative theoretical basis for this approach is given in Chapter IV.

It is characteristic of the force record, in the region of zero velocity, that its value remains quite constant. Another means of obtaining an average value of resistance is to calculate  $R_0$  in equation 1.1 at many points between the point of maximum velocity and the point of zero velocity. The resulting values are then averaged for a predicted capacity. This is equivalent to assuming that the constants in the Poncelet resistance law equation 1.2,  $k_1, k_2,$  are all zero except the first one. In all subsequent discussions the resistance predictions obtained using this modification will be referred to as  $R_0$  avg.

### 3.2 Small Scale Test Results

In the previous project phase equipment was developed for driving small scale piles, obtaining dynamic measurements during driving, and performing static load tests. A number of these piles were driven and tested at a site in Cleveland in a course

sand. (Figure 3.2). They were previously reported (Reference 1). Since these piles were driven during the time when equipment and procedures were being developed, the measurements taken were not always complete in the light of present knowledge. Complete results were obtained for the "after setup" tests on piles 15-3, 15-4, 15-6 and 15-7. The results were given again in Table 3.1. During the present phase three additional piles were driven at this site, and the results are also reported in Table 3.1. The identification for these piles has the following meaning: The first number indicates the number of the pile in the sequence. The letter T is used to avoid confusion with the piles driven earlier, and the last number indicates the length of the pile in feet. The notation 15/20 means that three five foot sections were used with instrumented sections at the tip and along the pile making a total pile length of 20 feet. Pile 1-T-15/20 was really an extension of Pile 1-T-10. In this case these piles will be referred to as two separate piles.

In these results the largest error occurred with pile 1-T-15/20. When full depth was reached a connection was broken on one of the transducer lead wires inside the pile. The pile was pulled, the connection repaired and it was driven back into the same hole. The dynamic prediction should apply in this circumstance just as if the pile had not been removed. However, due to the unusual circumstances this record will be neglected. The average error on the remaining ten tests is 16.1 percent for  $R_0$  and 13.8 percent for

$R_o$  avg. The nature of the data is such that further statistical investigation is not justified.

The same rigid body model was applied to a series of reduced scale piles driven into a silt soil. The soil had a laminated structure i.e. layers of silt ranging from 1/2 to 1 inch in thickness separated by a thin layer of very fine sand. The soil profile is given in Figure 3.3. The predicted bearing capacity obtained from equation 1.1 was much higher than the actual static bearing capacity obtained from the load tests, as shown in Table 3.2. Each of the five ten foot piles had similar predicted bearings and similar static bearings. It was determined that various static bearing capacities could be obtained dependent on the rate on which the C.R.P. Test was performed. This indicated that the ultimate soil-pile interface stress was velocity dependent. In fact, from the results obtained from three load tests performed on a particular pile at different rates, the soil appeared to behave as pseudoplastic material as evidenced by Figure 3.4.

The ultimate static bearing capacity obtained from a fast C.R.P. Test, at the rate of approximately 1.5 inches/min., approached the predicted bearing as shown for the case of pile 15-5 in Table 3.2. Upon recovering the piles after all required data was obtained, there was a layer of silt ranging from 1/16" to as much as 1/4" adhering to the pile surface. For every pile recovered this layer of silt existed, suggesting that failure did not occur at the soil-pile interface but rather at some distance from the

pile surface.

Both the ground acceleration and the acceleration at the top of the pile were measured in the hope that the use of the relative acceleration would improve the results both by shifting the zero velocity point and by changing the magnitude of the acceleration. Even though the ground acceleration was as high as 25% of the pile acceleration, the relative acceleration used in equation 1.1 did not improve the predicted bearing results. Since there was no knowledge of the motion of the soil below grade, no further analytical evaluation was made.

Three reduced scale piles were driven into a soil consisting of silt and clay. The soil profile is given in Figure 3.5. The piles were tested at various depths and all of them were driven to a depth of 20 feet. The results of the tests were given in Table 3.3. On some piles tests were made both at the end of driving and after a setup time. Thus, fourteen sets of records were obtained.

The correlation obtained is not satisfactory. In general, the  $(R_o)_{avg}$  value is in closer agreement with the measured static capacity than the  $(R_o)_{avg}$ . It is interesting to note the following comparison:  $(R_o)_{avg}$  is about the same as  $(R_o)_{avg}$  for the ten foot piles at the end of driving. It is substantially less than  $(R_o)_{avg}$  for all the 15 foot piles and for the ten foot piles after setup, but it is substantially larger for the 20 foot piles after setup. Further study of this apparent length effect is warranted.

### 3.3 Full Scale Test Results

Since the beginning of the project a number of test results have been obtained on full scale piles. A description of the piles and some of the driving equipment and conditions is given in Table 3.4. Some of these pile tests were reported in Reference 1 but are repeated here to present some further analysis which has been made of the data and to summarize all of the test results.

The experimental procedure which was employed on most of the piles was as follows: after a test pile, required by the Ohio Department of Highways, was driven it was allowed to setup for a few days. State personnel then performed their specified Maintained Load (M.L.) test. After completion of this test, with the cooperation of the contractor, a Constant Rate of Penetration (C.R.P.) test was performed by research project personnel. The C.R.P. test was continued to the ultimate load while the M.L. test was stopped at the yield load defined in Reference 3. After completion of the C.R.P. test the pile was restruck sufficiently to cause it to experience some permanent set. Dynamic records were obtained during this re-driving operation. This procedure proved more workable than attempting to obtain dynamic records at the end of driving. Furthermore, it gave dynamic records which reflected the condition of the pile at the time it was load tested and approached its service condition. This procedure developed gradually and, therefore, some of the results were obtained with a somewhat



different method or sequence of operation and are not complete in the present view.

Table 3.5 gives some results for dynamic records taken at the end of driving. For the first two piles in the table the dynamic prediction is compared with static tests made at a much later date. The ultimate load given for the M.L. test was obtained by extrapolating the test results upward from the yield load. Pile number 138 of Pier 4, Br. No. I-71-1826 shows very poor agreement between dynamic prediction and static measurement. However, the soil into which it was driven could be expected to show considerable strength gain in the nine days which elapsed between the two tests. The "F" piles in Akron were driven under the control of this project. A detailed description of their driving is contained in Section 3.4. Table 3.6 contains the results for a number of piles driven and tested according to the procedure outlined above. Comments are appropriate on some of the results. Pile 692 in Youngstown represented the first research project experience with a diesel hammer. A good appearing record was obtained. All subsequent experience with this type of hammer has given an acceleration record with considerable high frequency "noise". An additional cushion had to be added in all cases to avoid this problem. This later experience causes question of the validity of the dynamic prediction for this pile. In those cases where a dashed line is shown through the data a change in predicted capacity was obtained. For pile 506 (Uhrichsville) and

pile 531-76 (where 76 indicates the length of the pile in feet) Abut. 2, Canton, a strength decrease was indicated. In the latter case it is quite rapid. Pile 534 was filled with concrete prior to the load test and, therefore, had a much larger mass than the typical steel pile. The prediction shows an apparent increase in the later blows. This is the only pile tested during the entire project which has the large mass characteristic of many types of piles.

If the correlation between C.R.P. test strength and  $(R_o \text{ avg})_{\text{avg}}$  is examined an average difference of 9.8% is observed. The  $R_o \text{ avg}$  prediction shows less scatter than  $R_o$ . Further statistical examination of the data is not considered justifiable.

### 3.4 Akron Tests

During the summer of 1967 the Ohio Department of Highways arranged with the contractor of an active bridge construction project in Akron, Ohio to drive and test one pile under the control of research project personnel. The contractor was paid for the additional costs involved. Therefore, it could be expected that the improved control would produce results which could not otherwise be obtained. In order to make the maximum use of the test pile and the load test setup the pile was partially driven and tested. It was then extended and the operation repeated. Thus, piles having lengths of 33, 51.5 and 60.5 feet were tested at a single test site. They will be referred to as F-30, F-50

and F-60, respectively.

The test pile was a 12 inch diameter pipe pile having a 1/4-inch wall thickness. Four three foot sections were instrumented for force measurements. Resistance strain gages were attached at 90° intervals inside each of these sections at their midheight with the axis of the gages parallel to the axis of the pile. Micro-Measurement gages, type EA-06-250BB-120, were used with Eastman 910 cement. The gage protection procedure has been previously described. Opposite pairs of gages were connected in series to form one 240 ohm arm of the bridge. Two pairs of gages were used so that a complete backup system was available at each instrumented section. Each of the pipe sections were calibrated in a universal testing machine. The test pile was assembled by welding instrumented sections at each end of a 27 foot section of pile. The lead wires were carried to the top of the pile and the lower end was closed with a 1/2-inch plate. During the welding operation the area near the strain gages was kept cool with water soaked pads. The lead wires were attached to the pile wall at each end of the section, three styrofoam plugs were inserted along the pile, and the lead wires passed through them to further restrain the wires. After completion of tests on the first pile section (F-30), it was extended with a 15-1/2 foot section and another instrumented section. All lead wires were spliced at the joint with the pile extension up in the driving leads. After completion

of tests on this pile (F-50) it was further extended by adding a six foot section and another instrumented section.

At the end of driving of each pile, dynamic records were taken from each instrumented section, from the force transducer on top of the pile and from accelerometers at the top of the pile. In addition, the motion of the pile was recorded by drawing a line along a straight edge attached to the ground on paper attached to the pile. The static load test system was then assembled and within about two hours a C.R.P. test was performed. After a setup period of a few days a M.L. test was performed following, in a general manner, the Ohio Department of Highways procedure. Some of the waiting times were reduced so that the test could be performed in less time, and the load was carried to ultimate.

The driving operation is shown in Figure 3.6 and the instrumentation in Figure 3.7. The assembled load test setup is shown in Figure 3.8.

Considerable difficulty was experienced with the instrumentation for F-50 and F-60. A change in capacitance occurred with time and eventually became so great that dynamic measurements could not be made. Therefore, many of the pile sections instrumented for force measurement could be used only for static measurements. The measurement of static capacity and the dynamic measurements at the top of the pile were very successful. The correlation of measured static ultimate strength and the dynamic prediction is

given in Tables 3.5 and 3.6. Sample dynamic records and load tests are included in Volume II.

### 3.5 Summary

The project experimental efforts during the past two years have produced a considerable amount of data. Representative acceleration and force records with velocity, displacement and resistance curves are presented in Volume II. The original records of force and acceleration were manually digitized. This data was processed by an electronic digital computer and predicted capacities were automatically determined. Then the data was reproduced and complete drawings prepared automatically using a plotter controlled by the computer. The data is available in digital form on punched cards and could be quite easily transmitted to other investigators.

In this project phase considerable difficulty was experienced with diesel hammers. The presence of a high frequency signal of considerable magnitude caused difficulty with electronic equipment and data analysis. An additional cushion was designed and introduced into the driving system to avoid this problem. It was described in Section 2.2. The records obtained from diesel hammers had a similarity to records previously obtained from systems in which metal-to-metal impact occurred. Of course, the normal driving system contained a commercial cushion. It is hypothesized that as the diesel hammer falls and pressure builds up in the chamber a force is transmitted to the driving column causing the cushion to

be "tightened" up. In this condition the hammer fires and apparently high frequency vibrations are induced. This "tightening" effect is shown by the initial part of the record in Figure 3.9.

As indicated in Section 3.4 considerable difficulty was experienced with instrumentation during the Akron tests. Force data along the pile would be very useful and further efforts in this direction are desirable. The most probable cause of the capacitance shift is the accumulation of moisture in the lead wires. A better quality wire will avoid part of the problem. The use of a full bridge of active gages inside the pile will also be effective in reducing the difficulty. Further tests of this type should be made.

The lack of correlation of the predicted capacity with the static load test on the model piles in cohesive soils compared with good agreement for full scale piles in similar materials is difficult to explain. One possibility is that pile length effects the results. Then for very long piles it is possible that agreement would be less satisfactory. Further studies would be desirable to explain this phenomenon.

It should be noted that only one pile has been tested where the pile mass was large (Pile 534 in Canton was filled with concrete prior to test). In this case correlation was good. However, this pile was tested prior to the development of the force transducer and some question exists as to the accuracy of the force

measurements. Further data of this type would be very useful for prestressed concrete piles.

The use of the averaging technique described in Section 3.1 produced results with less scatter than the previous method. The results obtained for full scale piles are very encouraging.

## CHAPTER IV

### ANALYTICAL STUDY

#### 4.1 Elementary Theoretical Models of an Elastic Pile

The similarity of the velocity and force responses given in many of the figures is not merely coincidental. In fact, that the two curves are related by a constant of proportionality will be shown in the following section by considering a very elementary mathematical model representing the pile and the passive resistance force acting on it.

Although much more elaborate models of pile driving already exist as discussed in Reference 4, it is very useful to construct a simplified theoretical model which has at least qualitative value. Visualization and assessment of pile driving effect seen in more complicated models or in the field are aided by such a model.

Consider the pile model of length  $L$  and constant cross-section  $A$  shown in Figure 4.1. The ground resistance of the pile-soil interface will be drastically oversimplified to a single force acting at the bottom of the pile, i.e. considering only point bearing. Acting at the top of the pile is the driving force  $F_1(t)$  and at the bottom the passive tip force designated by  $F_2(t)$  as shown in this same figure.



Let  $x$  be the distance coordinate along the undisturbed pile which moves with the pile and  $X$  be the rigid body displacement measured from a fixed reference. Let  $\xi$  be the elastic displacement of the point  $x$  away from its rest position.

Consider a differential element of length  $dx$  at the point  $x$  acted upon by a positive (tensile) stress  $\sigma$  at this point and a positive tensile stress of  $\sigma + \frac{\partial \sigma}{\partial x}$  at  $x + dx$  as shown in Figure 4.2. The corresponding forces are obtained by assuming the stress  $\sigma$  to be uniformly distributed over the cross-sectional area  $A$ . The strain at  $x$  is given by  $\epsilon = \frac{\partial \xi}{\partial x}$ . Assuming the material of the pile to be elastic under dynamic conditions with a modulus of elasticity of  $E$ , then the simple stress-strain relation follows:

$$\sigma = E \frac{\partial \xi}{\partial x} \quad 4.1$$

If  $\rho$  is the density of the pile material, then equating the elastic and gravitational forces to the inertia forces in the  $x$  direction leads to the following equation:

$$A \frac{\partial \sigma}{\partial x} dx + \rho A g dx = \rho A \frac{\partial^2 (X + \xi)}{\partial t^2} dx \quad 4.2$$

where  $\frac{\partial^2 (X + \xi)}{\partial t^2}$  is the total acceleration of the pile. Using the elastic stress-strain relation given by 4.1, the above equation simplified to the following wave equation of the pile:

$$\frac{\partial^2 \xi}{\partial x^2} - \frac{1}{c^2} \ddot{\xi} = \frac{1}{c^2} (\ddot{X} - g) \quad 4.3$$

where  $C = \sqrt{E/\rho}$  is the speed of sound in the pile.

The boundary conditions at each end are as follows:

$$\frac{\partial \xi}{\partial x} = - \frac{F_1(t)}{EA} \quad \text{at } x = 0 \quad 4.4a$$

$$\frac{\partial \xi}{\partial x} = - \frac{F_2(t-L/C)}{EA} \quad \text{at } x = L \quad 4.4b$$

which states that the strain is compressive under the forces  $F_1$  and  $F_2$  at top and bottom respectively. The assumption is made throughout that the stresses are uniformly distributed over any cross-sectional area. A further assumption is made that the pile initially has no displacement or velocity (i.e. quiescent initial conditions).

The Laplace transform of each quantity in equations 4.3 and 4.4 a, b, taking into consideration the quiescent initial conditions becomes:

$$\frac{d^2 \bar{\xi}}{dx^2} - \frac{p^2}{C^2} \bar{\xi} = \frac{1}{C^2} (p^2 \bar{x} - \frac{q}{p}) \quad 4.5$$

$$\frac{d\bar{\xi}}{dx} = - \frac{F_1}{EA} \quad \text{at } x = 0 \quad 4.6a$$

$$\frac{d\bar{\xi}}{dx} = - \frac{F_2}{EA} \quad \text{at } x = L \quad 4.6b$$

where  $L\xi = \int_0^{\infty} \xi e^{-pt} dt \equiv \bar{\xi}$ , etc. Since the rigid body term  $X$

is only a function of time, and not of the spatial coordinate  $x$ , the solution of equations 4.5 and 4.6 a,b is:

$$\bar{\xi}(x) = \frac{C}{p \sinh \frac{pL}{C}} \left[ \frac{\bar{F}_1}{EA} \cosh \frac{pL}{C} - \frac{F_2}{EA} \right] \cosh \frac{px}{C} - \frac{C \bar{F}_1}{p EA} \sinh \frac{px}{C} - \bar{X} + \frac{g}{p^3} \quad 4.7$$

Since the top of the pile at  $x = 0$  is of particular interest because both strain and acceleration are measured in the field at this point, the above transformed solution reduces to:

$$(\bar{\xi} + \bar{X}) \Big|_{x=0} = \frac{C}{p \sinh \frac{pL}{C}} \left[ \frac{\bar{F}_1}{EA} \cosh \frac{pL}{C} - \frac{F_2}{EA} \right] + \frac{g}{p^3} \quad 4.8$$

The inversion of equation 4.8 can take several forms. The most appropriate solution would be written as either

$$(\bar{\xi} + \bar{X}) \Big|_{x=0} = \int_0^t F_1(\tau) Q'_{R1}(t-\tau) d\tau + \int_0^t F_2(\tau) Q'_{R2}(t-\tau) d\tau + g \frac{t^2}{2} \quad 4.9$$

or

$$(\bar{\xi} + \bar{X}) \Big|_{x=0} = \int_0^t F'_1(\tau) Q_{R1}(t-\tau) d\tau + \int_0^t F'_2(\tau) Q_{R2}(t-\tau) d\tau + g \frac{t^2}{2} \quad 4.10$$

In these equations the functions  $Q_{R1}$  and  $Q_{R2}$  are the solution of equation 4.8 when we have  $F_1 = H(t)$ ,  $F_2 = 0$  and  $F_1 = 0$ ,  $F_2 = H(t)$ , i.e. the responses of the pile to unit step inputs at either end and where  $H(t)$  represents the Heaviside unit step function with a

magnitude of unity. The primed quantities  $Q'_{R1}$  and  $Q'_{R2}$  are the first derivative of  $Q_{R1}$  and  $Q_{R2}$  with respect to  $t$ .

In order to make the solutions given by equations 4.9 and 4.10 more explicit, let us take the particular case when  $F_1 = F_{10}H(t)$ ,  $F_2 = 0$ . The Laplace transform of  $F_1$  becomes  $\bar{F}_1 = F_{10}/p$  and  $F_2$  becomes  $\bar{F}_2 = 0$ . In this case the solution to equation 4.8 reduces simply to:

$$(\bar{\xi} + \bar{X}) \Big|_{x=0} = \frac{C F_{10}}{p^2 EA} \left[ \frac{\cosh \frac{pL}{C}}{\sinh \frac{pL}{C}} \right] + \frac{g}{p^3} \quad 4.11$$

However the quantity in brackets can be expanded as follows:

$$\frac{\cosh \frac{pL}{C}}{\sinh \frac{pL}{C}} = 1 + 2(e^{-\frac{2pL}{C}} + e^{-\frac{4pL}{C}} + e^{-\frac{6pL}{C}} + \dots) \quad 4.12$$

Thus, using the expansion given by 4.12 and multiplying equation 4.11 through by  $p^2$  we obtain:

$$p^2(\bar{\xi} + \bar{X}) \Big|_{x=0} = \frac{C F_{10}}{AE} [1 + 2(e^{-\frac{2pL}{C}} + e^{-\frac{4pL}{C}} + e^{-\frac{6pL}{C}} + \dots)] + \frac{g}{p} \quad 4.13$$

But the left side of this equation is merely the Laplacian of  $(\xi + X)$ . Taking the inverse transform of equation 4.13 we obtain

$$(\ddot{\xi} + \ddot{X}) \Big|_{x=0} = \frac{C F_{10}}{AE} [\delta(t) + 2[\delta(t - \frac{2L}{C}) + \delta(t - \frac{4L}{C}) + \delta(t - \frac{6L}{C}) + \dots]] + g \quad 4.14$$

where  $\delta(t-\tau)$  is the Dirac delta function at time  $t = \tau$ . The velocity expression can be obtained by integrating equation 4.14 as follows:

$$\left. \dot{(\xi + \dot{X})} \right|_{x=0} = \frac{C F_{10}}{AE} [H(t) + 2[H(t-\frac{2L}{C}) + H(t-\frac{4L}{C}) + H(t-\frac{6L}{C}) + \dots]] + gt \quad 4.15$$

where the constant of integration is zero because of the quiescent initial velocity condition. Second integration yields the displacement:

$$F_{10} Q_{R1} = (\xi + X) \Big|_{x=0} = \frac{C F_{10}}{AE} [t+2 [(t-\frac{2L}{C}) H(t-\frac{2L}{C}) + (t-\frac{4L}{C}) H(t-\frac{4L}{C}) + (t-\frac{6L}{C}) H(t-\frac{6L}{C}) + \dots]] + \frac{gt^2}{2} \quad 4.16$$

Therefore an explicit form for  $Q_{R1}$  has been obtained for use in equations 4.9 or 4.10. A similar expression is obtained for  $Q_{R2}$

by taking  $F_1 = 0$  and  $F_2 = F_{20} H(t)$  as:

$$F_{10} Q_{R1} = (\xi + X) \Big|_{x=0} = \frac{2C F_{20}}{AE} [(t-\frac{L}{C}) + (t-\frac{3L}{C}) H(t-\frac{3L}{C}) + (t-\frac{5L}{C}) H(t-\frac{5L}{C}) + \dots] + \frac{gt^2}{2} \quad 4.17$$

It is now possible to select one of the simple solutions of equations 4.14, 4.15, or 4.16 for illustrative purposes and to compare it with the corresponding results obtained by the assumption that the pile is a rigid body. To this end, equation 4.15 is

selected and compared with the results obtained from the following rigid body analysis.

Assuming as before that the force  $F_1(t)$  is represented as a unit step force of magnitude  $F_{10}$  and  $F_2(t) = 0$ , we have:

$$F_1(t) = F_{10} H(t) \quad 4.18$$

Taking the mass of the pile  $\rho AL$  to be represented by  $m$ , then the force equilibrium equation of the rigid pile becomes:

$$m \ddot{X} = F_{10} H(t) + mg \quad 4.19$$

Upon integrating this equation, the velocity of the rigid pile is:

$$\dot{X}(t) = \frac{F_{10} t}{m} + gt \quad 4.20$$

The results shown in Figure 4.3 are obtained where gravity effects are neglected, by non-dimensionalizing the results of equations 4.15 and 4.20 by dividing each term by the factor  $\frac{F_{10}}{\rho AC}$  and then plotting the response against time.

The rigid body velocity response of a constant force suddenly applied to the top of the rigid pile, increases linearly with time. On the other hand, the elastic pile velocity responds in steps separated by the travel time  $2L/C$  of a wave down the length of the pile  $L$  and back with a speed  $C$ . Furthermore, the average of the elastic velocity is the linearly increasing rigid velocity as shown in Figure 4.3.

Solutions from equations 4.9 or 4.10 can be obtained for several types of forcing functions  $F(t)$ , or Figure 4.3 can be used as a basic form from which a number of solutions can be obtained.

Let it be supposed that instead of applying a constant force to the pile, a force  $F_1(t)$  consisting of a square pulse with a duration time  $T$  and amplitude  $F_{10}$  is applied suddenly to the top of the pile. This force can be written as:

$$F_1(t) = [H(t) - H(t-T)] F_{10} \quad 4.21$$

The velocity response for this particular forcing function can be obtained in the same way as for the case given by equation 4.18. However, the results of Figure 4.3 can be used instead since both terms of the right side of equation 4.21 are similar with the exception of time lag  $t-T$ . To obtain the velocities it suffices to subtract from the given results, results similar to those of Figure 4.3, starting at  $t=T$ . Taking for illustrative purposes,  $T = L/C$  yields the results given in Figure 4.4 where gravity effects are neglected.

In this figure the rigid body and elastic body results are rather dissimilar, but still the rigid body results are a kind of average of the elastic body results. The short force pulse at the top of duration  $T$  is seen to traverse down the pile and reflect back to the top in intervals of  $2L/C$ . It is to be emphasized that in actuality, successive reflections would probably be damped out as will be demonstrated in the following section, so that the

figure represents only a hypothetical situation.

Further cases can be developed, for example, assuming various rules of action governing the force  $F_2(t)$  at the lower tip. A possible situation is discussed here. Since, in fact, the force  $F_2(t)$  is a soil reaction force, it would be reasonable to assume that this force does not arise until  $t = L/C$ , i.e. until the stress wave has reached the bottom of the pile. Evidence of this time lag in the tip resistance has been confirmed several times from field data. These forces can be represented as:

$$F_1(t) = F_{10} \delta(t) \quad 4.22a$$

$$F_2(t) = F_{20} \delta(t-L/C) \quad 4.22b$$

where

$$\int_0^{\infty} \delta(t) dt = 1 \quad 4.22c$$

i.e. the two forces are hammer blows of "infinite height and infinitesimal duration". Upon substituting the transforms of 4.22a and b into equation 4.8 and expanding the hyperbolic function into its equivalent exponential form, the following transformed displacement is obtained:



$$(\bar{\xi} + X) \Big|_{x=0} = \frac{C}{EA\rho} \left\{ [1 + 2(e^{-\frac{2pL}{C}} + e^{-\frac{4pL}{C}} + e^{-\frac{6pL}{C}} + \dots)] F_{10} - 2[e^{-\frac{2pL}{C}} + e^{-\frac{4pL}{C}} + e^{-\frac{6pL}{C}} + \dots] F_{20} \right\} + \frac{g}{p^3} \quad 4.23$$

The transformed velocity becomes:

$$\rho(\dot{\bar{\xi}} + \dot{X}) \Big|_{x=0} = \frac{C}{AE} [F_{10} + 2(F_{10} - F_{20}) (e^{-\frac{2pL}{C}} + e^{-\frac{4pL}{C}} + e^{-\frac{6pL}{C}} + \dots)] + \frac{g}{p^2} \quad 4.24$$

This yields for the velocity:

$$(\dot{\bar{\xi}} + \dot{X}) \Big|_{x=0} = \frac{C}{EA} F_{10} \delta(t) + \frac{2C}{EA} (F_{10} - F_{20}) [\delta(t - \frac{2L}{C}) + \delta(t - \frac{4L}{C}) + \delta(t - \frac{6L}{C}) + \dots] + gt \quad 4.25$$

and for the displacement:

$$(\bar{\xi} + X) \Big|_{x=0} = \frac{C F_{10} H(t)}{EA} + \frac{2C}{EA} (F_{10} - F_{20}) [H(t - \frac{2L}{C}) + H(t - \frac{4L}{C}) + H(t - \frac{6L}{C}) + \dots] + \frac{gt^2}{2} \quad 4.26$$

By taking  $2F_{20} = F_{10}$  and nondimensionalizing the displacement by the factor  $\frac{F_{10}}{\rho AC}$ , the results shown in Figure 4.5 are obtained. The corresponding rigid body displacement obtained, for the forces given equations 4.22a, b, is:

$$x(t) = \frac{F_{10}}{m} H(t) t - \frac{F_{20}}{m} [H(t-L/c) \cdot (t-L/c)] + \frac{gt^2}{2} \quad 4.27$$

This result is also shown in Figure 4.5. Here again the rigid body displacement response is the average of the elastic response for this assumed model and boundary conditions.

The first treatment of an elastic pile model, given above, has lent some insight to pile action. However, it lacks some realistic features. A second model will be considered here. As shown in Figure 4.6 the soil resistance will be simulated by a uniformly distributed force  $f_r$  along the pile having dimensions of lbs/ft. as:

$$f_r = K_1 + K_2 (\dot{X} + \dot{\xi}) + K_3 (\dot{X} + \dot{\xi})^2 + \dots \quad 4.28$$

i.e.  $f_r$  may consist of frictional force  $K_1$ , a viscous force  $K_2(\dot{X} + \dot{\xi})$  and higher order resistance forces in powers of the total velocity. For ease in analysis, only the first two terms  $K_1$  and  $K_2$  will be retained.

Again assume the pile to have a uniform cross-section  $A$  and length  $L$  which receives an impulsive blow  $F_0 \delta(t)$  on top as shown in Figure 4.6. The basic equilibrium of an element  $dx$  long is given by

$$\rho A (\ddot{X} + \ddot{\xi}) dx = A \frac{\partial \sigma}{\partial x} dx - f_r dx \quad 4.29$$

This leads to the following equation of motion:

$$\frac{\partial^2 \xi}{\partial x^2} - \frac{1}{c^2} (\ddot{X} + \ddot{\xi}) - \beta (\dot{X} + \dot{\xi}) = \alpha \quad 4.30$$

where

$$\alpha = \frac{K_1}{AE} \quad \text{and} \quad \beta = \frac{K_2}{AE} \quad 4.31$$

a,b

Assuming quiescent initial conditions the Laplace transform of equation 4.30 yields

$$\frac{d^2 \bar{\xi}}{dx^2} - \lambda^2 \bar{\xi} = \frac{\alpha}{p} + \lambda^2 \bar{X} \quad 4.32$$

where  $\lambda^2 = \frac{p^2}{c^2} + \beta p$ . The solution of the above equation with the following boundary conditions:

$$\frac{\partial \xi}{\partial x} = - \frac{F_0 \delta(t)}{AE} \quad \text{at } x = 0 \quad 4.33a$$

$$\frac{\partial \xi}{\partial x} = 0 \quad \text{at } x = L \quad 4.33b$$

becomes:

$$\bar{X} + \bar{\xi} = \frac{F_0}{AE\lambda} \left[ \frac{\cosh \lambda L \cosh \lambda x}{\sinh \lambda L} - \sinh \lambda x \right] - \frac{\alpha}{\lambda^2 p} \quad 4.34$$

Considering the particular point  $x = 0$  the above equation reduces

$$\text{to:} \quad \bar{X} + \bar{\xi} = \frac{F_0}{AE\lambda} \frac{\cosh \lambda L}{\sinh \lambda L} - \frac{\alpha}{\lambda^2 p} \quad 4.35$$

The inversion of equation 4.35, after using a series expansion for the term containing the hyperbolic functions, yields:

$$\begin{aligned}
(X+\xi) \Big|_{x=0} &= \frac{CF_0}{AE} e^{-\beta \frac{C^2 t}{2}} \left\{ I_0\left(\beta \frac{C^2 t}{2}\right) + 2 \left[ I_0\left(\frac{\beta C^2}{2} \sqrt{t^2 - \left(\frac{2L}{C}\right)^2}\right) \right. \right. \\
&+ I_0\left(\frac{\beta C^2}{2} \sqrt{t^2 - \left(\frac{4L}{C}\right)^2}\right) + I_0\left(\frac{\beta C^2}{2} \sqrt{t^2 - \left(\frac{6L}{C}\right)^2}\right) + \dots \left. \left. \right] \right\} \\
&+ \frac{K_1}{K_2} \left[ \frac{1}{\beta C^2} (1 - e^{-\beta C^2 t}) - t \right] \qquad 4.36
\end{aligned}$$

where  $I_0$  is the hyperbolic Bessel function having the property that  $I_0\left(\frac{\beta C^2}{2} \sqrt{t^2 - \tau^2}\right) = 0$  for  $t < \tau$ . Differentiating the above equation yields the following velocity expression:

$$\begin{aligned}
(\dot{X}+\dot{\xi}) \Big|_{x=0} &= \frac{C^3 \beta F_0}{2 AE} e^{-\beta \frac{C^2 t}{2}} \left\{ -I_0\left(\frac{\beta C^2 t}{2}\right) - 2 \left[ I_0\left(\frac{\beta C^2}{2} \sqrt{t^2 - \left(\frac{2L}{C}\right)^2}\right) \right. \right. \\
&+ I_0\left(\frac{\beta C^2}{2} \sqrt{t^2 - \left(\frac{4L}{C}\right)^2}\right) + I_0\left(\frac{\beta C^2}{2} \sqrt{t^2 - \left(\frac{6L}{C}\right)^2}\right) + \dots \left. \left. \right] \right. \\
&+ I_1\left(\frac{\beta C^2 t}{2}\right) + 2t \left[ \frac{I_1\left(\frac{\beta C^2}{2} \sqrt{t^2 - \left(\frac{2L}{C}\right)^2}\right)}{t^2 - \left(\frac{2L}{C}\right)^2} + \frac{I_1\left(\frac{\beta C^2}{2} \sqrt{t^2 - \left(\frac{4L}{C}\right)^2}\right)}{t^2 - \left(\frac{4L}{C}\right)^2} + \dots \right] \left. \right\} \\
&+ \frac{K_1}{K_2} (e^{-\beta C^2 t} - 1) \qquad 4.37
\end{aligned}$$

where

$$I_1 = \frac{d I_0}{dt}$$

Letting  $\rho AL = m$  be the mass of the rigid pile and including only the first two terms of the resistance law given in equation

4.28, then the equation of motion becomes:

$$m \ddot{X} + K_2 L \dot{X} = F_0 \delta(t) - K_1 L \quad 4.38$$

with quiescent initial conditions. However, this equation may be rewritten as:

$$m \ddot{X} + K_2 L \dot{X} + K_1 L = 0 \quad 4.39$$

with the initial conditions being:

$$X(0) = 0, \quad \dot{X}(0) = \frac{F_0}{m} \quad 4.40$$

a, b

The solution to equation 4.39 with initial conditions given by equations 4.40 a, b has the following form:

$$X(t) = \frac{m}{K_2 L} \left( \frac{F_0}{m} + \frac{K_1}{K_2} \right) - \frac{K_1}{K_2} t - \frac{m}{K_2 L} \left( \frac{F_0}{m} + \frac{K_1}{K_2} \right) e^{-\frac{K_2 L t}{m}} \quad 4.41$$

for which the velocity is:

$$\dot{X}(t) = -\frac{K_1}{K_2} + \left( \frac{F_0}{m} + \frac{K_1}{K_2} \right) e^{-\frac{K_2 L t}{m}} \quad 4.42$$

Taking  $K_1 = 0$  and  $\beta = \frac{1}{LC}$  (i.e.  $K_2 = \frac{AE}{LC}$ ) permits a sample plot of responses as given in equations 4.36 and 4.41, 4.37 and 4.42. These results are shown in Figures 4.7 and 4.8 respectively.

The two theoretical pile models assumed up to this point are still not sufficiently realistic for all time,  $t$ , to permit more than qualitative conclusions for actual piles. They do clearly indicate however, the effect of wave action traveling up and down the pile, and the oscillation of the elastic pile about the rigid

body position. Another important qualitative result is that the velocity is proportional to the force when the soil-pile interface resistance is assumed zero as seen in equation 4.15. This result is also borne out in the initial portions of actual field data for all piles encountered so far. A more realistic resistance law, if the Laplace transform solution technique is used, would require much more sophisticated solutions as evidenced by the already involved solution given in equation 4.36 for a simple resistance law.

#### 4.2 Elastic Wave Equation Using Finite Fourier Transform

The application of the Laplace transform in the previous section to the basic wave equation with various assumed forms of soil-pile resistance laws yielded qualitative insight as to the behavior of the pile under an impact force,  $F(t)$ . The assumed models, however, were not sufficiently realistic for all time,  $t$ . In this section an attempt will be made, through the use of a continuous elastic pile model, to reproduce the acceleration, velocity, and displacement response of several piles resulting from a measured impact force,  $F(t)$ . As a result of matching theoretical and measured responses, this section undertakes to predict the static bearing capacity of example piles. The field measurements with reference to both full-scale piles and reduced-scale piles, consisted of the force and acceleration measured as functions of time at the top of the pile.

The matching and prediction scheme employs a four-parameter model of an elastic and rigid-body pile response to the measured hammer force input. The theoretically predicted bearing is rather satisfactorily verified by direct comparison with static tests made in the field.

Important qualitative results are also obtained from this analytical study. The most important of these results is an explanation for the successful predictions which resulted from the application to full-scale piles at the simplified rigid-body model, discussed in Section 3.1.

Consider again a pile model of length  $L$  and having a uniform cross-sectional area  $A$  shown in Figure 4.9 where  $X$  represents the rigid body motion of the pile and  $x$  the spatial coordinate along the pile of a system of axes moving with the pile. Let  $\xi$  be the elastic deflection of the point  $x$  away from its equilibrium position. Let the applied force acting on the pile resulting from the measured hammer force be designated as  $F_T(t)$  and the passive resistance force at the bottom of the pile be given by  $F_B(t)$ . This bottom force is assumed zero when  $t \leq \frac{L}{C}$ . Let  $R_L(x,t)$  be the distributed resistance force resulting from the soil-pile interaction along the length of the pile. Both  $F_B(t)$  and  $R_L(x,t)$  are passive forces.

Considering an elementary volume from the pile at position  $x$  with the passive resistance force  $R_L(x,t)$  as shown in Figure 4.9,

assuming the material of the pile to be elastic under dynamic conditions with a modulus of elasticity,  $E$ , results in the following basic governing equation for the pile:

$$\frac{\partial^2 \xi}{\partial x^2} - \frac{1}{C^2} \frac{\partial^2 \xi}{\partial t^2} = \frac{1}{C^2} \frac{\partial^2 X}{\partial t^2} + \frac{R_L(x,t)}{AE} \quad 4.43$$

where  $C = \sqrt{E/\rho}$  is the wave velocity in the pile material of density  $\rho$  and elastic modulus  $E$ . The above wave equation is valid on the domain  $0 \leq x \leq L$  for all time  $t \geq 0$ .

The boundary conditions to be employed are:

$$\frac{\partial \xi}{\partial x} = - \frac{F_T(t)}{AE} \quad \text{at } x = 0 \text{ for } t \geq 0 \quad 4.44a$$

$$\frac{\partial \xi}{\partial x} = - \frac{F_B(t)}{AE} \quad \text{at } x = L \text{ for } t \geq 0 \quad 4.44b$$

The total initial displacement and velocity conditions are assumed quiescent:

$$X(0) + \xi(x,0) = 0 \quad 4.45a$$

$$\dot{X}(0) + \dot{\xi}(x,0) = 0 \quad 4.45b$$

for all  $x$  between  $0 \leq x \leq L$ .

By defining the total displacement at a point  $x$  on the pile as:

$$Z(x,t) = X(t) + \xi(x,t) \quad 4.46$$



and since the motion of the rigid body is not a function of  $x$ , the governing equation 4.43 becomes:

$$\frac{\partial^2 Z(x,t)}{\partial x^2} - \frac{1}{c^2} \frac{\partial^2 Z(x,t)}{\partial t^2} = \frac{R_L(x,t)}{AE} \quad 4.47$$

The soil resistance laws will be assumed to consist of a frictional force and a viscous force similar to equation 4.28 as:

$$R_L(x,t) = R_0(x,t) + D \dot{Z}(x,t) \quad 4.48$$

where  $R_L(x,t)$  has dimensions of force per length and where  $D = dAE$  for an appropriate "damping coefficient",  $d$ , to be defined later.

Substitution of equation 4.48 into equation 4.47 and the application of the finite Fourier cosine transform to the results with the aid of the transformed boundary condition yields:

$$\ddot{\bar{Z}}_c(n,t) + c^2 d \dot{\bar{Z}}_c(n,t) + \left(\frac{n\pi c}{L}\right)^2 \bar{Z}_c(n,t) = \frac{c^2}{AE} [(-1)^{n+1} \bar{F}_B(t) + \bar{F}_T(t) - \bar{R}_c(n,t)] \equiv G(n,t) \quad 4.49$$

where the barred quantities represent the cosine transform, as for example

$$\bar{Z}_c(n,t) = \int_0^L Z(x,t) \cos \frac{n\pi x}{L} dx \quad 4.50$$

It is remarked in passing that the cosine transform is employed

because of its appropriateness to the present boundary conditions. If the sine transform were used, the transform of the first term on the left side of equation 4.47 would be written as:

$$\int_0^L \frac{\partial^2 Z}{\partial x^2} \sin \frac{n\pi x}{L} dx = \int_0^L \frac{\partial^2 \xi}{\partial x^2} \sin \frac{n\pi x}{L} dx = \frac{n\pi}{L} [(-1)^{n+1} \xi(L) + \xi(0)] - \left(\frac{n\pi}{L}\right)^2 \bar{\xi}_s(n,t) \quad 4.51$$

For this case the integral relation of equations 4.44 a,b would be required. Since no knowledge of the variation of  $F_T(t)$  along the pile existed, (the series of piles driven in Akron, Ohio excepted), the sine transform was not used.

The general solution of equation 4.49 is:

$$Z_c(n,t) = \int_0^t g(t,\tau) G(n,t) d\tau \quad 4.52$$

where  $g(t,\tau)$  is the associated Green's function of the homogeneous equation 4.49 with the following transformed initial conditions:

$$Z_c(n,0) = \dot{Z}_c(n,0) = 0 \quad 4.53 \text{ a,b}$$

Then the solution of equation 4.49 is given by:

$$Z_c(n,t) = \bar{\xi}_c(n,t) = \int_0^t \frac{G(n,\tau) e^{-\gamma(t-\tau)} \sin \beta(t-\tau) d\tau}{\beta} \quad 4.54$$

for  $n = 1, 2, 3, \dots$

where

$$\gamma = \frac{C^2 d}{2} \quad 4.55$$

$$\beta = \frac{n\pi C}{L} \left[ 1 - \left( \frac{dC L}{2n\pi} \right)^2 \right]^{1/2} \quad 4.56$$

and d is defined as:

$$d = \frac{2n\pi\zeta}{CL} \quad 4.57$$

with  $\zeta$  equal to the ratio of damping to critical, so that each mode of the response has the same damping ration,  $\zeta$ . For each value of  $N \geq 1$ , equation 4.54 represents the elastic response of the pile for a given forcing function  $G(n,t)$ .

For the case  $n = 0$ , equation 4.49 yields the rigid body contribution:

$$\ddot{Z}_c(0,t) = \ddot{X}_c(t) = \frac{C^2}{AE} [-F_B(t) + F_T(t) = \bar{R}_c(0,t)] = G(0,t) \quad 4.58$$

from which  $\dot{X}_c(t)$  and  $X_c(t)$  are obtained by successive time integrations. It can be proven that when  $n = 0$  the solution to equation 4.49 represents only the rigid body portion. The inverse transform of equation 4.49 with  $n = 0$  is:

$$\ddot{Z}(0,t) = \frac{\ddot{Z}_c(0,t)}{L} = \frac{G(0,t)}{L} \quad 4.59$$

or using the notation  $\ddot{X}(t) \equiv \ddot{Z}(0,t)$ , yields:

$$\ddot{X}(t) = \frac{C^2}{AEL} [-F_B(t) + F_T(t) - R_0(x,t)] \quad 4.60$$

Since  $c^2 = E/\rho$ , the implication is:

$$\frac{c^2}{AEL} = \frac{1}{V\rho} = \frac{1}{m} \quad 4.61$$

where  $m$  is the total mass of the pile. Consequently, equation 4.60 can be written as:

$$M \ddot{X}(t) = F_T(t) - F_B(t) - R_0(x,t) = \sum F(t) \quad 4.62$$

which is merely the application of Newton's second equation of motion of a rigid body. It is noted in passing that 4.62 resembles eq. 1.1, i.e. the rigid body model.

The total displacement of a point on the pile is given by:

$$Z(x,t) = \frac{X_c(t)}{L} + \frac{2}{L} \sum_{n=1}^{\infty} \bar{\xi}_c(n,t) \cos \frac{n\pi x}{L} \quad 4.63$$

where  $Z(x,t)$  is the net solution of equation 4.47.

Considering in particular the point  $x = 0$ , the above solution reduces simply to:

$$Z(0,t) = \frac{X_c(t)}{L} + \frac{2}{L} \sum_{n=1}^{\infty} \bar{\xi}_c(n,t) \quad 4.64$$

This point is of particular interest since the measured field data was obtained at the top of the pile and the above solution will be matched to the field data response.

The form and application of the soil resistance force law, given by 4.48, needs further elucidation. In this present

section the constant contribution term,  $R_0(x,t)$ , will be defined and applied operationally as an active force as follows:

$$R_0(x,t) = 0 \quad \text{for } 0 \leq t \leq t_1 \quad 4.65a$$

$$R_0(x,t) = \frac{C_0}{L} \quad \text{for } t_1 < t \leq \infty \quad 4.65b$$

where  $C_0$  is constant for all  $x$  and time  $t > t_1$ . The time  $t_1$  is arbitrarily taken as the time when the measured velocity was at a maximum. In several cases considered this time can be approximated as  $t_1 = \frac{L}{C}$ , i.e. the time for an elastic wave to travel from top to bottom of the pile; the exact value chosen for  $t_1$  however, can be considered a parameter of the solution.

While many definitions of  $R_0(x,t)$  might be made, further experimentation in this direction is presently being undertaken. The above definition, however, has proven adequate in several examples studied to date as will be shown. In other words, a total static soil resistance of amount  $C_0 + F_B(t)$  is assumed to begin acting instantly once the time  $t_1$  has been reached.

In order to simulate an elastic-plastic failure law for the pile-soil resistance law, a slight modification of the above scheme for  $R_0(x,t)$  has also been employed. The resistance law was alternately taken in the form:

$$R_0(x,t) = \frac{C}{L} \int_0^{t_1} K(x) Z\left(0, \frac{t-\tau}{C}\right) d\tau \quad \text{for } 0 \leq t \leq t_1 \quad 4.66a$$

$$R_0(x,t) = \frac{c_0}{L} \quad \text{for } t_1 < t \leq \infty \quad 4.66b$$

where the coefficient  $K(x)$  depends on the soil shear resistance at the pile-soil interface. For extra simplicity  $K(x)$  was taken as a constant  $K(x) = K_0$  throughout the pile length. Also the displacement function appearing in equation 4.66a was taken as that measured in the field in order to simplify the solution given by equation 4.54. It may be pointed out prior to discussing the examples that this resistance law for the time preceding  $t_1$ , essentially an elastic-plastic law, had slight effect upon the response, whatever the value of  $K_0$  chosen. It caused only slight changes in the early and less significant portion of the calculated pile displacement response. As shown previously the responses in the early portion of the acceleration, velocity, and displacement are proportional to the measured input force  $F_T(t)$ . The form of the resistance law suggested by equations 4.66a, b is shown in Figure 4.10.

Before comparing the results of this analysis to the measured responses, a few comments should be made on the convergence problems encountered in calculation. If it is assumed in the present discussion that the forcing function given by the right side of equation 4.49 is independent of time so that the integral expression can be evaluated, and the assumed resistance law given by either equations 4.65 a,b or equations 4.66 a,b is independent of  $n$ , i.e.

$$G_0 = G(n, t)$$

then the transformed solution  $\bar{Z}_c(n, t)$  given by equation 4.54 would be written as:

$$\bar{Z}_c(n, t) = G_0 \int_0^t \frac{e^{-\gamma(t-\tau)} \sin \beta(t-\tau)}{\beta} d\tau \quad 4.67$$

where  $\gamma$  and  $\beta$  are given by equations 4.55 and 4.56. Differentiating the above equation results in the following velocity relation:

$$\dot{\bar{Z}}_c(n, t) = -G_0 \frac{\gamma}{\beta} \int_0^t e^{-\gamma(t-\tau)} \sin \beta(t-\tau) d\tau + G_0 \int_0^t e^{-\gamma(t-\tau)} \cos \beta(t-\tau) d\tau \quad 4.68$$

Upon integrating it can be easily shown that the velocity expression  $\dot{\bar{Z}}_c(n, t)$  is a function of the following:

$$\frac{1}{n}, \frac{e^{-nt} \cos nt}{n}, \frac{e^{-nt} \sin nt}{n} \quad 4.69$$

The inverse transform of the velocity at the top of the pile is given by:

$$\dot{Z}(0, t) = \frac{\dot{X}_c(t)}{L} + \frac{2}{L} \sum_{n=1}^{\infty} \dot{\bar{Z}}_c(n, t) \quad 4.70$$

Therefore, substituting the functions displaced in 4.69 into 4.70

leads to a divergent series because of the sum  $\sum_{n=1}^{\infty} \left(\frac{1}{n}\right)$ . Similarly,

the acceleration is represented by a non-convergent series in the variable  $n$ .

In order to avoid this mathematical problem a central finite difference scheme was used to represent the velocity and acceleration responses from the convergent series representation of the displacement response given by equations 4.54 and 4.64.

A piecewise linear approximation was used to represent the measured forced  $F_B(t)$  and  $F_T(t)$  appearing in equation 4.49 instead of some approximate analytical function with continuous derivatives.

#### 4.3 Comparison of Theoretical Predictions with Experimental Results

The analytical method outlined in Section 4.2 was employed on a number of practical examples for which static bearing test results were available to compare with dynamic predictions. The measured hammer force at the top of the pile is taken as the known input to the analytic problem. The first aim of the calculation is then to predict the pile displacement response. The four parameters of each calculation were taken as  $C_0$ ,  $K_0$ ,  $t_1$ , and  $\zeta$ . Of these,  $C_0$  had by far the greatest importance; the other parameters acted as "trimming" parameters only. By choosing  $K_0 = 0$ ,  $\zeta = 0.90$  and  $t_1$  approximately equal to the time of peak velocity or in some cases equal to  $\frac{L}{C}$ , these trimming parameters would be effectively removed from the calculation for most of the piles considered. The parameter  $K_0$ , as mentioned earlier, did not prove to be of great significance. The damping ratio  $\zeta$  was taken



as being large in most cases, representing highly damped oscillations of the pile response modes. The speed of sound in steel was checked by direct experiment and a value of 17,200 feet per second was used in all cases.

The computer-aided procedure then used was as follows: Given the measured force inputs  $F_T(t)$  at the top of the pile and when possible, the force  $F_B(t)$  at the toe, the best possible match was sought for the pile displacement independently obtained through double integration of the measured acceleration using any reasonable values for the four parameters mentioned. The comparison of predicted bearing, using the mathematical model of Section 4.2, to the measured bearing is the principal object of this section.

Both the acceleration and velocity responses were used as aids in determining a good displacement match by taking into account the location of peaks occurring at the same time as the measured acceleration and velocity responses. When a "best" match was thought to have been obtained, the corresponding sum of  $C_0 + F_B(t)$  employed was compared to the ultimate static bearing capacity obtained either by the performance of a C.R.P. Test or a standard M.L. Test. The matching technique is valid only in that portion of the time domain for which the velocity is positive. No provision was made to incorporate a resistance after the time of zero velocity. In the cases where no toe force measurements were made,  $F_B$  was taken to be zero in the analysis; the predicted  $C_0$  thus represents

the total predicted bearing capacity. It will be shown in the next section that the inclusion of  $F_B(t)$  in  $C_0$  or consideration of the sum  $C_0 + F_B(t)$  slightly affects the total predicted value.

The above analysis and algorithm were applied to several full-scale and reduced-scale piles. In this section the toe force  $F_B(t)$  was taken as zero, thus incorporating it into  $C_0$ . The parameter  $C_0$  in this section thus will represent the total predicted bearing.

The results shown in Figure 4.11 are those of full-scale pile 103 of North pier, last blow. The pile had a length of 74 feet and cross-sectional area of 7.83 sq. in. The theoretical displacement response from the above analysis matches well the displacement obtained by twice integrating the measured acceleration data. Both the theoretical velocity and acceleration responses resemble the experimental results. For this pile the predicted static bearing is  $C_0 = 222$  kips as opposed to 214 kips extrapolated from an M.L. Test. The predicted bearing is less than 4% higher than the static bearing.

Figure 4.12 shows the results of another full-scale pile, pile 692, driven in Youngstown, Ohio. Here the match of theoretical and experimental response curves is very encouraging. The periodicity of the acceleration response is very close to that measured in the field. The predicted bearing of 300 kips is approximately the same as the ultimate bearing of 296 kips

obtained from a C.R.P. Test as shown in Table 3.7. The error is approximately 1.3%.

The comparison of theoretical displacement to the measured displacement for pile 506 in Uhrichsville, Ohio, is shown in Figure 4.13. Here again the match is very good, while the match of acceleration and velocity to the corresponding experimental results is fairly good. The predicted bearing of 280 kips was slightly lower than the static bearing of 295 kips obtained from a C.R.P. Test. In this case it was found that the ratio of damping to critical damping was 0.65 and a  $K_0$  of 25 ksf was used in order that the displacement curves would match. The error in prediction here is approximately 5%.

The results shown in Figures 4.14 to 4.19 are those of the full-scale pile driven under the supervision of project personnel in Akron, Ohio. Figure 4.14 shows the results of a 30 foot pile at the end of driving. The match between theoretical and measured responses is fair but the correlation of predicted bearing  $C_0=119$  kips as opposed to an ultimate of 104 kips measured in a static C.R.P. Test is good. The results shown in Figure 4.15 are for the same pile but after a ground "set-up" period of approximately one week's duration. Here the match of theoretical displacement and measured displacement is good while the acceleration and velocity results are only fair. Both the predicted and measured ultimate bearing show an increase in strength due to the set-up period. The

dynamic prediction of ultimate bearing of 134 kips agrees fairly well with the actual static test results of 114 kips.

Figure 4.16 shows the results for Pile F-60, at the end of driving with approximately 60 feet below grade, with theory being a very good match as to curve shape in displacement, velocity, and acceleration. The static capacity predicted is  $C_0 = 220$  kips as opposed to a measured ultimate value of 204 kips obtained from a C.R.P. Test. The dynamic prediction error is 8% high. Figure 4.17 presents the results for the same pile which was restruck after a 2 week set-up period. Again, the match of the theoretical responses to the experimental results is good. The dynamic prediction of ultimate static bearing coincides with the actual static test results obtained from a C.R.P. Test.

Because of the excellence of the dynamic prediction in this case, it becomes a good object for test of the sensitivity of the prediction method to the value of  $C_0$  chosen. Figure 4.18 illustrates this, where values of  $C_0 = 232, 242$  and  $252$  kips have been tried, with corresponding theoretical displacements compared to the experimental test results. It is clear from this that close displacement match sharply delineates the proper  $C_0$  value within the theoretical method presented. This sensitivity in choosing the proper  $C_0$  existed in all piles considered.

The results presented in Figure 4.19 are those of a 12 inch diameter fluted pipe-pile driven 58 feet below grade into a coarse sand. The pile is designated as C-1, Canton, Ohio, Blow No. 2A.

The match of the theoretical responses to the experimental results is good up to 13 milliseconds at which time the curves begin to deviate from one another. The dynamic predicted bearing of 192 kips coincides with the actual static bearing obtained from a C.R.P. Test performed a few days earlier. Even though there is a discrepancy in time between measured and predicted bearing, further increase in static bearing would probably be small. This is so because the pile had already had a set-up period of approximately two weeks.

Figure 4.20 presents the results of full-scale pile No. 113 of North Pier at the end of driving. The match of theoretical displacement to the experimental displacement is excellent while the correlation between predicted static bearing to actual bearing is poor. An attempt was made to consider an overdamped response for this particular pile. The reason for such an attempt was that the measured acceleration response appeared to be highly damped due to the lack of oscillatory motion. When  $\zeta$  is greater than one, the solution for the transformed displacement given by equation 4.54 becomes as follows:

$$\bar{Z}_c(n,t) = \bar{\xi}_c(n,t) = \int_0^t \frac{G(n,t)[e^{(n-\gamma)(t-\tau)} - e^{-(n+\gamma)(t-\tau)}]}{2n} d\tau \quad 4.71$$

where  $\gamma$  is defined in equation 4.55 and  $n$  has the following form:

$$n = \frac{n\pi C}{L} \sqrt{\zeta^2 - 1} \quad 4.72$$

with  $\zeta$  being the ratio of damping to critical damping. Even though there was an improvement in the ratio of the predicted bearing to the static bearing, the match of the theoretical and experimental displacement nevertheless became worse. Thus, further overdamped calculations were not attempted for this pile.

Figure 4.21 shows the results for pile No. A of wall No. 91, another full-scale pile with a length of 74 feet below grade. Here the match of theoretical and experimental curves is less satisfactory than the previous piles considered but the static bearing prediction remains fair:  $C_0 = 290$  as opposed to a measured ultimate static value of 252 kips, the dynamic prediction error here is 15% too high.

The same analysis and matching techniques, used on the full-scale piles just considered, were employed to a few reduced-scale piles. The results shown in Figure 4.22 are those of pile 15-7 driven into sand 15 feet below grade. The results are for the first blow upon restriking the pile after a one week set-up period. The match of velocity and acceleration curves are fair in comparison to displacement match as shown in this figure. The discontinuity in the velocity at the time  $t_1$  resulted because of the discontinuity in the assumed soil resistance law. It was found that an increase in rigidity of a pile results in an increased dependence on or sensitivity to what type of soil-resistance law is assumed. In other words, the variation of soil-resistance as a function of time depends more on the rigid body motion of the

pile than on its elastic motion. This is the basis of Poncelet's law mentioned in Chapter 1. In the following section a variable resistance law is hypothesized and applied to a few reduced-scale piles. Discussion of the results will be reserved until that time.

The theoretical predicted bearing for pile 15-7 is 18 kips in contrast to the measured static bearing of 14 kips with a corresponding error of 28%, high. Again, the necessary assumed ratio of damping to critical damping was found to be large, a value of 0.90.

Figure 4.23 illustrates the dynamic prediction method for another reduced scale pile 1-T-10 having a length of 12 feet. The match achieved is the worst of all cases treated as far as curve shape is concerned, though general trends are preserved. However, the predicted ultimate static bearing capacity is  $C_0 = 9.9$  kips as opposed to a measured static bearing of 9.5 kips, the prediction being high by 4%.

#### 4.4 Elastic Wave Equation with Variable Static Resistance Law

Questions arose as to the justification of assuming a constant resistance law when applying the above-mentioned analysis to reduced-scale piles. An attempt was made to approximate the shape of static resistance  $R_0(x,t)$  given in equation 4.48 to the measured force at the top of the pile. This approximation scheme is shown in Figure 4.24. At the time  $t_1$ , the static resistance  $C_0$  is activated as in the previous analysis but only exists up to the time  $t_2$ , at which point a new resistance  $C'_0$  is activated. This

new resistance is also assumed constant on the time interval

$$t_2 \leq t \leq \infty.$$

The results of applying a variable resistance law to reduced-scale pile 1-T-10 are shown in Figure 4.25. The variable resistance law assumed is superimposed on the measured force at the top of the pile as shown in Figure 4.26. There is an improvement in the velocity and acceleration responses during the first two milliseconds as compared to the corresponding responses of a constant resistance law given in Figure 4.23. The improved predicted bearing was found to be 9.0 kips as opposed to the measured static bearing of 9.5 kips. In this case the toe force was incorporated into the resistance parameters  $C_0$  and  $C'_0$ .

The results shown in Figure 4.27 are those of the same reduced-scale pile 1-T-10, except that the toe force was not combined in the parameters  $C_0$  and  $C'_0$  but was considered separately in the right side of equation 4.49. Shown in Figure 4.28 is the toe force for blow 2A of this particular pile. The predicted bearing increased slightly from 9.0 kips to 9.2 kips. The velocity and acceleration responses of Figure 4.30 are similar to those of Figure 4.25.

#### 4.5 Summary of Results

The results of the approximate schemes, given in Chapter 1 and Sections 3.1 and 4.2, are summarized in Tables 4.1 and 4.2 for some of the piles studied. In these tables column 3 repre-



sents the theoretical predicted bearing using one of the assumed resistance laws discussed in either Section 4.2 or in Section 4.4. The results listed in column 5 are those obtained by applying the averaging scheme discussed in Section 3.1 to the assumed rigid body equation 1.1. Column 6 presents actual static test results obtained from either a M.L. or a C.R.P. Test for the ultimate load bearing capacity. The results,  $R^*(t_0)$ , in column 4 represent the application of equation 1.1 using only the rigid body acceleration obtained from the theoretical analysis discussed in Sections 4.2 and 4.4 at the point where the velocity passes through zero. The results in this column are in close agreement to the predicted values of  $C_0$ .

Comparing the results of columns 3, 5, and 6 it may be argued that the very practical graphical averaging method described in Section 3.1 (i.e. the application of Newton's equation to the measured field data), does in fact yield good results in the cases considered, especially in cases of full scale piles. Thus, this approximate scheme seems to suffice for practical applications while the more elaborate computer analysis remains fruitful as a research tool.

In the cases where reduced-scale piles are driven into silt and clay soils, a critical and closer examination of the behavior of the soil-pile interaction should be carried out.

## CHAPTER V

### SPECIAL PURPOSE COMPUTER

#### 5.1 General Description

A special-purpose digital computer has been built to operate with the pile driving instrumentation console presently used by the project. The function of the computer is to make real time calculations, (during driving), of the static resistive capacity of a pile. Calculations of the capacity are made within 2 milliseconds after each blow. Thus, each blow could conceivably be recorded.

The computer accepts two channels of acceleration and one channel of strain. These are the same signals which are inputs to the oscillograph. High impedance amplifiers at the input to the computer isolate the computer from the oscillograph. One or both of the acceleration input channels may be used. The computer will compute the load according to equation 1.1 to be

$$\text{LOAD} = K\epsilon - M(A_1 + A_2)/2 \quad 5.1$$

where  $\epsilon$  is the strain in microinches/inch,  $A_1$  and  $A_2$  are the two acceleration inputs in g's,  $M$  is the mass of the pile, and  $K$  is the strain calibration.

#### 5.2 Computer Organization

Figure 5.1 shows the system organization of the computer. Following will be a brief description of each of the functional

components of the system.

### Operator Controls

The operator control panel is shown in figure 5.2. A toggle switch allows the operator to select whether the computer operates in either the "manual" mode or the "automatic" mode. When operating in the automatic mode each blow will be recorded and the load will be displayed in the Nixie tube readout for approximately 1 second, after which the computer will automatically reset in preparation to receive the next blow. When operating in the "manual" mode a blow will not be recorded until after the operator has pushed the "READY" pushbutton. Once a blow has been recorded, the load will remain displayed until the operator pushes the "READY" pushbutton again. Thus, in manual the operator can select which blows are recorded.

$V_1$ ,  $V_2$ , and  $V_3$  are the input gain controls as shown in Figure 5.1. When toggle switch  $S_1$  is in the left position, the acceleration inputs to the computer are zero. When  $S_1$  is in the right position the acceleration is the average of the inputs to the two acceleration channels. Switch  $S_2$  operates in the same manner for the strain input as  $S_1$  does for the acceleration. Switch  $S_3$  is a 3-position toggle switch. When  $S_3$  is in the right position, the velocity input to the system control is

$$vel. = \int_0^t \frac{(A_1 + A_2)}{2} dt \quad 5.2$$

If  $S_3$  is in the center position, the velocity input to the control system is positive, and if  $S_3$  is to the left, the velocity input is zero. A more detailed description of the use of these switches is given in section 5.3 on computer calibration.

#### Input Control

The function of the input control circuitry is to detect when a blow has occurred and determine the zero velocity point where the data is to be sampled. Figure 5.3 shows the functional components of the input control. The integrator is AC coupled so that any drift on the acceleration channel inputs will not cause the integrator output to latch up (i.e. - go to infinity).

The positive velocity detector uses feedback to prevent it from triggering when the velocity goes from zero to positive until the signal is significantly positive. This is to ensure that a blow has been detected and will disregard any small positive velocity signal caused by low amplitude 60 cps noise on the acceleration channel inputs. However, when the velocity is going from positive to zero, the output of the detector does not change until the velocity does become less than or equal to zero as shown in Figure 5.4.

#### Analog-Digital Converter

The analog-digital converter accepts an analog input ( $A_a$ ) signal and the output of a digital register. The output of the digital register is converted to an analog signal ( $A_d$ ) which is

then compared with ( $A_a$ ). If  $A_a > A_d$  a signal is sent to system control to tell the digital register to increment. If  $A_a < A_d$  a signal is sent to tell the register to decrement. In this manner the digital register tends to follow the analog input in value.

#### Digitized Signal Register

These registers contain the digitized values of the analog input signals. The digital data is in binary-coded decimal format. Each of these registers can count up and down between the values of 0 and 1900.

#### Multiplier

The multiplier multiplies an input frequency by the fractional value set in the thumb-wheel switches. When one of the digitizing registers is counted down, a pulse is sent to the multiplier for each step of the counter. Thus, if the digitized acceleration register were to contain 800, and .125 were set in the MASS thumb-wheel switches and the register were counted down to zero, then the MULTIPLIER would receive 800 pulses from the register and put out  $(800)(0.125) = 100$  pulses to the ADDER.

#### System Control

System Control is composed primarily of state control logic which can best be described by the flow chart shown in Figure 5.5.

#### Adder and Accumulator

The Accumulator is a binary coded decimal register which can be incremented by pulses from the Adder and reset to zero

by control signals. The Adder is a gate which allows pulses from the acceleration channel Multiplier to be sent to the Accumulator during control state number 2, and pulses from the strain channel multiplier during control state number 3.

### 5.3 Computer Calibration

#### Strain Channel

- 1) Zero acceleration input by switching "S<sub>1</sub>" to left position.
  - 2) Set .999 in Strain Cal. thumb-wheel switches.
  - 3) Deflect strain beam on recorder to the left with calibration input at instrumentation console. This deflection will be some known number of micro-strains.
  - 4) Set computer to manual and set "S<sub>2</sub>" to right.
  - 5) Set "S<sub>3</sub>" to center position.
  - 6) Push "Ready" pushbutton.
  - 7) Switch "S<sub>3</sub>" to left - strain should appear in Nixie readout.
  - 8) Adjust "V<sub>2</sub>" (clockwise to decrease and repeat steps 5 through 8 until calibrated strain reading is reached.
- Note: only the 3 most significant digits of the registers are displayed in the Nixie tubes. Calibration numbers up to 1800 can be used. If numbers over 1000 are being used, sometime during the calibration procedure, the thumbwheel switches should be changed to .099 and the reading should appear in the third digit of the display.

9) The strain calibration used during recording should then be set into the thumb-wheel switches. The decimal point is to the left of the most significant digit in the thumb-wheel switches, so the strain calibration should be scaled so that the final result will have the most significant digit in the most significant position of the Nixie readouts.

Acceleration Channel

- 1) Zero strain channel by switching "S<sub>2</sub>" to left.
- 2) Set .999 in MASS thumb-wheel switches
- 3) Computer should be in MANUAL
- 4) Switch "S<sub>1</sub>" to right
- 5) The output of the positive velocity is taken to one of the visicorder inputs. This signal can be seen to deflect by
  - a) moving "S<sub>3</sub>" to left.
  - b) pushing "READY"
  - c) moving "S<sub>3</sub>" to center

The amplitude of this deflection can be adjusted by an "ADJ" knob on a small panel next to the operators panel, until the deflection is the same as for a calibrated acceleration deflection. This signal is then introduced to the acceleration channel of the computer by switching the toggle switch on the small panel to the "CAL" position.

- 6) Turn "V<sub>1</sub>" and "V<sub>3</sub>" clockwise as far as they will go.
- 7) Switch "S<sub>3</sub>" to center position

- 8) Push "READY"
- 9) Switch "S<sub>3</sub>" to left position
- 10) Rotate "V<sub>1</sub>" counter-clockwise while repeating steps 7-9 until the Nixie readout is one half of the calibrated acceleration value.
- 11) Rotate "V<sub>3</sub>" counter-clockwise while repeating steps 7-9 until the Nixie readout gives the calibrated acceleration value.
- 12) Set weight in MASS thumb-wheel switches scaled to match strain channel.

Recording

1. Switch "S<sub>1</sub>", "S<sub>2</sub>", and "S<sub>3</sub>" to the right
2. Switch toggle switch on small panel to "REC" position.



## CHAPTER VI

### CONCLUSIONS

During the past two year phase of this project, two different types of transducers have been developed which provide a satisfactory measurement of the force at the top of the pile. One of these is a strain gage load cell type device which attaches on top of the pile. The other type makes the force measurement by means of a clip-on strain transducer. Both methods are satisfactory. The load cell is more accurate due to the direct calibration but it is large and heavy to handle.

The modified rigid pile mathematical model shows less scatter and better correlation than is obtained from the previous method. Correlation between measured and predicted static resistance is good for full scale piles in all soil types encountered. Small scale piles did not show such good agreement particularly for cohesive soils. Further study is necessary to explain this difference.

The force measurements along the pile in Akron were only partially successful. The experience gained there will help to avoid these difficulties in future tests of this type.

The elastic pile analytical work provides an explanation of some aspects of pile behavior. It explains the basis for the modified rigid pile model. It is particularly interesting that

the oscillation of the acceleration after the peak of velocity is fairly well reproduced. This motion is not due to the return of the stress wave as indicated by its rather short period.

The special purpose computer shows promise of being capable of making the necessary computations for the dynamic prediction of the static resistance. If this can be accomplished on a routine basis there is every indication that the proposed method can provide a very rapid and inexpensive load test system.

## REFERENCES

1. Goble, G.G., Scanlan, R. H. and Tomko, J.J., "Dynamic Studies on the Bearing Capacity of Piles", Vol. I and Vol. II, Case Institute of Technology, July, 1967.
2. "A Performance Investigation of Pile Driving Hammers and Piles", Michigan State Highway Commission, Lansing, Michigan, March, 1965.
3. "Construction and Materials Specification", State of Ohio, Department of Highways, Columbus, Ohio, Jan. 1963.
4. LaPay, W. S., "Dynamic Pile Behavior-Literature Survey and Response Studies", Master's Thesis. Case Institute of Technology 1965.

TABLE 3.1  
 Comparison of Static Bearing Capacity with Dynamic Prediction  
 For Reduced Scale Pile

Pile Description	Blow Number	Ultimate Static Load from C.R.P. Test in Kips	Dynamic Results at $x(t_0)=0$ in Kips		$R_0 = F(t_0) - m\ddot{x}(t_0)$ In Kips	$R_0$ avg. In Kips
			$-m\ddot{x}(t_0)$	$F(t_0)$		
15-3	326	14.8	-5.5	6.7	12.2	13.4
	327		-6.3	7.0	13.3	13.4
	Average		-5.9	6.9	12.8	13.4
15-3 (After Set-Up)	1 A	18.3	-7.0	13.7	20.7	17.5
	2 A		-4.9	10.3	15.2	15.4
	3 A		-3.5	8.3	11.8	16.0
Average		18.3	-5.1	10.8	15.9	16.3
15-4 (After Set-Up)	1 A	10.6	-5.6	6.8	12.4	12.4
	2 A		-2.8	7.4	10.2	10.2
	3 A		-4.7	6.9	11.6	11.6
Average		10.6	-4.4	7.0	11.4	11.4
15-6 (After Set-Up)	1 A	12.1	-5.5	10.0	15.5	14.2
	4 A		-5.1	9.0	14.1	13.9
	9 A		-2.6	6.5	9.1	11.0
Average		12.1	-4.4	8.5	12.9	13.0

TABLE 3.1

cont.

Pile Description	Blow Number	Ultimate Static Load from C.R.P. Test in Kips	Dynamic Results at $x(t_0)=0$ in Kips		$R_0 = F(t_0) - m\ddot{x}(t_0)$ In Kips	$R_0$ avg. In Kips
			$m\ddot{x}(t_0)$	$F(t_0)$		
15-7 (After Set-Up)	1 A	14.0	-6.9	10.1	17.0	15.0
	2 A		-4.8	8.6	13.4	14.9
	4 A		-4.0	7.9	11.9	14.6
	Average		-5.2	8.9	14.1	14.8
1-T-10	115	5.6	-1.6	2.4	4.0	8.0
	117		-1.4	3.2	4.6	9.6
	Average		-1.5	2.8	4.3	8.8
	1-T-10 (After Set-Up)		-7.0	2.2	9.2	12.3
1-T-15/20	1 A	9.5	-5.2	4.2	9.4	10.0
	2 A		-6.1	3.2	9.3	11.2
	Average		-19.4	10.4	29.8	25.4
	1-T-15/20 (After Set-Up)		-12.8	12.2	25.0	21.7
2-T-15/20	1 A	17.4	-12.0	11.6	23.6	20.6
	2 A		-14.4	12.2	26.6	20.3
	4 A		-13.1	12.0	25.1	20.9
	Average		-13.2	9.2	22.4	17.4
2-T-15/20 (After Set-Up)	1 A	22.0	-7.8	13.2	21.0	21.6
	2 A		-10.2	13.2	23.4	22.2
	Average		19.0	13.2	22.2	21.9

TABLE 3.2

Comparison of Static Bearing Capacity with Dynamic Prediction  
For Reduced Scale Pile After Set-Up Period

Pile Description	Blow Number	Ultimate Static Load from C.R.P. Test in Kips	Dynamic Results at $x(t_0)=0$ in Kips		$R_0 = F(t_0) - mx(t_0)$ In Kips	$R_0$ avg. In Kips	
			$\frac{mx(t_0)}{F(t_0)}$	$F(t_0)$			
10-1	4 A	7.5	-2.5	11.3	13.8	15.2	
	5 A		-4.3	8.9			13.2
	8 A		-7.3	8.0			15.3
	Average		-4.7	9.4			14.1
10-2	1 A	7.0	-5.9	6.9	12.8	12.2	
	3 A		-4.1	4.8			8.9
	Average		-5.9	6.9			12.8
	1 A		-6.0	8.7			14.7
10-4	1 A	8.0	-6.8	6.6	13.4	13.6	
	2 A		-6.7	7.6			14.3
	Average		-6.8	7.1			13.9
	4 A		-6.9	7.6			14.5
10-5	5 A	9.3	-6.7	6.9	13.6	12.5	
	Average		-6.8	7.3			14.1
	2 A		-14.3	18.3			32.6
	4 A		-13.5	16.2			30.8
15-1	5 A	10.6	-14.0	16.8	30.8	26.5	
	Average		-14.3	17.1			31.4
	1 A*		-3.9	8.1			12.0
	3 A*		-6.5	9.0			15.5
15-5	11 A*	10.3	-9.7	7.3	17.0	16.0	
	Average		-5.2	8.6			13.8

1.51

1.33

\* Average of 2 accelerometers

TABLE 3.3

Comparison of Static Bearing Capacity with Dynamic Prediction  
For Reduced Scale Piles at End of Driving and After Set-Up Period  
in Silt and Clay

Pile Description	Blow Number	Ultimate Static Load from C.R.P. Test in Kips	Dynamic Results at $x(t_0)=0$ in Kips		$R_0 = F(t_0) - m\ddot{x}(t_0)$ In Kips	$R_0$ avg. In Kips
			$m\ddot{x}(t_0)$	$F(t_0)$		
1-R-10 (After Set-Up)	1 A	10.2	-6.0	7.9	13.8	13.0
	2 A		-6.9	7.9	14.8	
	3 A		-7.8	8.1	15.9	
	Average		-6.9	7.9	14.8	
1-R-15 (After Set-Up)	1 A	14.6	-9.2	10.6	19.8	19.8
	2 A		-8.1	17.9	26.0	
	Average		-8.7	14.2	22.9	
2-R-10	130	12.2	-8.6	9.8	18.4	18.0
	131		-1.2	11.8	13.0	
	135		-3.4	14.6	18.0	
	Average		-4.4	12.0	16.4	
2-R-10 (After Set-Up)	1 A	12	-11.4	12.4	23.8	17.0
	4 A		-8.0	9.8	17.8	
	Average		-9.6	11.0	20.8	
2-R-15	212	12.2	-24.4	14.2	38.6	21.4
	214		-7.2	4.4	11.6	
	215		-15.6	14.6	30.2	
	Average		-15.8	11.0	26.8	

TABLE 3.3  
con't.

Pile Description	Blow Number	Ultimate Static Load from C.R.P. Test in Kips	Dynamic Results at $\dot{x}(t_0)=0$ in Kips		$R_0 = F(t_0) - m\ddot{x}(t_0)$ In Kips	$R_0$ avg. In Kips
			$m\ddot{x}(t_0)$	$F(t_0)$		
2-R-15 (After Set-Up)	2 A	15.4	-14.4	16.0	30.4	25.5
	3 A		-18.0	15.0		
	5 A		-14.6	14.6		
	Average		-15.6	15.2		
2-R-20	309	18.2	-9.2	22.0	31.2	27.4
	311		-3.8	29.6		
	315		-5.6	29.0		
	316		-5.0	28.4		
	Average		-5.8	27.2		
2-R-20 (After Set-Up)	4 A	20.2	-11.8	20.4	32.2	33.1
	7 A		-6.0	35.0		
	9 A		-5.8	27.4		
	Average		-7.8	27.6		
3-R-10	122	11.0	-1.6	6.8	8.4	9.8
	123		-2.6	16.0		
	124		-2.8	16.4		
	Average		-2.4	13.0		
3-R-10 (After Set-Up)	1 A	11.6	-18.6	9.6	28.2	15.6
	2 A		-12.2	11.0		
	4 A		-19.0	9.6		
	Average		-16.6	10.0		

1.6

1.9

2.0 ~~2.0~~



TABLE 3.3  
con't.

Pile Description	Blow Number	Ultimate Static Load from C.R.P. Test in Kips	Dynamic Results at $x(t_0)=0$ in Kips		$R_0 = F(t_0) - m\ddot{x}(t_0)$ In Kips	$R_0$ avg. In Kips
			$m\ddot{x}(t_0)$	$F(t_0)$		
3-R-15	198	11.2	-15.4	9.6	25.0	14.5
	199		-11.0	10.0	21.0	13.5
	200		-5.6	9.4	15.0	12.8
	Average		-10.6	9.6	20.4	13.6
3-R-15 (After Set-Up)	6 A	16.8	-20.0	12.8	32.8	22.4
	7 A		-9.8	14.0	23.8	22.6
	Average		-14.9	13.4	28.4	22.5
3-R-20	268	16.2	-18.0	11.6	29.6	20.1
	271		-13.4	10.6	24.0	19.2
	Average		-15.6	11.1	26.8	19.7
3-R-20 (After Set-Up)	1 A	18.2	-8.2	27.4	35.6	38.2
	3 A		-12.0	34.4	46.4	47.4
	10 A		-4.2	32.6	36.8	45.9
	15 A		-21.0	13.6	34.6	25.5
	16 A		-19.4	12.2	31.6	25.6
Average		18.2	-13.0	24.0	37.0	36.5

1.2

1.34

1.21

2.00

TABLE 3.4

## Physical Characteristics of Full Scaled Piles Tested

Pile No. and Description	Type of Soil	Nominal Diameter In Inches	Wall Thickness In Inches	Area In In. <sup>2</sup>	Length of Pile in Ft. Below		Weight of Pile Lb./Ft.	Type of Hammer Used	
					Grade	Strain Gages Driving Load Tests			
113 North Pier of Br. No. Cuy 21-21-1431	Sand	12*	0.250	9.82	53	59.5	-	33.5	Steam Vulcan 0
138 of Pier 4 of Br. No. I-71-1826	Sand, Silt & Clay	12*	0.179	6.67	85	110	87	22.8	Steam Vulcan 50 C
A of Pier 5 of Br. Cuy 290-0040	Sandy Silt	12*	0.210	7.83	62	-	78.5	26.8	Diesel Link Belt 520
103 of Pier 2 of Br. No. 290-0040	Sandy Silt	12*	0.210	7.83	74	-	75.0	26.8	Diesel Link Belt 520
A of Wall 91A. Br. Cuy. 90-1395	Gray Silt & Clay	12*	0.210	7.83	74	-	76.5	26.8	Steam Vulcan 1
692 I-80 Youngstown, Ohio	Gray Silt & Clay	18**	3 & 5 gage	14.5	73	-	74	40.2 <sup>+</sup>	Diesel Link Belt 520
506 of Br. No. 1880 Uhrichs-ville	Sand, Silt & Clay	12*	.179	6.67	77	-	78	22.8	?

Pile No. And Description	Type of Soil	Nominal Diameter In Inches	Wall Thickness In Inches	Area In In. <sup>2</sup>	Length of Pile in Ft. Below		Weight Of Pile Lb./Ft.	Type of Hammer Used	
					Grade	Strain Gages Driving Load Tests			
534 <sup>1</sup> of Abut. 2 Br. 77-0937 Canton, Ohio	Gravelly Sand	12**	9 Gage Fluted	5.81	75	-	76	122.5 <sup>+</sup>	Diesel Delmag. D-12
531-70A & 70B Abut. 2 Br. 77-0937 Canton	Gravelly Sand	12**	9 Gage Fluted	5.81	70	-	71	18.0 <sup>+</sup>	Diesel Delmag D-12
531-76 Abut. 2 Canton	Gravelly Sand	12**	9 Gage Fluted	5.81	76	-	77	18.0 <sup>+</sup>	Diesel Delmag D-12
531-83 Abut. 2 Canton	Gravelly Sand	12**	9 Gage Fluted	5.81	83	84	84	18.0 <sup>+</sup>	Diesel Delmag D-12
Canton Test Pile C-1 of Br. No. 77-0937	Gravelly Sand	12**	9 Gage Fluted	5.81	58	-	59	18.0 <sup>+</sup>	Diesel Delmag D-12
F-30 Akron, Ohio	Silt & Sand	12*	.250	9.83	31	31.5	31.5	33.5	Diesel Link Belt
F-50 Akron, Ohio	Silt & Sand	12*	.250	9.83	50	50	50	33.5	Diesel Link Belt
F-60 Akron, Ohio	Silt & Sand	12*	.250	9.83	59	59	59	33.5	Diesel Link Belt

TABLE 3.4 cont'd.

Pile No. and Description	Type of Soil	Nominal Diameter In Inches	Wall Thickness In Inches	Area In In. <sup>2</sup>	Length of Pile in Ft. Below			Weight of Pile Lb./Ft.	Type of Hammer Used
					Grade	Strain Gages Driving	Load Tests		
3914 of Br. No. 1799 Great Miami River Hamilton County, Ohio	Coarse Gravel and Sand	12	0.179	6.67	61	71	63	22.8	Diesel
272 of Br. No. Luc. 75-0427	Clayey Silt	12	0.179	6.67	51	52	52	22.8	Diesel Link Belt

\* Spiral Welded Pipe Pile

\*\* Fluted - Tapered Pile

+ Average Weight per Foot

1 Pile filled with Concrete

TABLE 3.5

Comparison of Static Bearing Capacity with Dynamic Prediction  
For Full Scale Piles at End of Driving

Pile Description Location, Soil Condition	Blow No.	Ultimate Static Load Capacity in Tons		Dynamic Results at $m\ddot{x}(t_0)=0$ in Tons		$R_0 = F(t_0) - m\ddot{x}(t_0)$ in Tons	$R_0$ avg. in Tons
		C.R.P. Test	M.L. Approx.	$m\ddot{x}(t_0)$	$F(t_0)$		
113 North Pier of Br. Cuy. 21-1431 Cleveland Sand	Last	---	100 - 140 (12/22/64)	-18	106	124	118 (12/15/64)
138 of Pier 4 Br. No. I-71-1826 Cleveland Silt and Clay	76	135+	130-150 3/10/66	-33	31	64	65 (3/ 1/66)
531-83, Abut. 2 Canton, Ohio Gravelly Sand	2*	125	---	-30	66	96	102
	5*			-40	63	103	104
	9*			-43	64	104	108
	Average	125	---	-37	64	101	105
F-30, Contract Akron, Ohio Fine Sand, Silt and Clay	13	52	---	-13	37	50	58
	14			-15	49	64	59
	15			-15	51	66	63
	16			-16	48	64	61
	17			-17	44	61	58
Average	52	---	-15	46	61	60	

TABLE 2.6  
cont'd.

Pile Description Location, Soil Condition	Blow No.	Ultimate Static Load Capacity in Tons		Dynamic Results at $m\ddot{x}(t_0)=0$ in Tons		$R_0 = F(t_0) - m\ddot{x}(t_0)$ in Tons	$R_0$ avg. in Tons
		C.R.P. Test	M.L. Approx.	$m\ddot{x}(t_0)$	$F(t_0)$		
F-50 Contract Akron, Ohio Fine Sand, Silt and Clay	18*	112	---	-76	70	146	94
	19*			-61	69	130	98
	20*			-69	71	140	99
	Average	112	---	-69	70	139	97
F-60, Contract Akron, Ohio Fine Sand, Silt and Clay	17*	102	---	-51	89	140	115
	18*			-44	86	130	99
	19*			-78	84	162	113
	Average	102	---	-58	86	144	109

\* Average of 2 accelerometers

+ Evidence of pile yielding structurally

TABLE 3.6

Comparison of Static Bearing Capacity with Dynamic Prediction  
For Full Scale Piles After Set-Up Period

Pile Description Location, Soil Condition	Blow No.	Ultimate Static Load Capacity in Tons		Dynamic Results at $m\ddot{x}(t_0)=0$ in Tons		$R_0 = F(t_0) - m\ddot{x}(t_0)$ in Tons	$R_0$ avg. in Tons
		C.R.P. Test	M.L. Approx.	$m\ddot{x}(t_0)$	$F(t_0)$		
A of Pier No. 5 of Br. Cuy. 290-0040 Cleveland Sandy Silt	10 A	---	64	-35	90	125	115
	12 A	---		-43	95	138	134
	13 A	---		-46	96	142	131
	37 A	---		-30	87	126	124
	Average	---	64	-41	92	133	126
103 of Pier 2 of Br. No. 290-0040 Cleveland Sandy Silt	1 A	---	98-115	-31	76	107	109
	2 A	---		-20	78	98	93
	9 A	---		-29	104	133	135
	10 A	---		-22	103	125	126
	Average	---	98-115	-26	90	116	116
A of Wall 91A Cr. Cuy. 90-1395 Cleveland Sand and Silt	1 A	126	115-140	-30	104	134	128
	3 A			-31	108	139	130
	7 A			-42	101	143	136
	Average	126	115-140	-35	104	139	131
	692 Youngstown, Ohio of Inter. 80 Med. Coarse Sand	7 A	148	140-155	-113	135	248
11 A				-34	133	167	170
12 A				-73	138	211	190
15 A				-75	100	175	150
Average		148	140-155	-74	126	200	174

TABLE 3.6

cont'd.

Pile Description Location, Soil Condition	Blow No.	Ultimate Static Load Capacity in Tons		Dynamic Results at $m\dot{x}(t_0)=0$ in Tons		$R_0 = F(t_0) - m\ddot{x}(t_0)$ In Tons	$R_0$ avg. In Tons
		C.R.P. Test	M.L. Approx.	$m\dot{x}(t_0)$	$F(t_0)$		
506 Uhrichsville, Ohio, Br. No. 1880 Clay	2 A	122**	130-160	-33	109	142	140
	6 A			-33	106	139	138
	10 A			-30	85	115	110
	11 A			-38	86	124	118
Average		122**	130-160	-33	108	141	139
Pile C-1 of Br. 77-0938 Canton, Ohio Gravelly Sand	2 A	96	---	-45	50	95	94
534 of Abut. 2 Br. 77-0937 Canton, Ohio Gravelly Sand	1 A*	106		-55	51	106	106
	2 A*			-70	43	113	106
	11 A*			-165	68	233	158
	14 A*			-135	65	200	160
	17 A*			-90	69	159	140
Average		106		-63	47	110	106
531-70A, Abut. 2 Br. 77-0937 Canton, Ohio	1 A	95		-19	66	85	84
	3 A			-14	65	79	79
	5 A			-34	64	98	110
	Average		95		-22	65	87



TABLE 2.0  
cont'd.

Pile Description Location, Soil Condition	Blow No.	Ultimate Static Load Capacity in Tons		Dynamic Results at $m\dot{x}(t_0)=0$ in Tons		$R_0 = F(t_0) - m\dot{x}(t_0)$ in Tons	$R_0$ avg. in Tons
		C.R.P. Test	M.L. Approx.	$m\dot{x}(t_0)$	$F(t_0)$		
531-70B <sup>++</sup> , Abut. 2 Br. 77-0937	14 A	100	---	-19	45	64	65
	33 A			-20	60	80	80
	Average	100	---	-19	53	72	73
531-76, Abut. 2 Br. 77-0937 Canton, Ohio Gravelly Sand	3 A*	99	---	-31	72	103	103
	5 A*			-23	57	80	80
	9 A*			-26	63	89	89
	11 A*			-22	50	72	72
	Average	99	---	-27	65	92	92
F-30 Contract Akron, Ohio Fine Sand, Silt and Clay	1 A	57	57	-21	57	76	70
	5 A			-9	48	57	59
	6 A			-17	42	59	65
	7 A			-5	36	41	49
	Average	57	57	-13	46	58	63
F-50 Contract Akron, Ohio Fine Sand, Silt And Clay	10 A	119	112	-44	98	142	118
	13 A			-34	108	142	120
	14 A			-45	108	153	121
	15 A			-53	76	129	94
	Average	119	112	-44	98	142	113

TABLE 3.6  
cont'd.

Pile Description Location, Soil Condition	Blow No.	Ultimate Static Load Capacity in Tons		Dynamic Results at $m\dot{x}(t_0)=0$ in Tons		$R_0 = F(t_0) - m\ddot{x}(t_0)$ in Tons	$R_0$ avg. in Tons
		C.R.P. Test	M.L. Approx.	$m\dot{x}(t_0)$	$F(t_0)$		
F-60 Contract Akron, Ohio Fine Sand, Silt and Clay	22 A*	121	110	-65	75	140	108
	26 A*			-117	80	197	117
	27 A*			-81	75	156	108
	Average	121	110	-88	77	164	111
Great Miami River HAM-27-1799 Cincinnati Sandy Gravel	3	95.0	---	-69.2	73.8	142.0	92.5
	4			-52.3	65.2	117.5	97.8
	15			-44.7	73.5	118.2	93.3
	Average	95.0	---	-55.1	70.8	126.2	94.5
Pile #272 of Bridge # Luc75-0427 (Lucas County Toledo)	11	110.5	108.0	-33.1	115.7	148.8	127.5
	12			-46.2	119.4	165.6	134.2
	14			-75.0	127.8	202.8	134.8
	17			-53.6	124.8	178.4	138.6
	22			-37.5	120.2	157.7	127.5
	28			-30.5	115.4	145.9	115.8
	33			-24.2	121.2	145.4	128.6
Average	110.5	108.0	-42.9	120.6	163.5	129.6	

+ Results extrapolated from Ohio Department of Highway's M.L. Test

++ Second series of restriking pile

\* Average of 2 accelerometers

\*\* Terminated Load Test because Load Test System appeared to be unstable.

TABLE 4.1

Bearing Capacity Results in Kips  
of Full Scale Piles

Pile Number	Blow No.	Constant Resistance Law $C_0$	$R^*(t_0)$	$R(t_0)$ avg.	Ultimate Static Load
103 of Pier 2	1-A	222	227	218	214
692 Youngstown	Last	300	309	300	296
506, Uhrichsville	2-A	280	283	280	295
F-30, Akron	13	119	121	116	104
F-30, Akron	1-A	134	131	140	114
F-60, Akron	17	220	222	230	204
F-60, Akron	26-A	242	245	234	242
C-1, Canton	2-A	192	178	188	192
113 of N. Pier	Last	350	360	236	240
A of Wall 91A	3-A	290	291	260	252

TABLE 4.2

Bearing Capacity Results in Kips  
of Reduced-Scale Piles

Pile Number	Blow No.	$C_0$ or $C'_0 + F_B(t_0)$	$R^*(t_0)$	$R(t_0)$ avg.	Ultimate Static Load
15-7, Sand	1A	18	18.4	15	14.0
1-T-10, Sand Constant Law	2A	9.9	10.5	9.4	9.5
1-T-10, Sand Variable with $F_B(t) = 0$	2A	9.0	9.4	9.4	9.5
1-T-10, Variable in- cluding $F_B(t)$	2A	9.2	9.7	9.4	9.5
1-T-15/20, Sand Constant Law	1A	20.5	20.3	22.5	16.7
1-T-15/20, Sand Variable, in- cluding $F_B(t)$	1A	16.5	16.4	22.5	16.7

Detail A

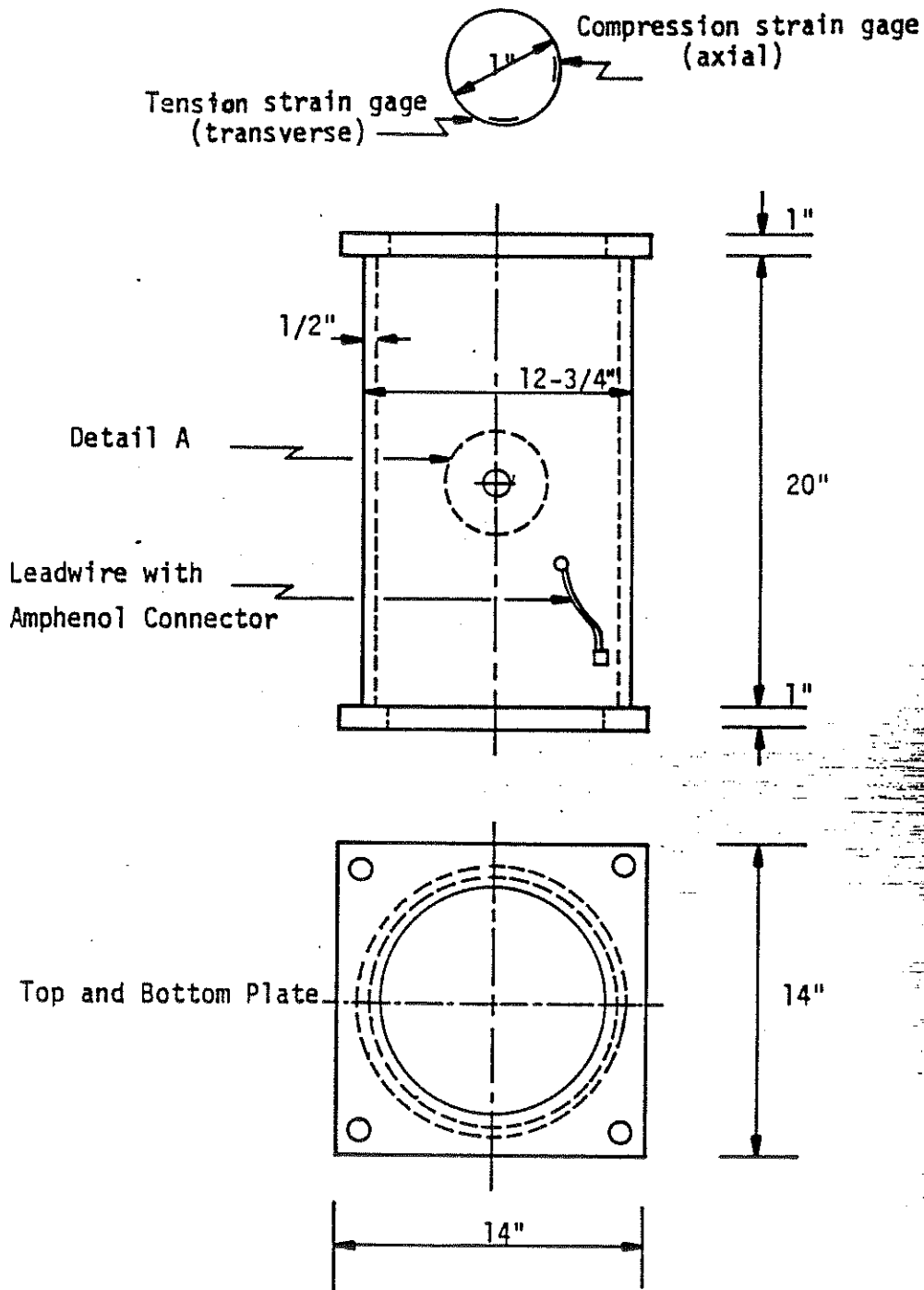


Figure 2.1

Drawing of Full Scale Pile Transducer

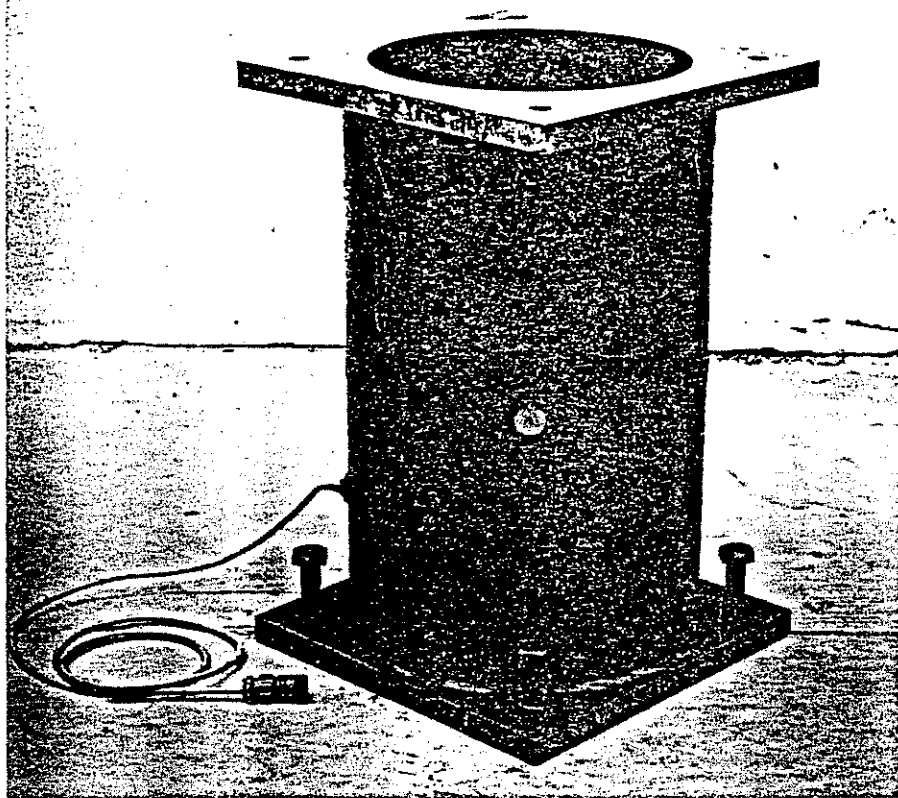


Figure 2.2

Full Scale Pile Transducer

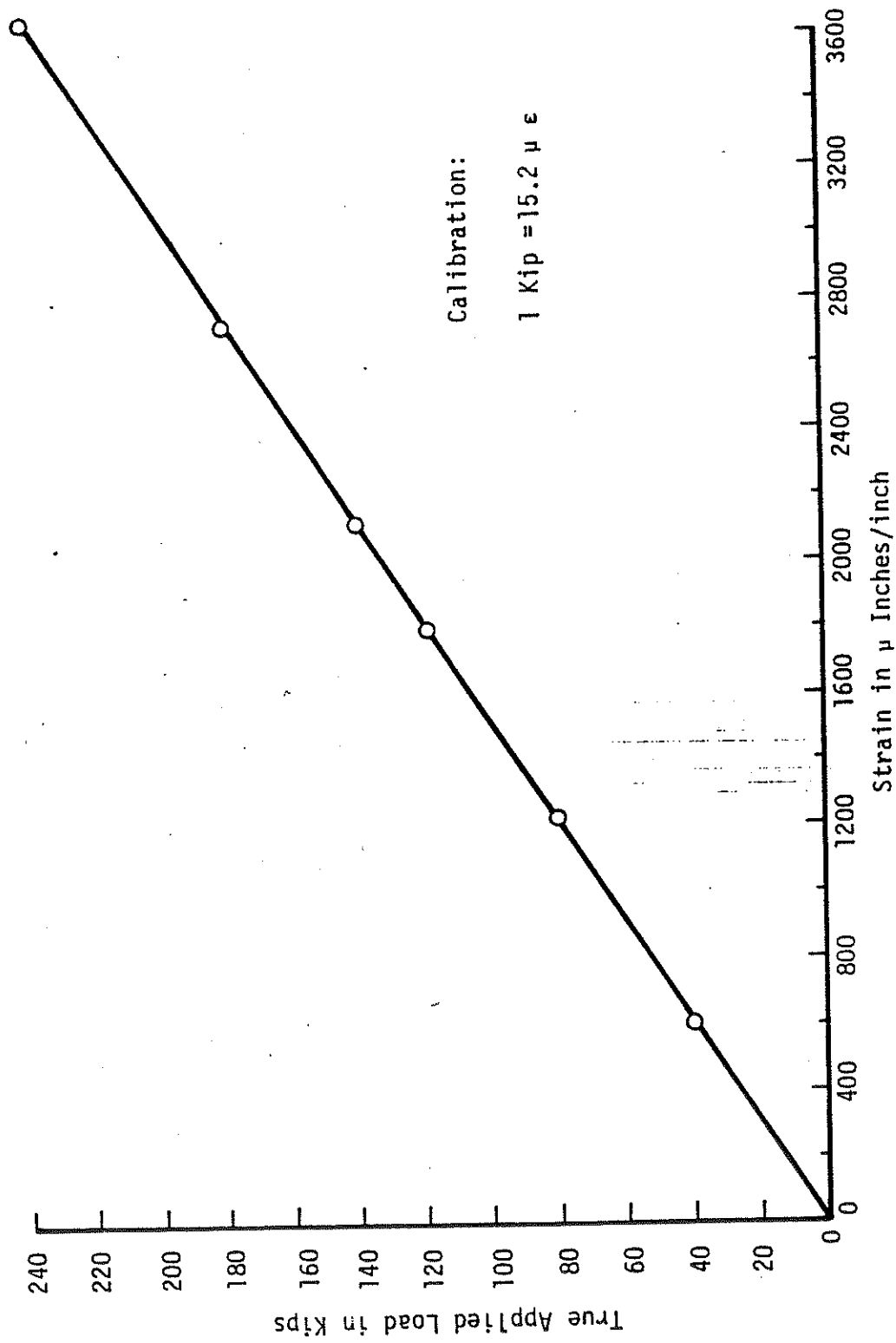


Figure 2.3  
Calibration of Full-Scale Pile Transducer

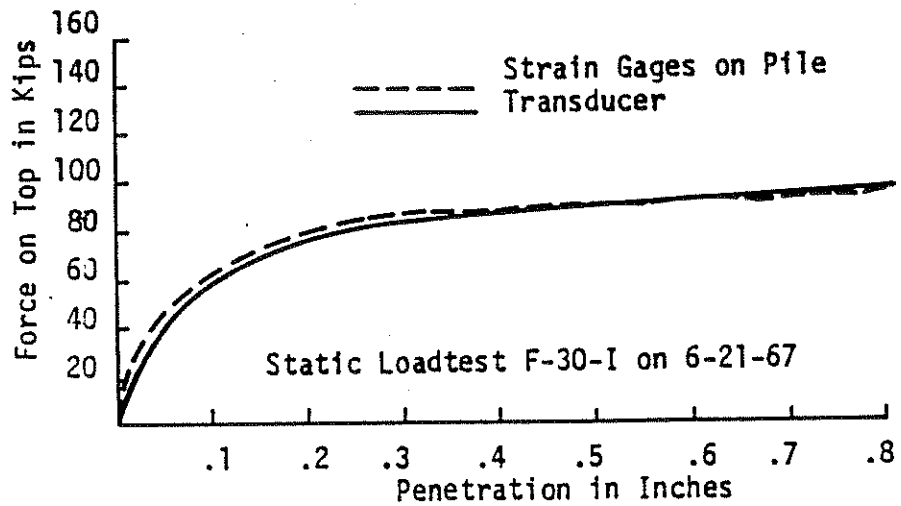


Figure 2.4 Transducer Comparison at Static Load Test

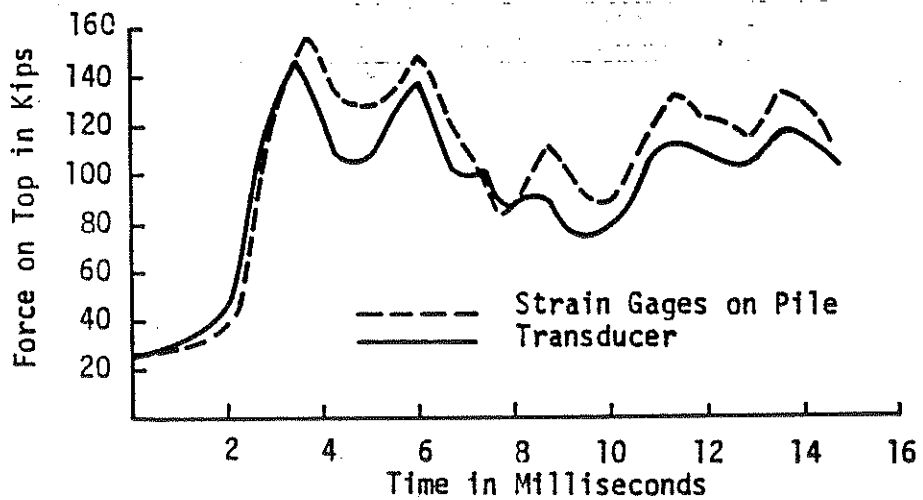


Figure 2.5 Transducer Comparison at Dynamic Test



BOTTOMVIEW

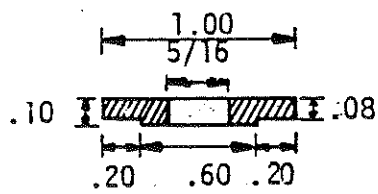
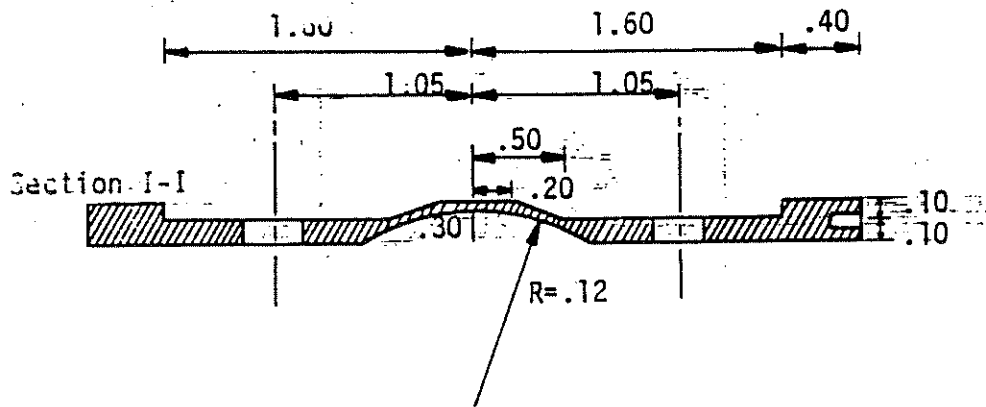
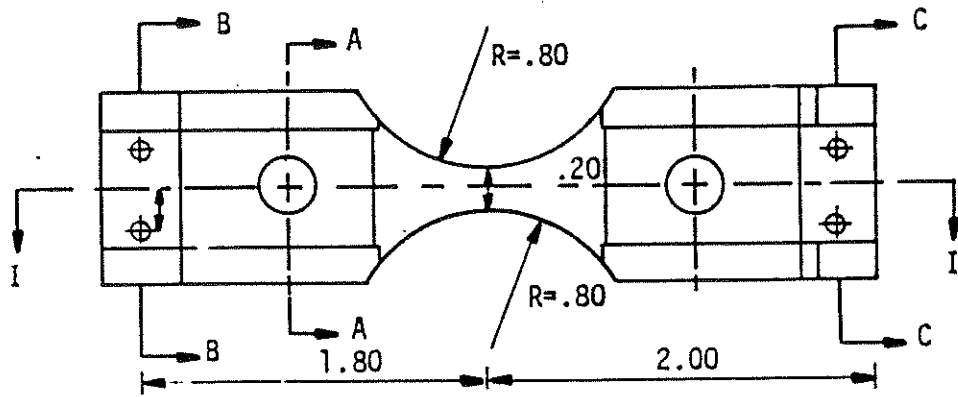


Figure 2.6

Clip On Transducers

Runs 1, 2, 3, & 4

- 1-  $\theta$
- 2-  $\times$
- 3-  $\triangle$
- 4-  $\square$

Points of unloading  
not shown for clarity

After run 1 and 2  
positions of transducers  
were switched

Calibration factor

$$k = \frac{1430}{500} = 2.86$$

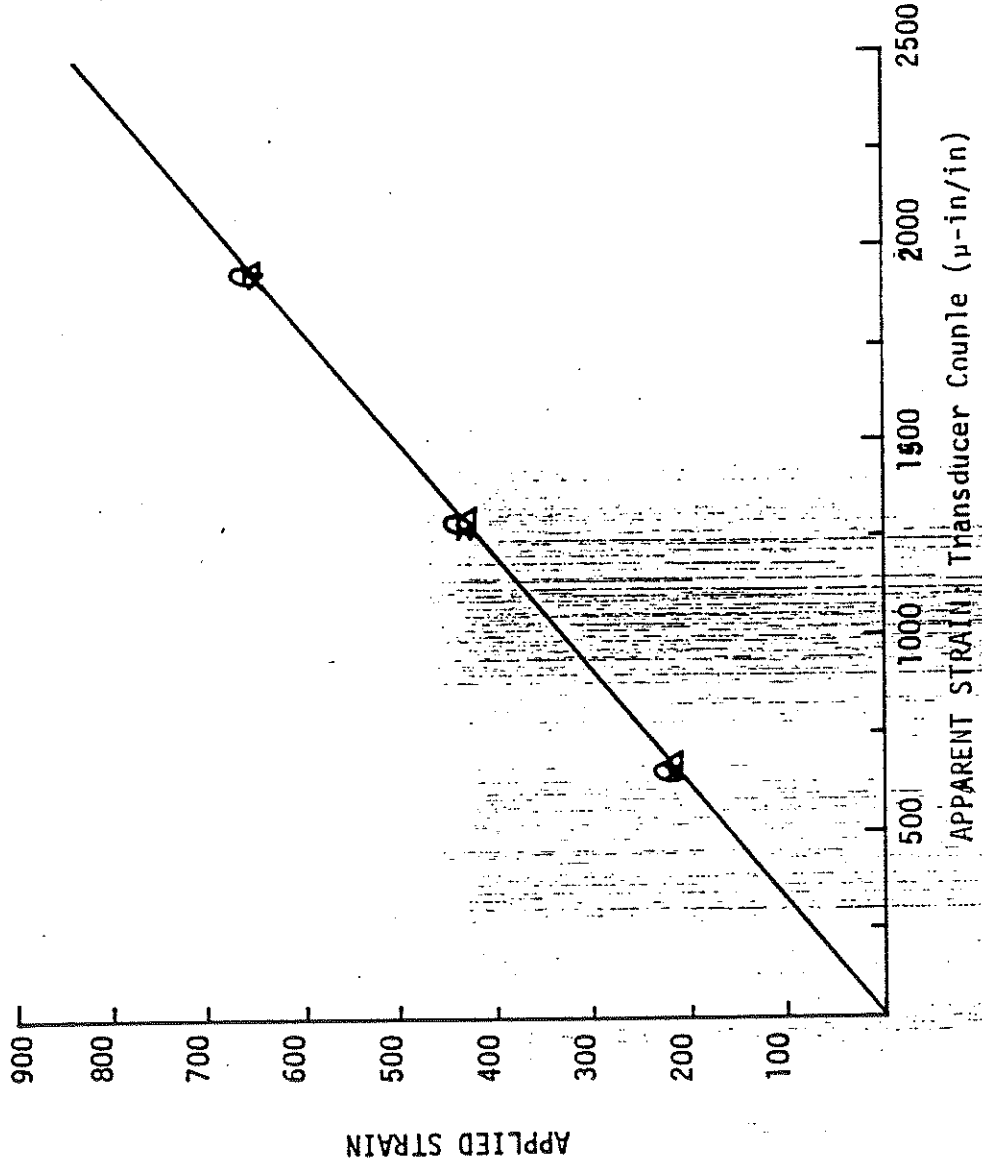


Figure 2.7

Calibration of Clip-On Transducers

Full Scale Pile Toledo on 4-18-68

Blow # 11

3 feet distance between transducers

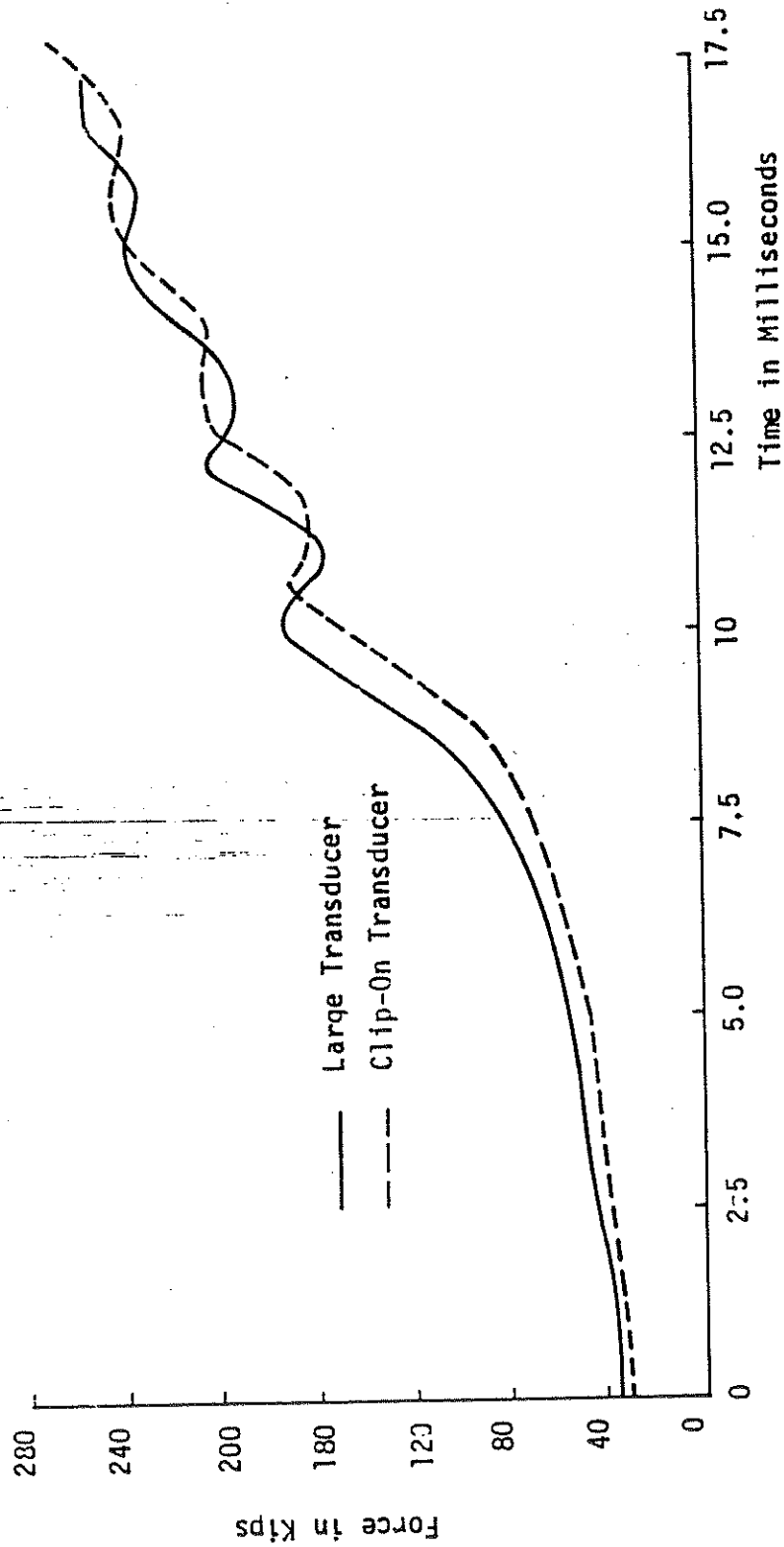


Figure 2.8  
Comparison of Clip On with Large Transducer

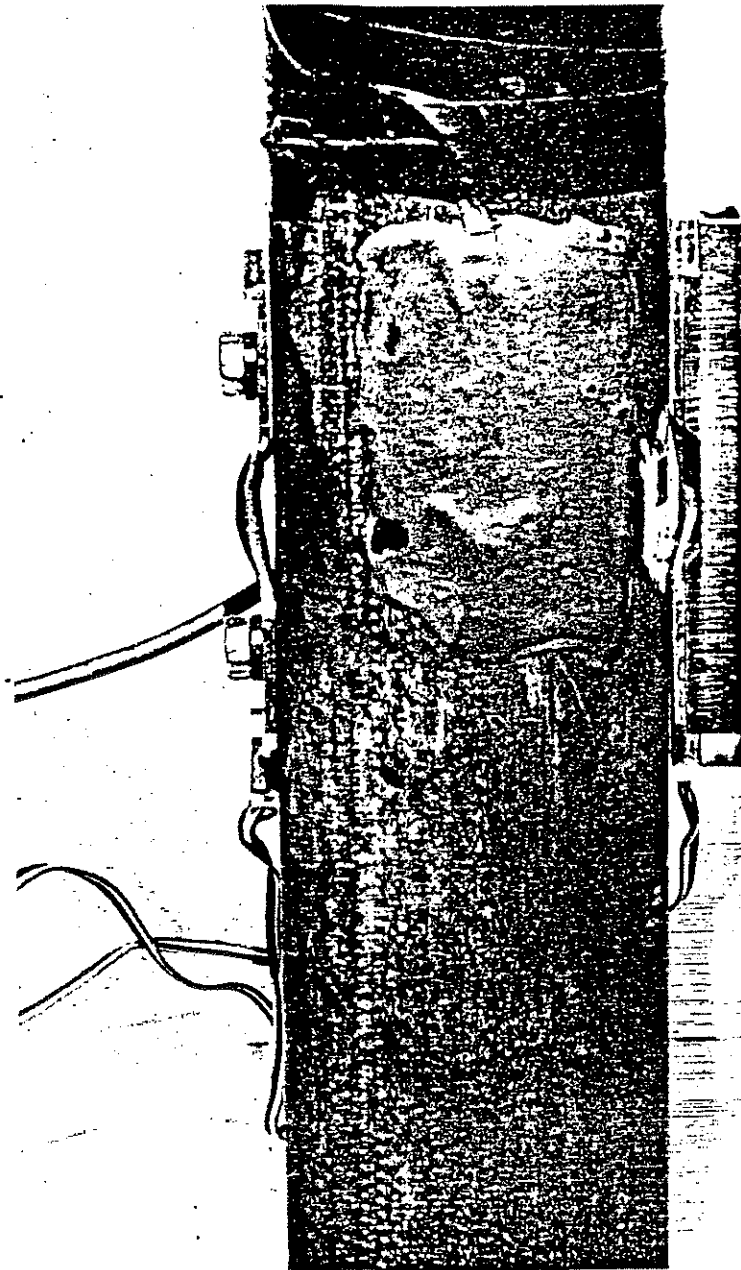


Figure 2.9

Clip-On Transducers Attached to Reduced Scale Pile Section

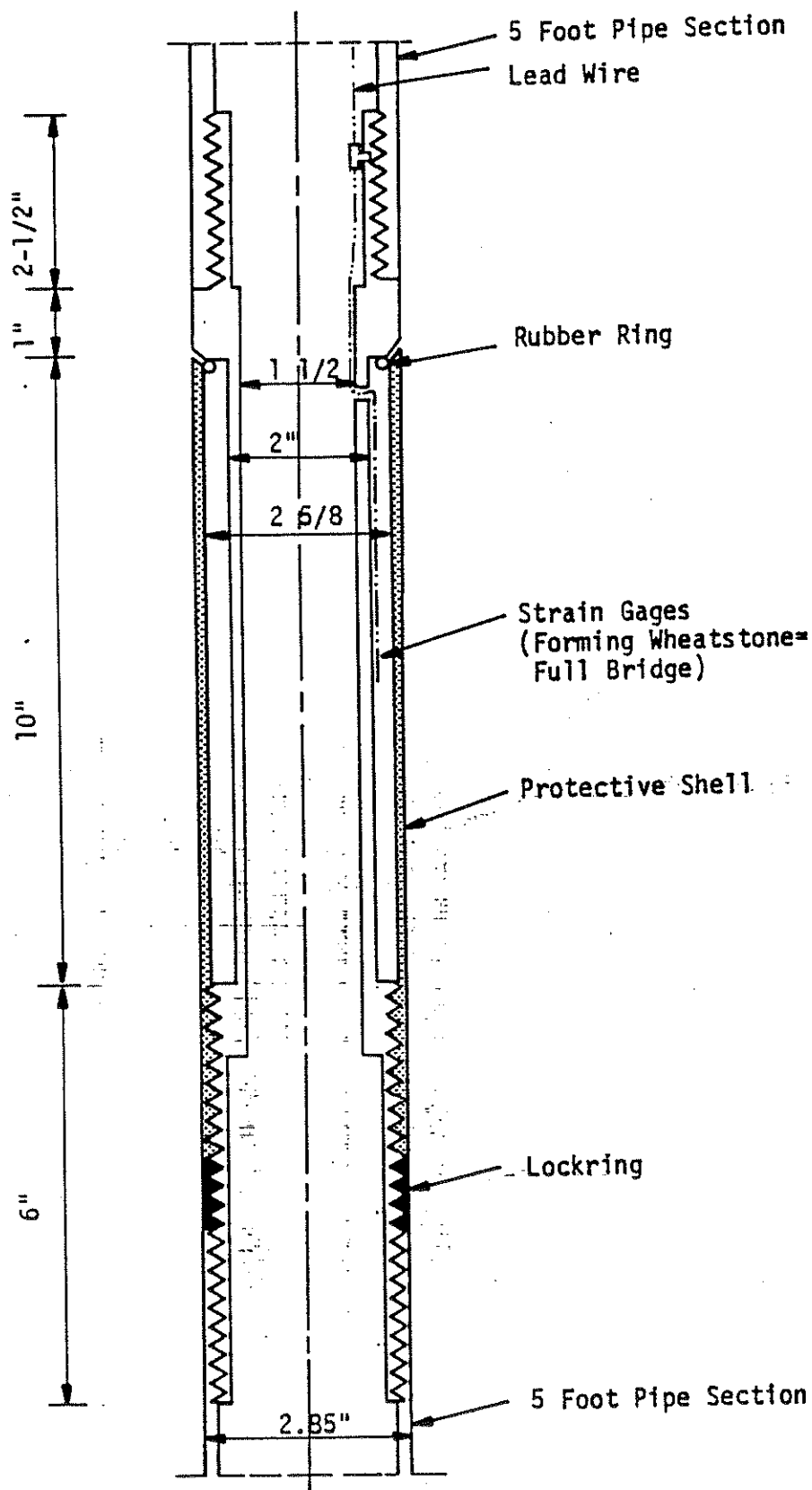


Figure 2.10

Design of an Intermediate Reduced Scale Pile Transducer

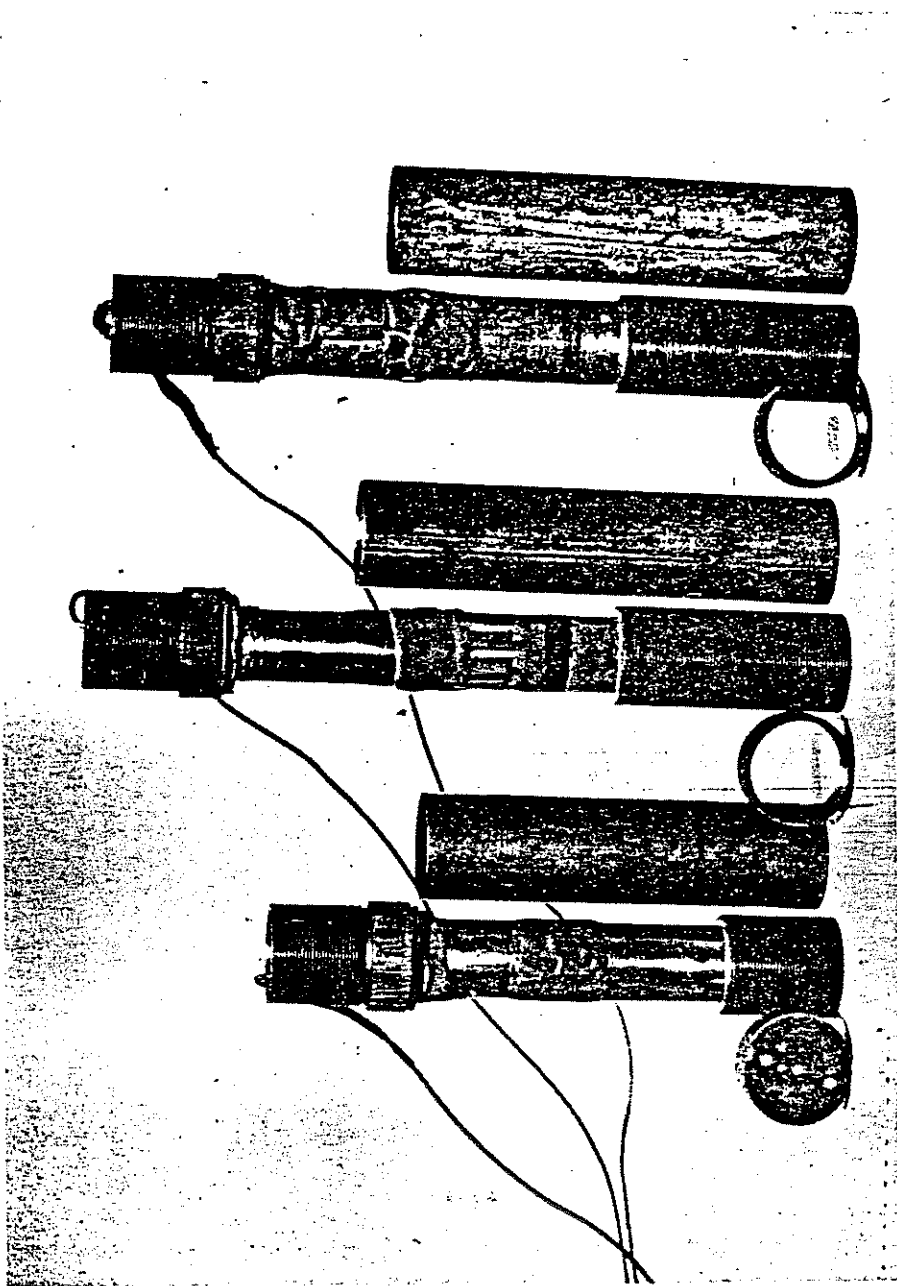


Figure 2.11

Reduced Scale Pile Transducers for Use Below Grade

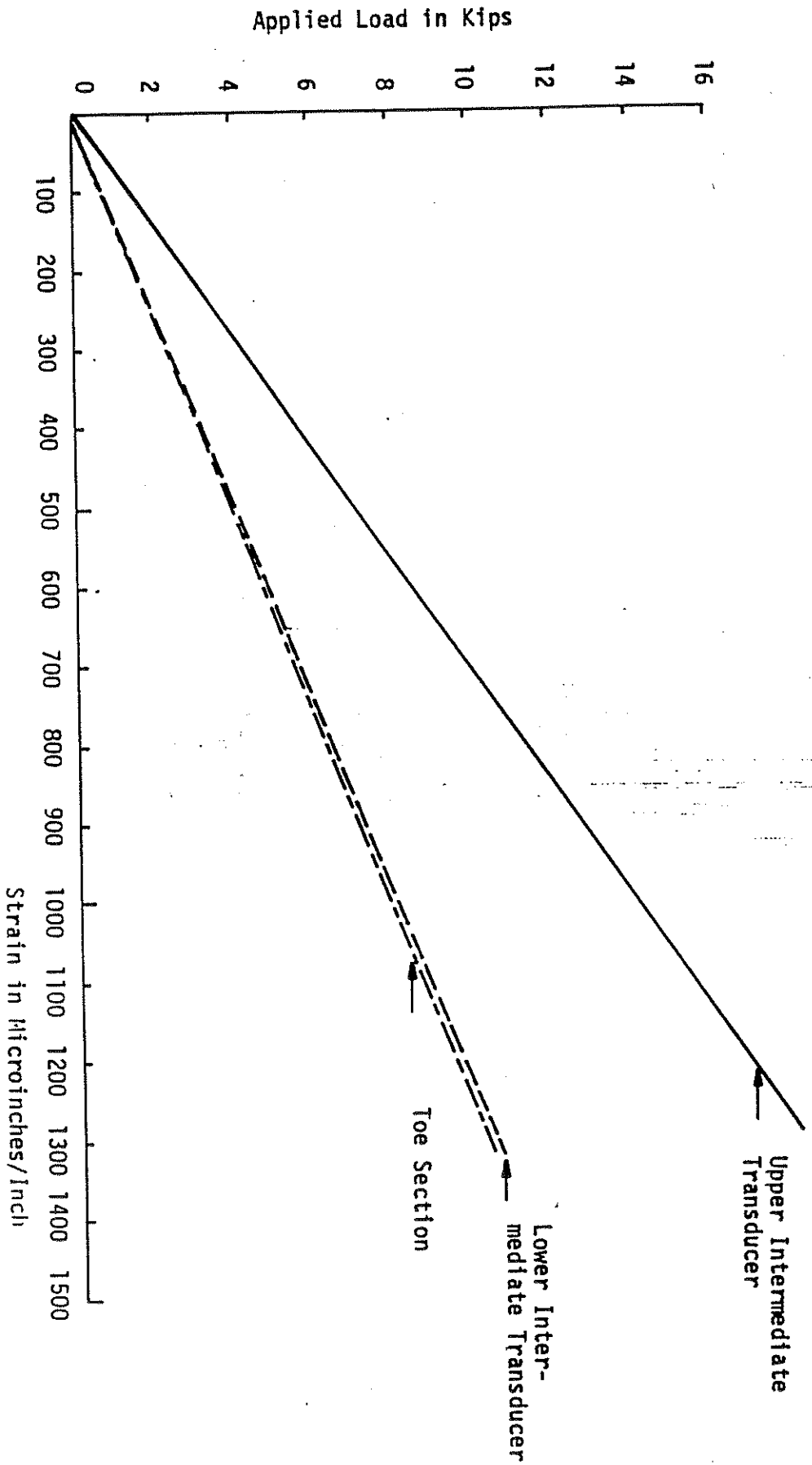


Figure 2.12  
Calibrations for Model Pile Transducers

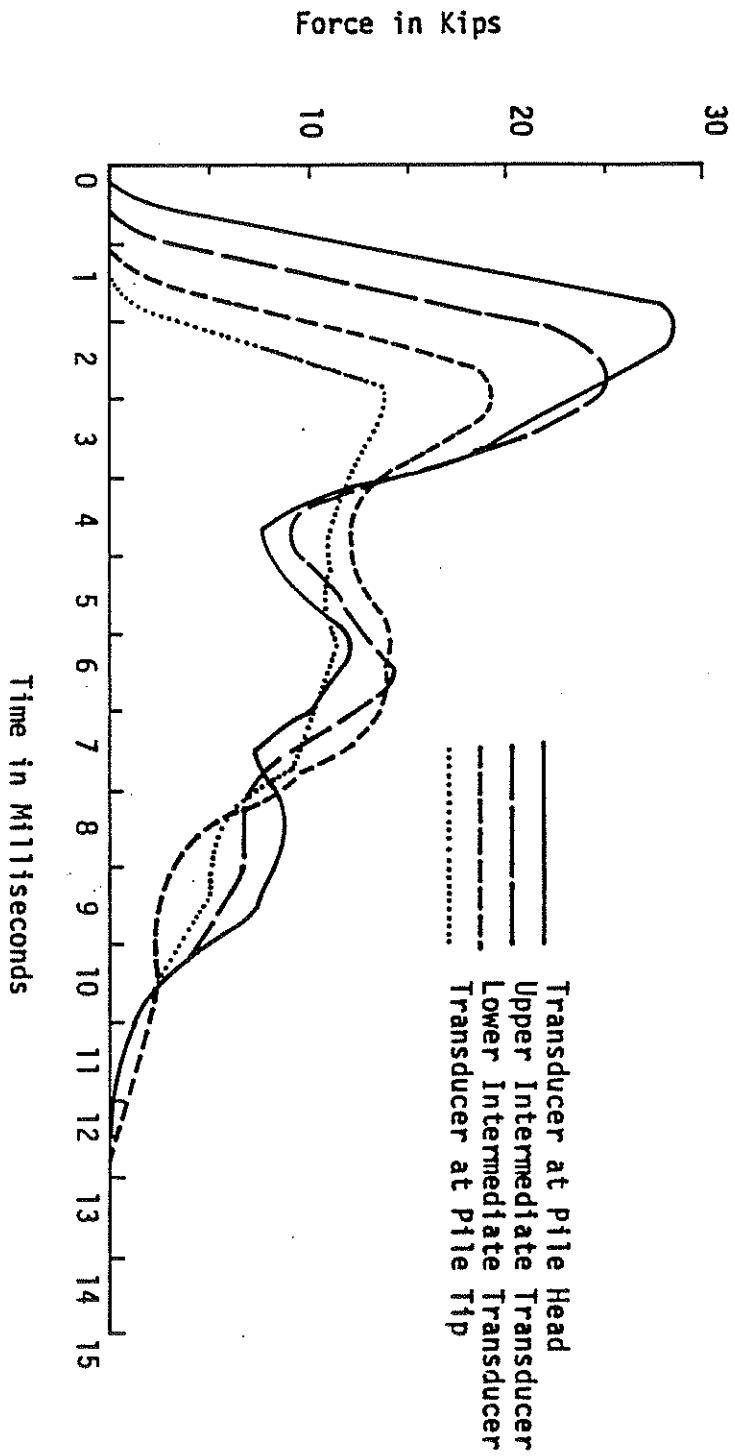


Figure 2.13 Force Results at Four Stations on Model Pile



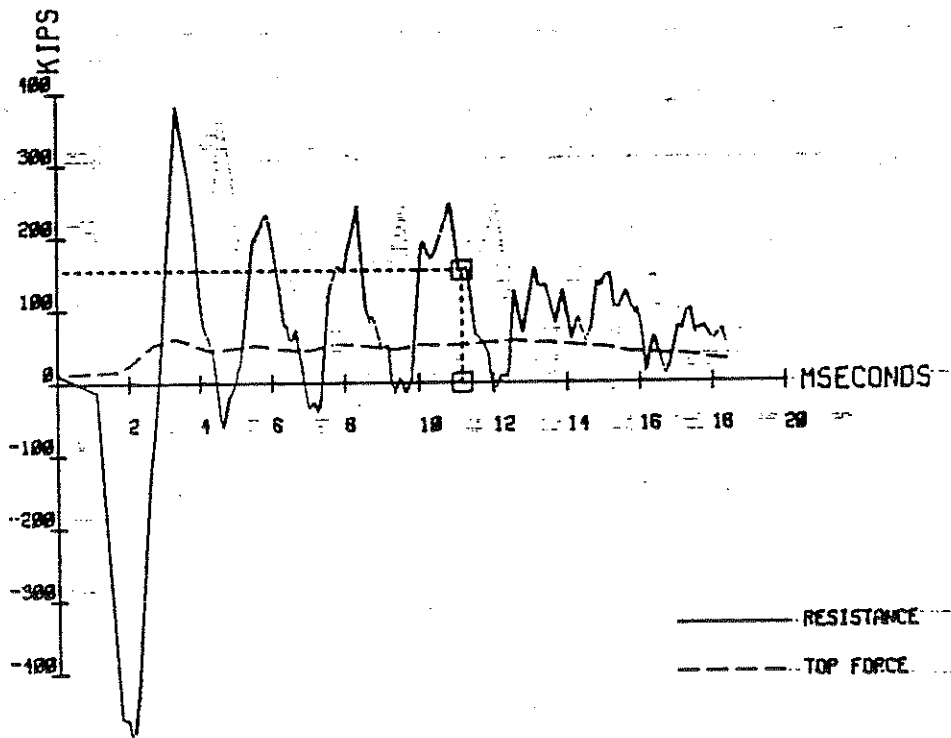
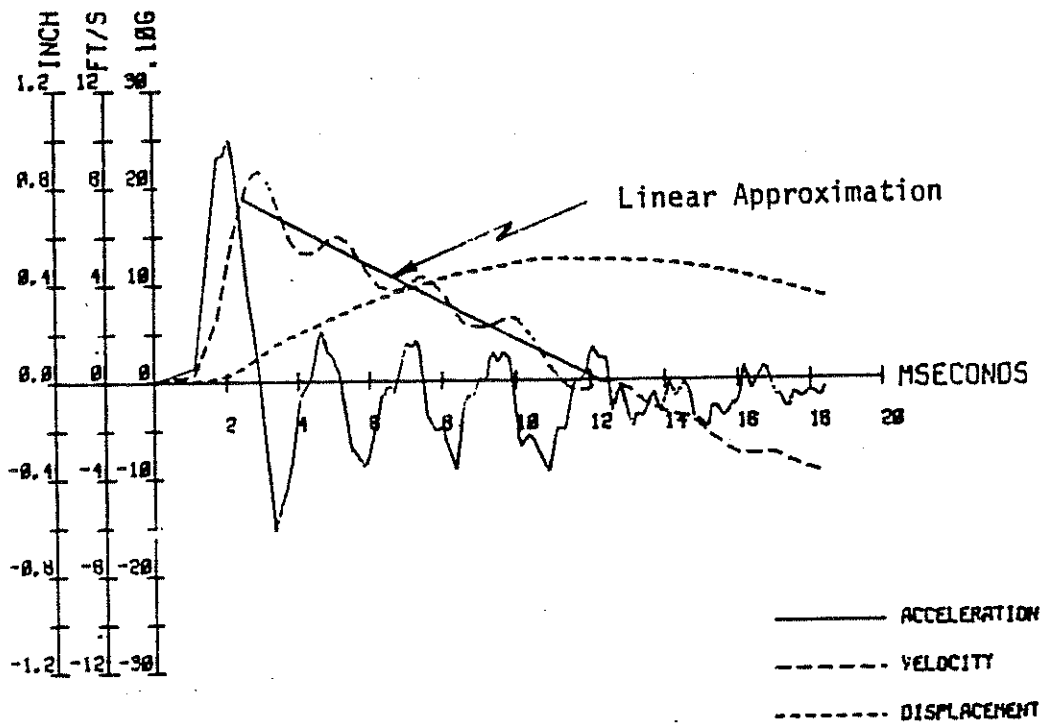


Figure 3.1  
Typical Full Scale Pile Results with  
Indicated Linear Velocity Descent

Surface Elevation at 675.0 Feet

Sample No.	Description	Physical Characteristics in %					
		Agg.	C.S.	F.S.	Silt	Clay	W.C.
10	Brown Silty Gravelly Sand	16	1	58	16	9	17
9	Brown Gravel	81	5	10	2	2	9
8	Brown Gravelly Sand	42	2	44	5	7	9
7	Brown Sand	13	10	67	0	10	17
6	Brown Sand	8	9	75	4	4	12
5	Brown Sandy Gravel	52	24	14	5	5	9
4	Brown Sandy Gravel	48	26	16	5	5	6
3	Brown Sandy Gravel	V	I	S	U	A	L
2	Brown Sandy Gravel	V	I	S	U	A	L
1	Brown Silty Gravelly Sand	33	23	29	7	8	8

Figure 3.2 Soil Characteristics at West 14th and Abbey Road

Surface Elevation at 627.0 Feet

Sample No.	Physical Characteristics in %					
	Agg.	C.S.	F.F.	Silt	Clay	L.C.
6	0	0	1	59	40	27
5	0	0	0	33	67	31
4	0	0	0	36	64	29
3	0	0	1	47	52	25
2	0	1	1	52	46	28
1	0	0	2	51	47	26

Description

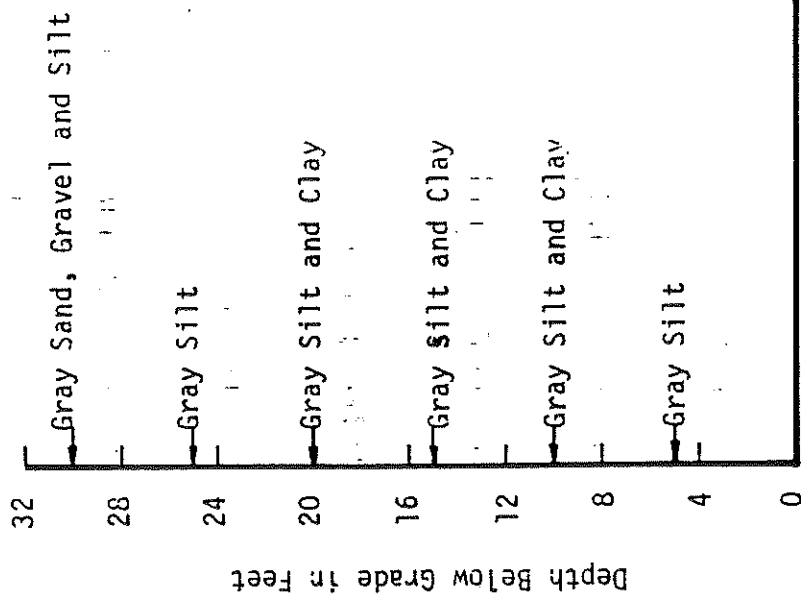


Figure 3.2 Soil Characteristics at Jennings Road Site

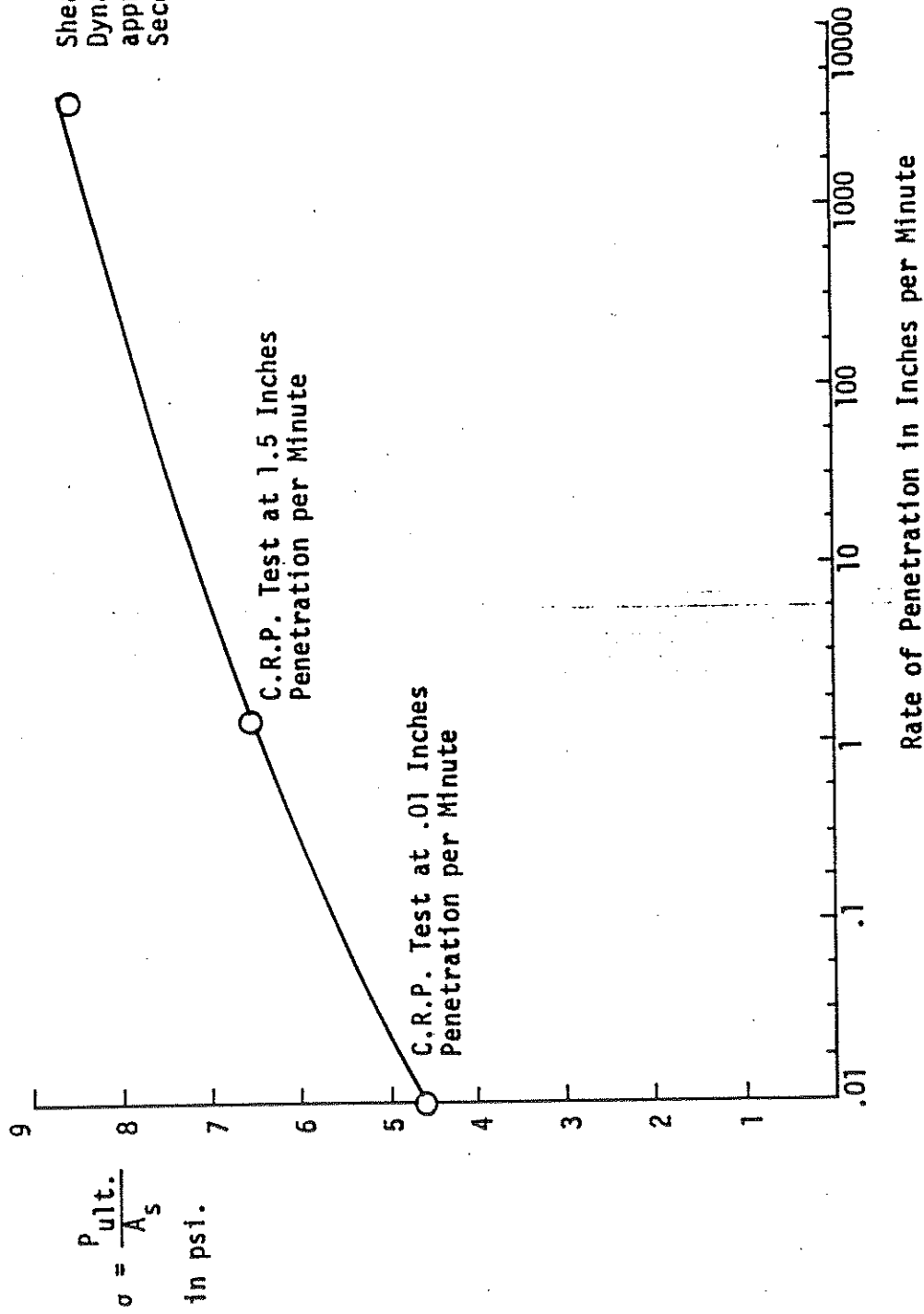


Figure 3.4 Variation of Shear Resistance with Rate of Penetration

Surface Elevation at 1045.0 Feet

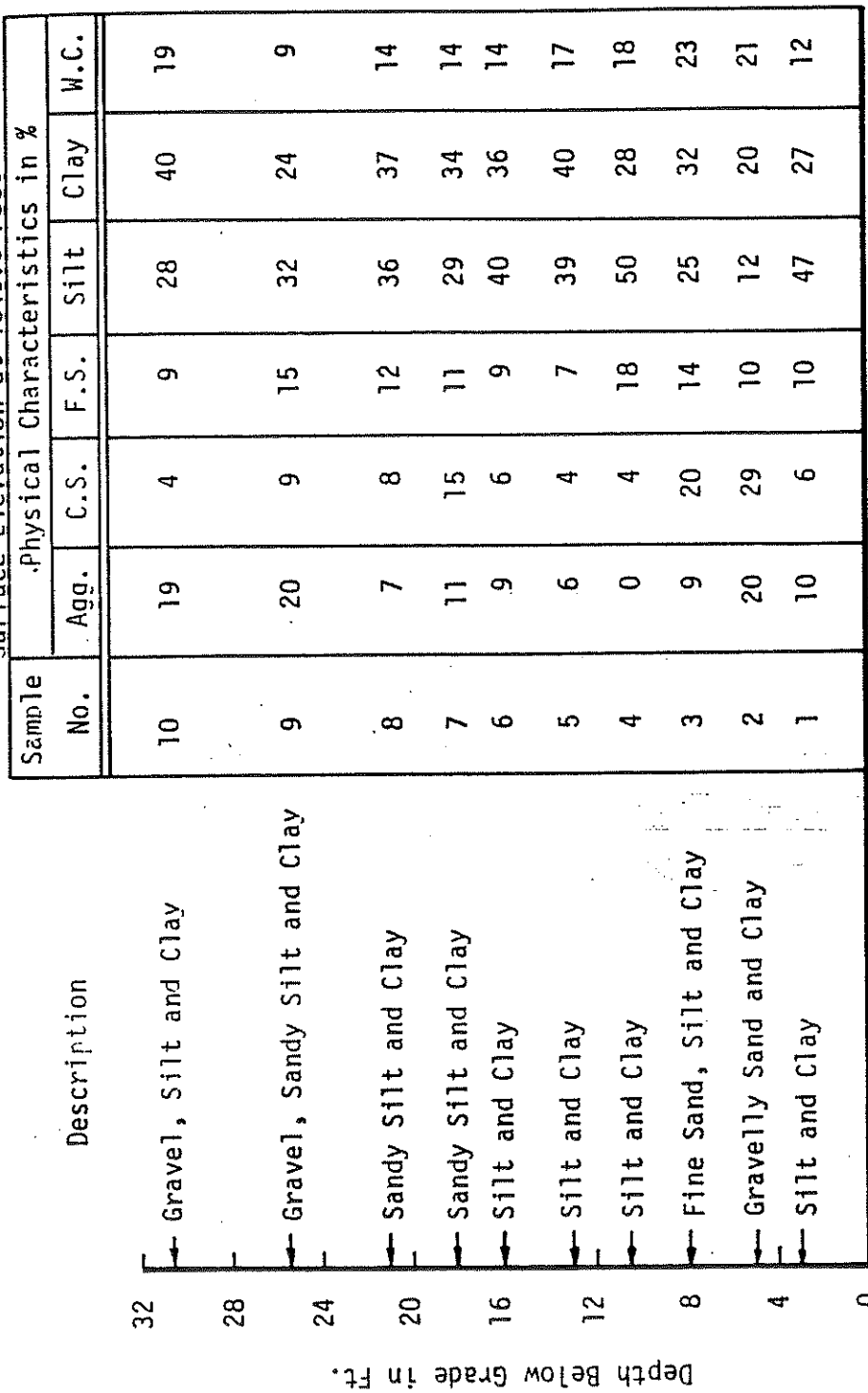


Figure 3.5 Soil Characteristics at Randall Yard Site

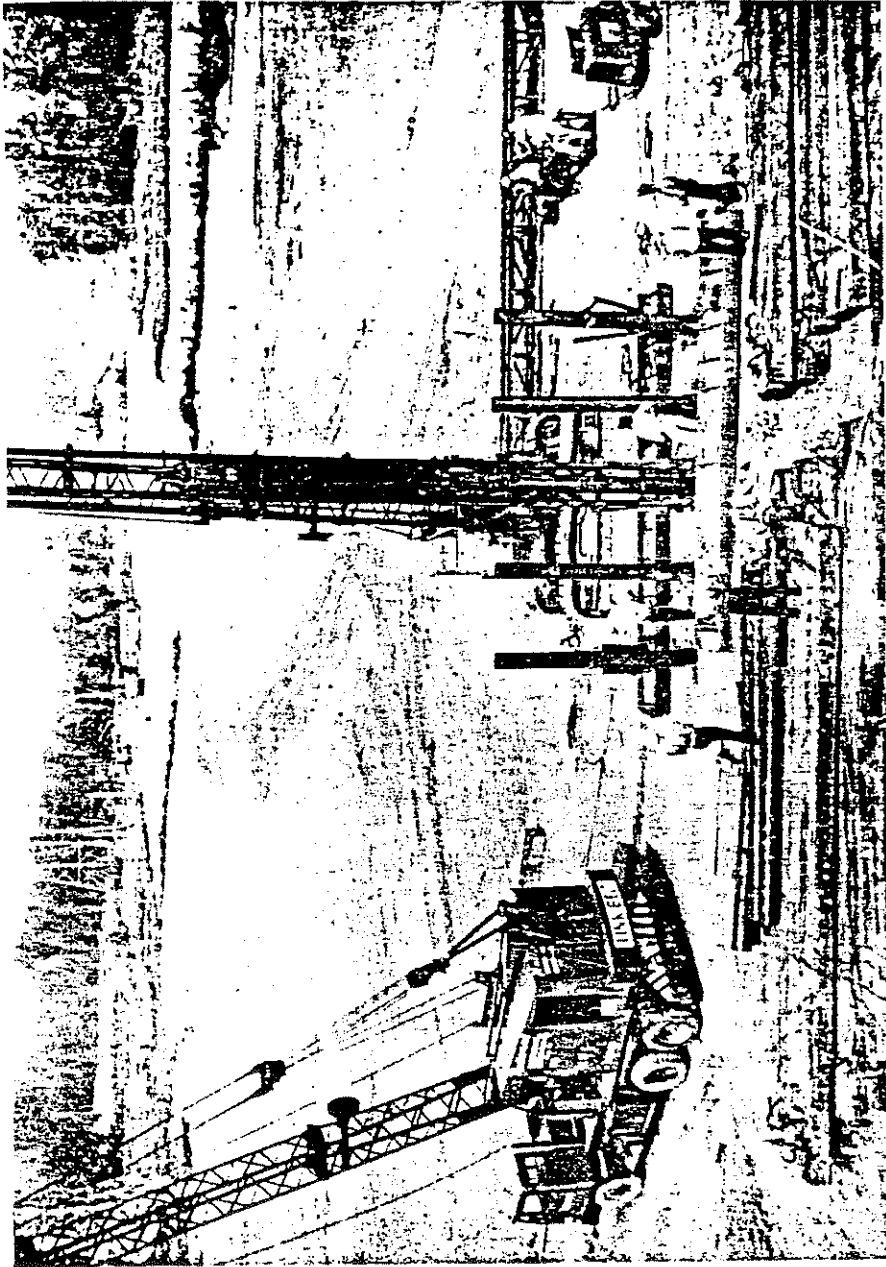


Figure 3.6

Driving Operation On Full Scale Pile in Akron

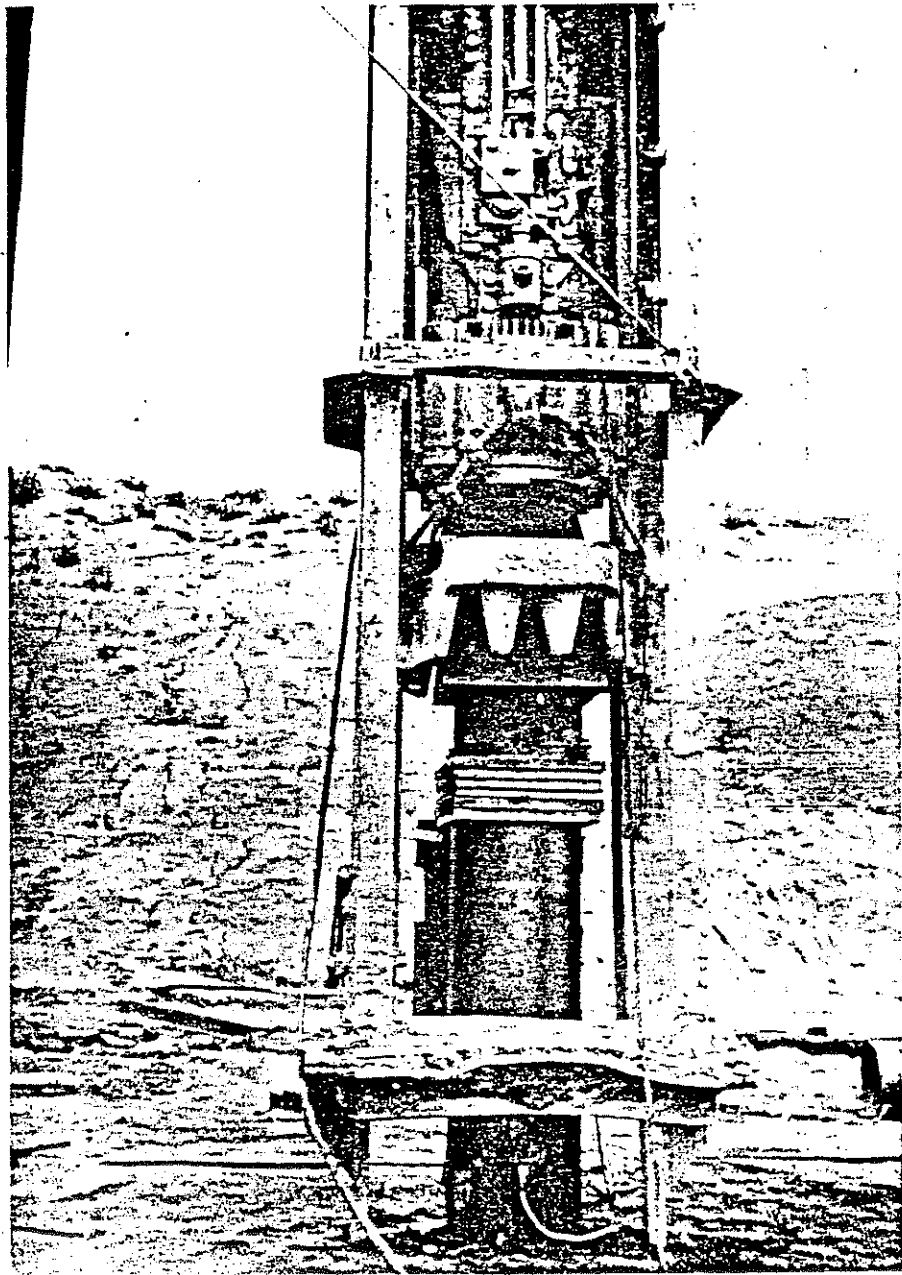


Figure 3.7

Accelerometer, Force Transducer, Cushion, and Driving Head

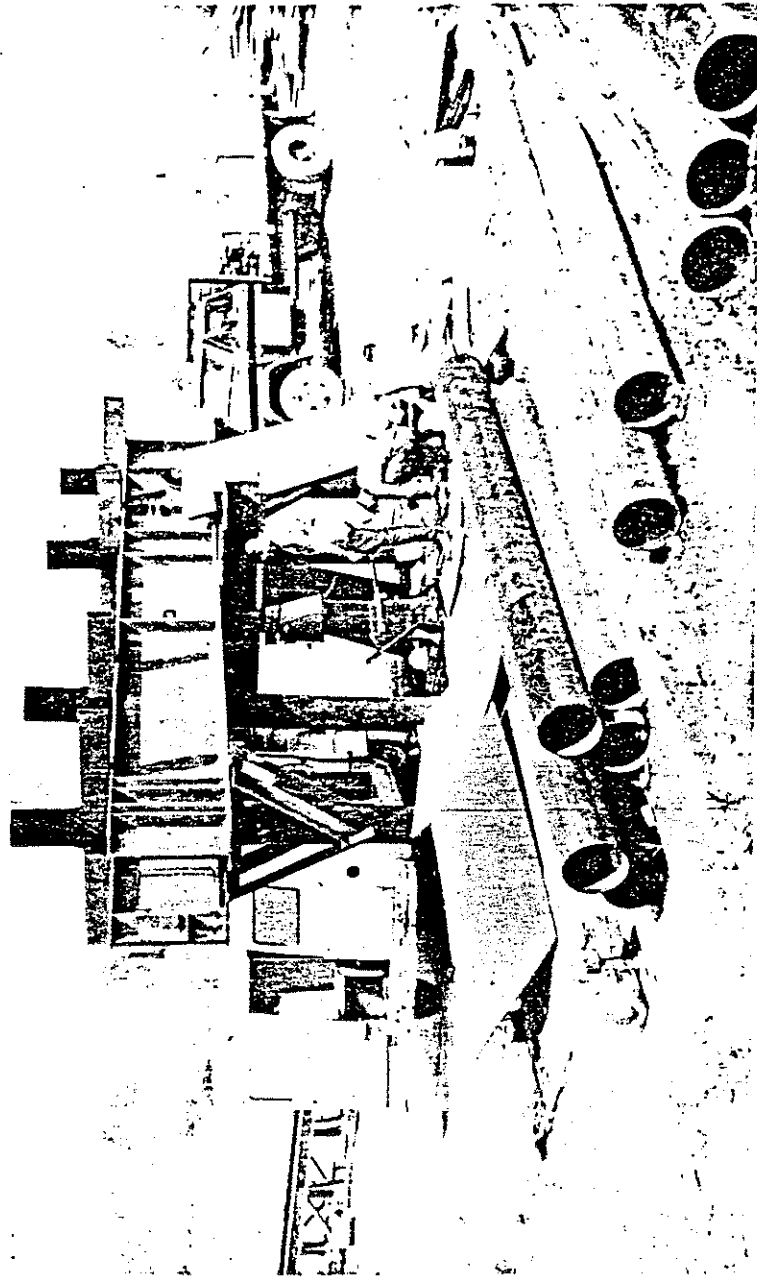


Figure 3.8

Assembled Load Test Setup on Full Scale Pile in Akron



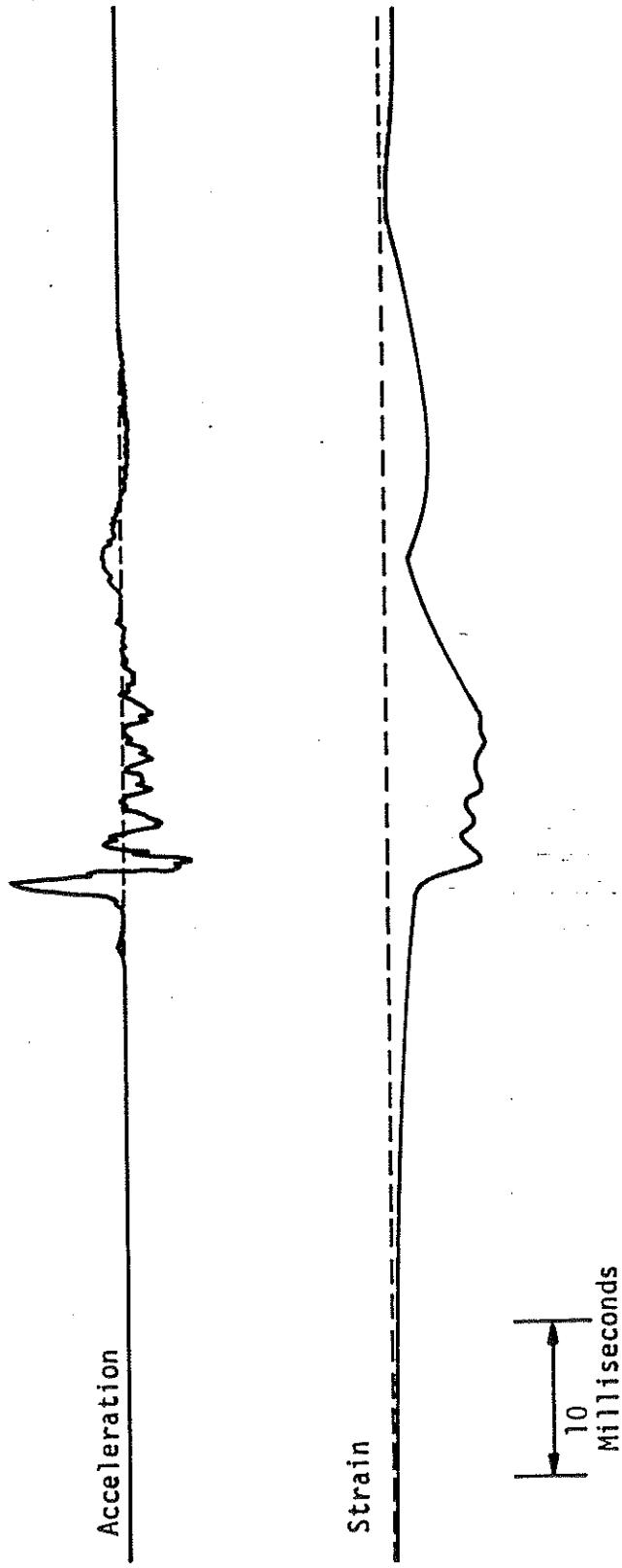


Figure 3.9

Typical Record of a Diesel Hammer Blow

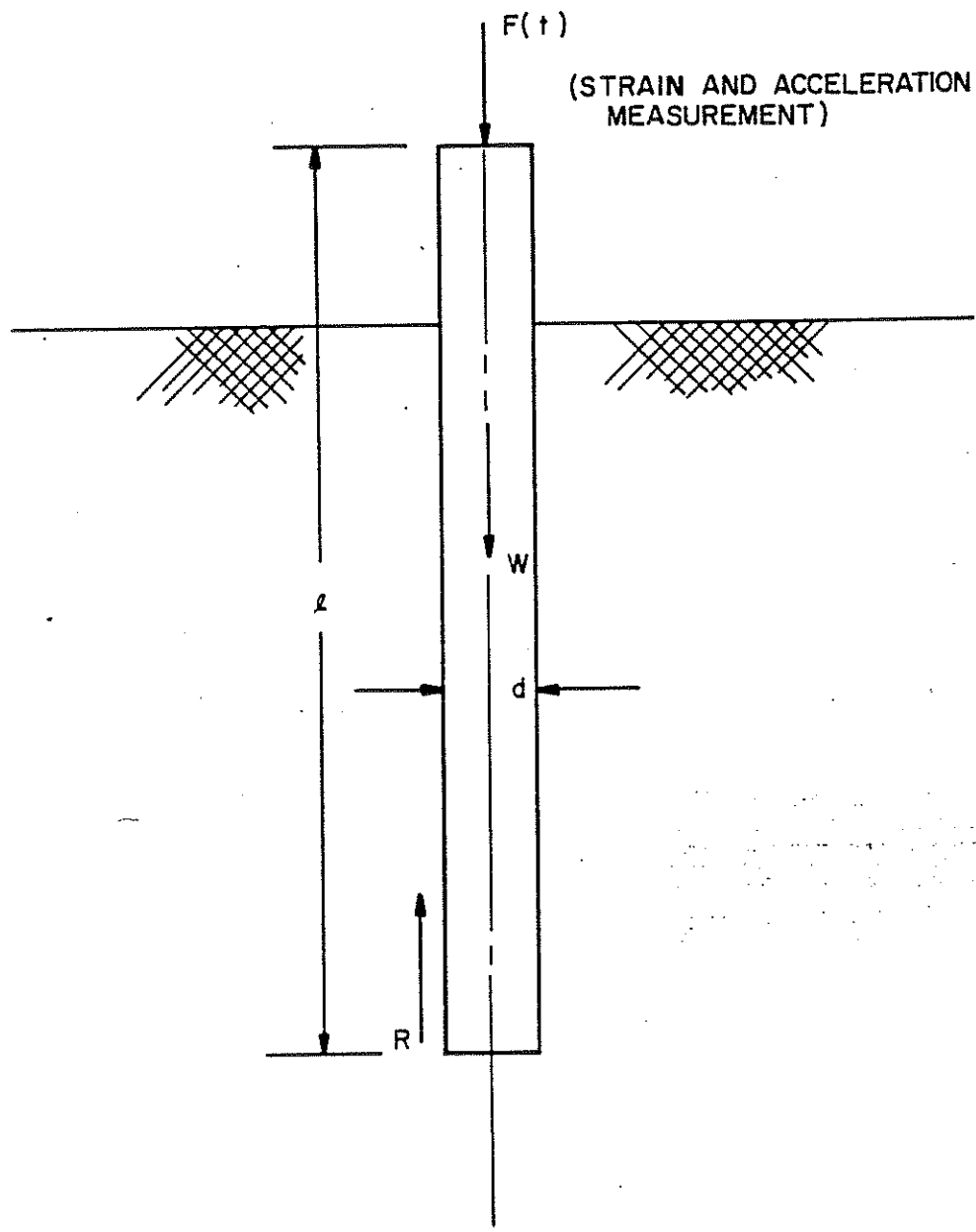


FIGURE 4.1  
SIMPLIFIED ANALYTICAL MODEL

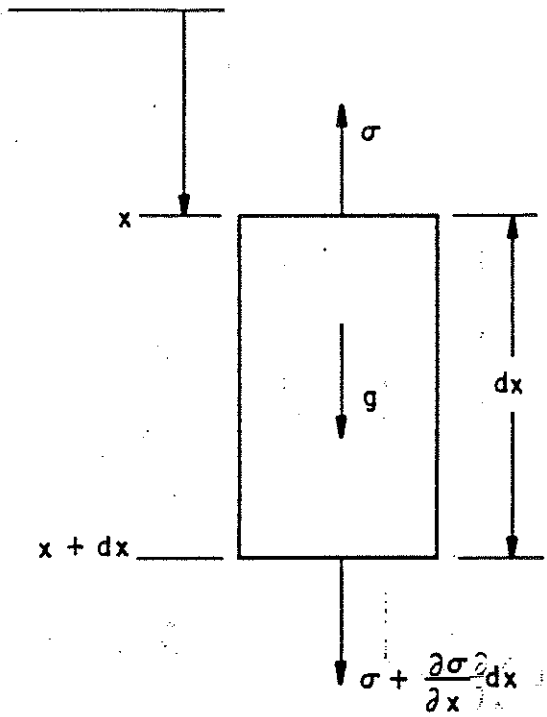


Figure 4.2

Stresses Acting on Differential Element

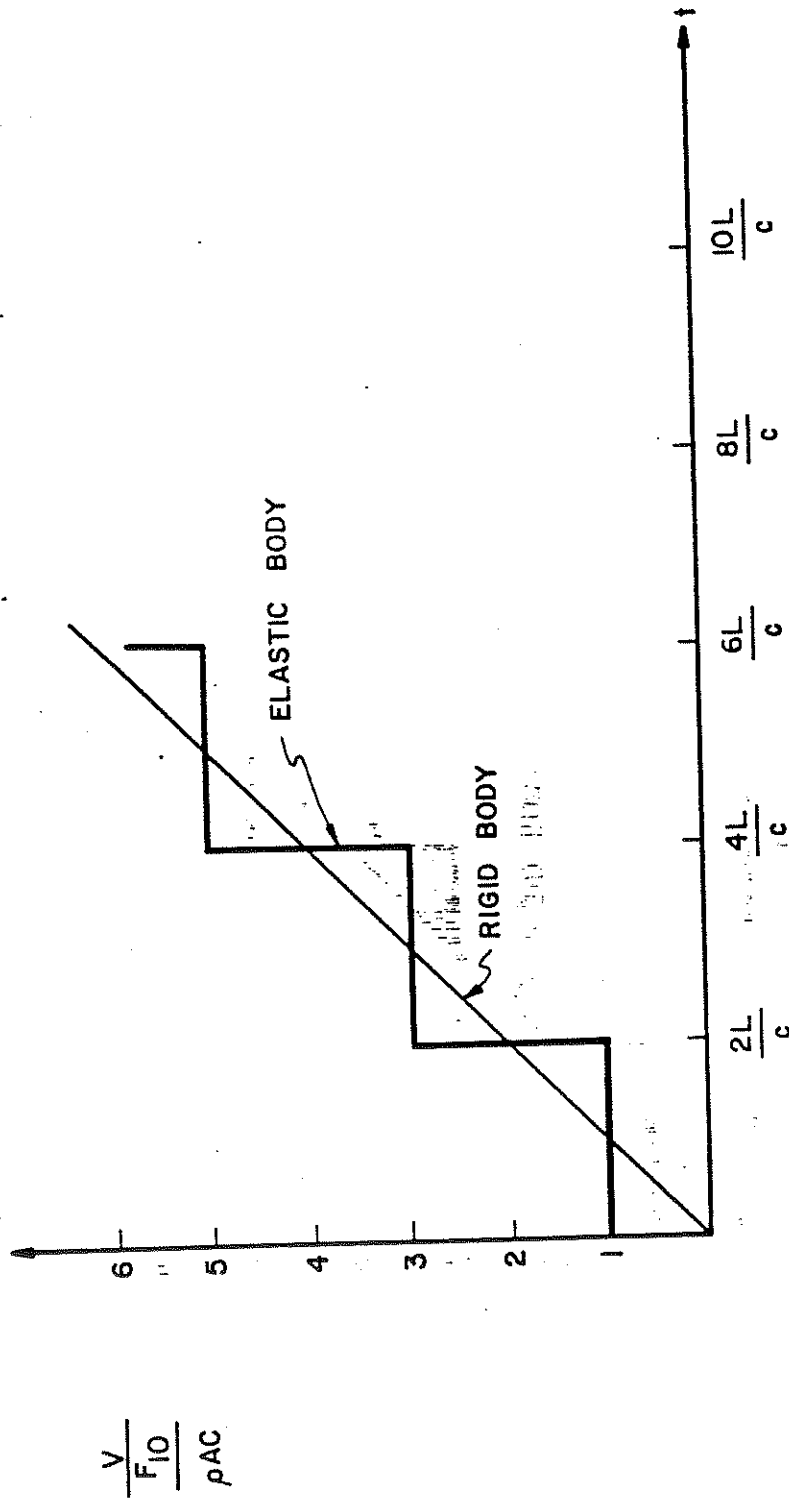


Figure 4.3  
Velocity under a Step Input Force at the Pile Top (Gravity Effect Omitted)

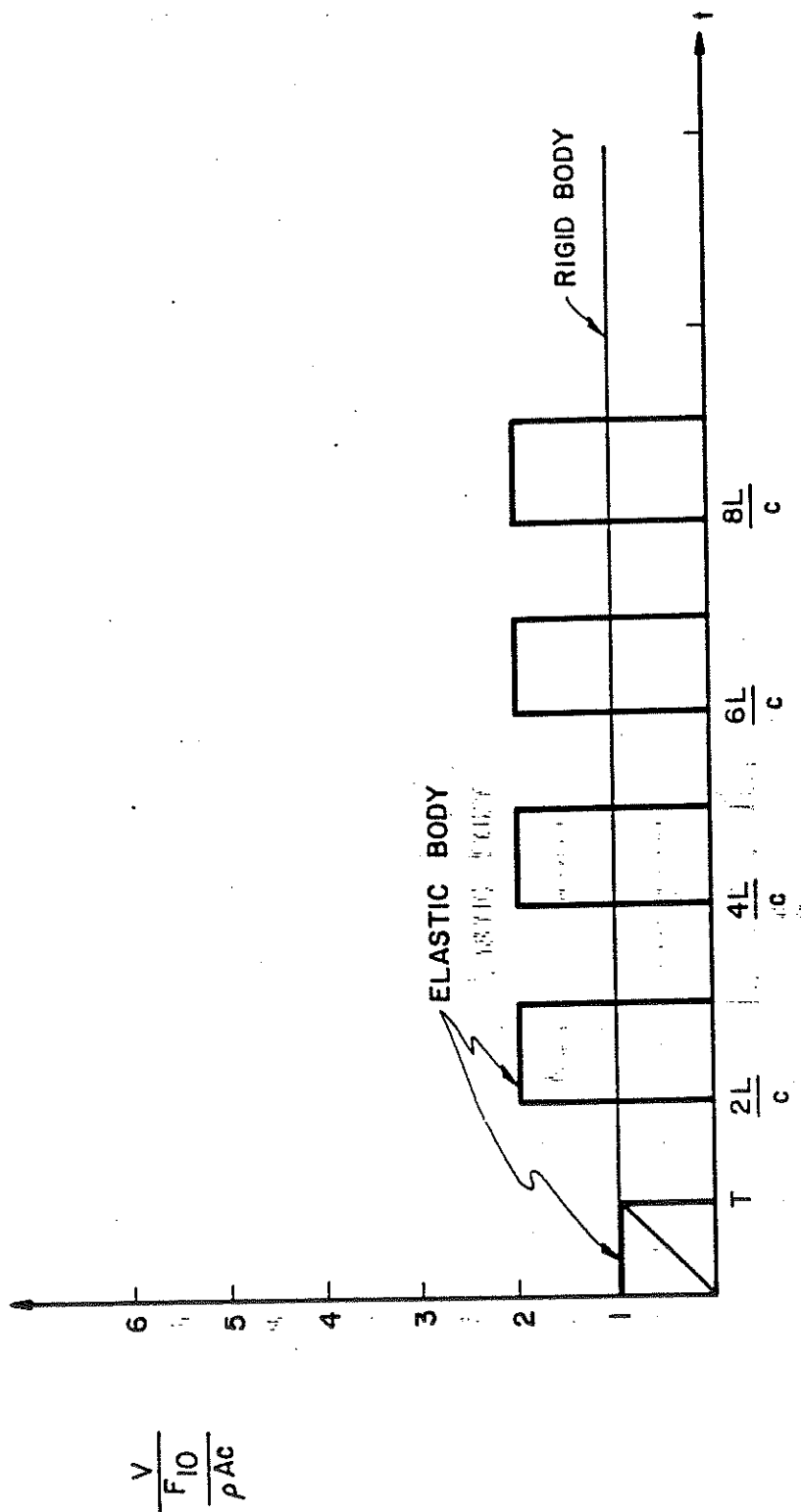


Figure 4.4

Velocity under a Top Force Pulse of Duration  $T$  (Gravity Effect Omitted)

$$\frac{x + \xi}{\frac{F_{10}}{\rho A c}}$$

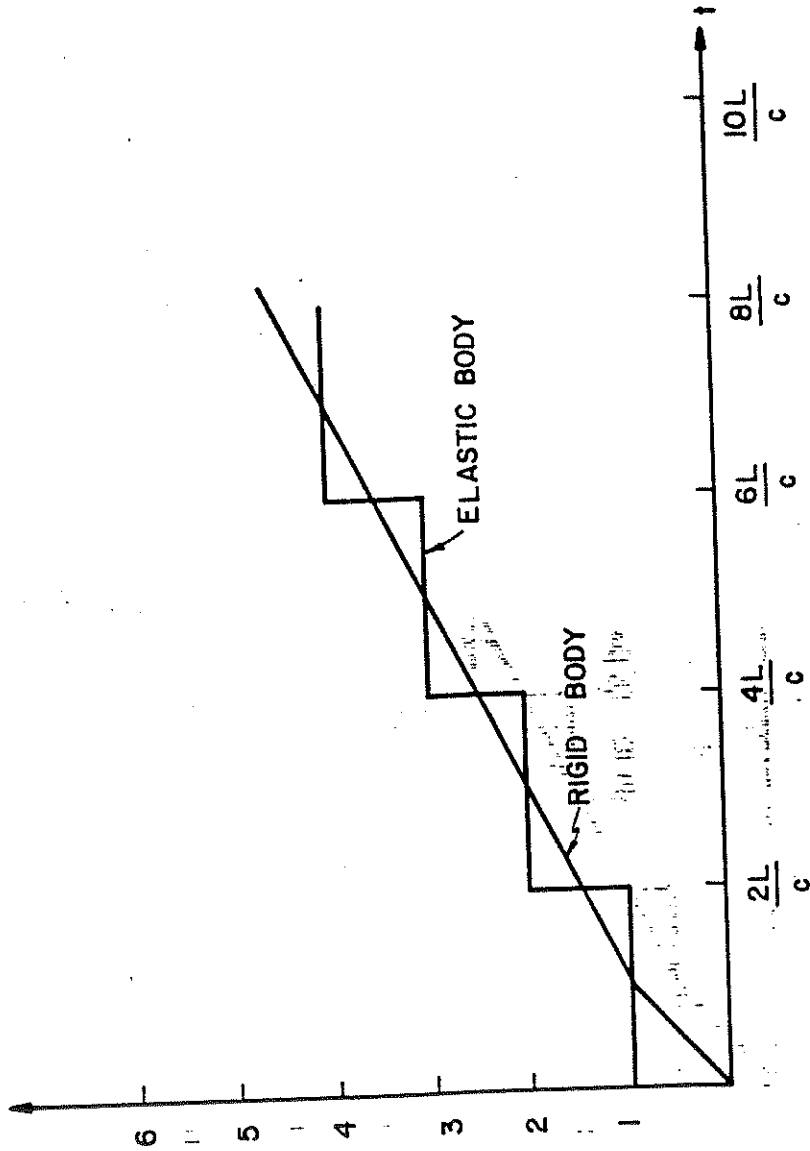


Figure 4.5

Displacement at Top of Pile Under Dirac  
Impulse Blows at Top and Bottom of Pile

$$(F_{20} = \frac{1}{2} F_{10})$$

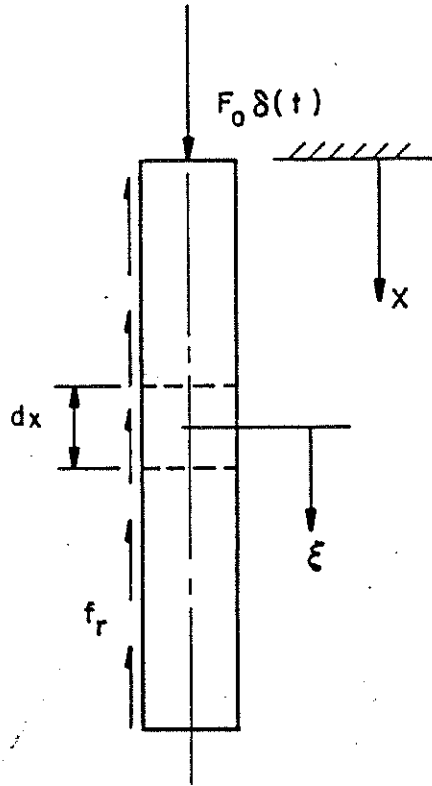


Figure 4.6  
Idealized Pile Model

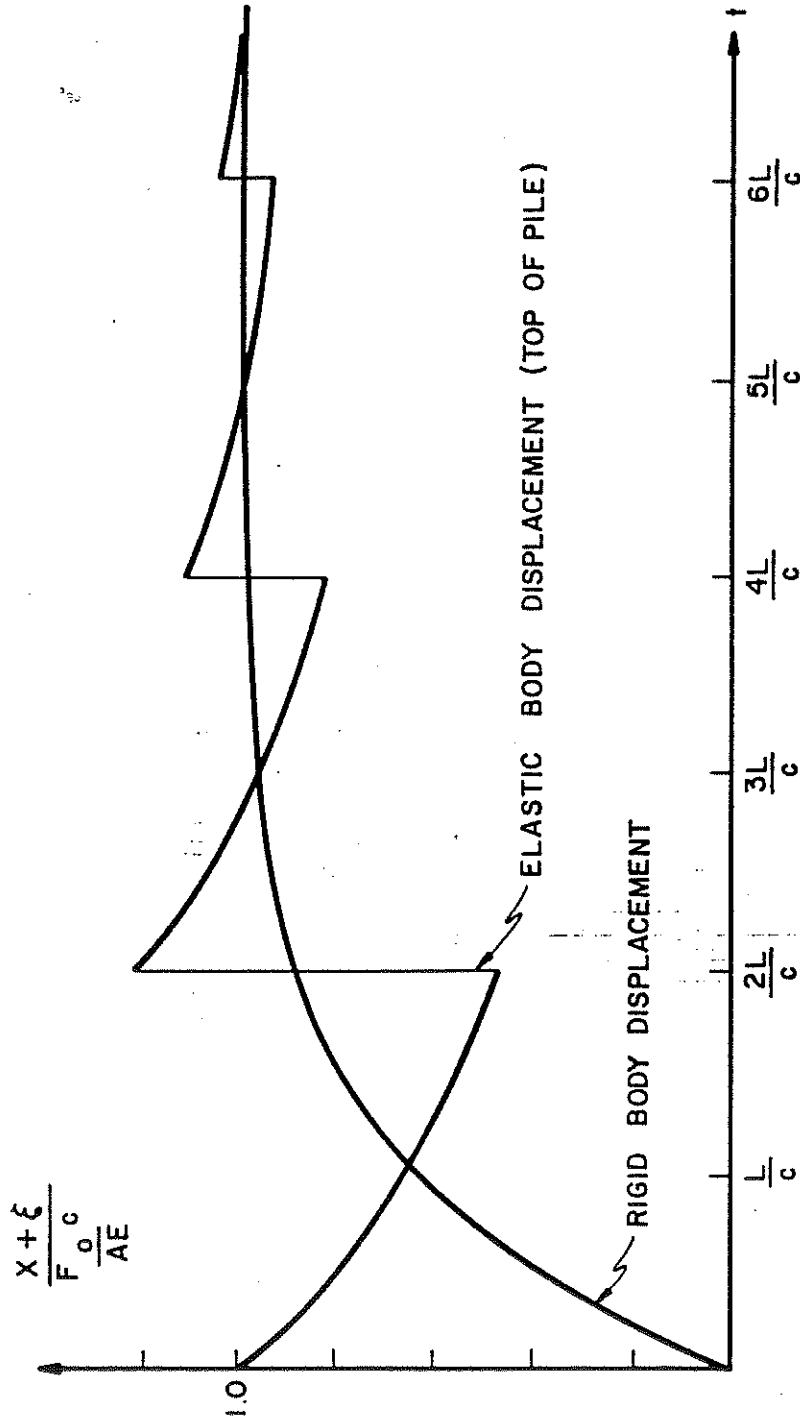


Figure 4.7

Pile Displacement Responses to Instantaneous Pulse



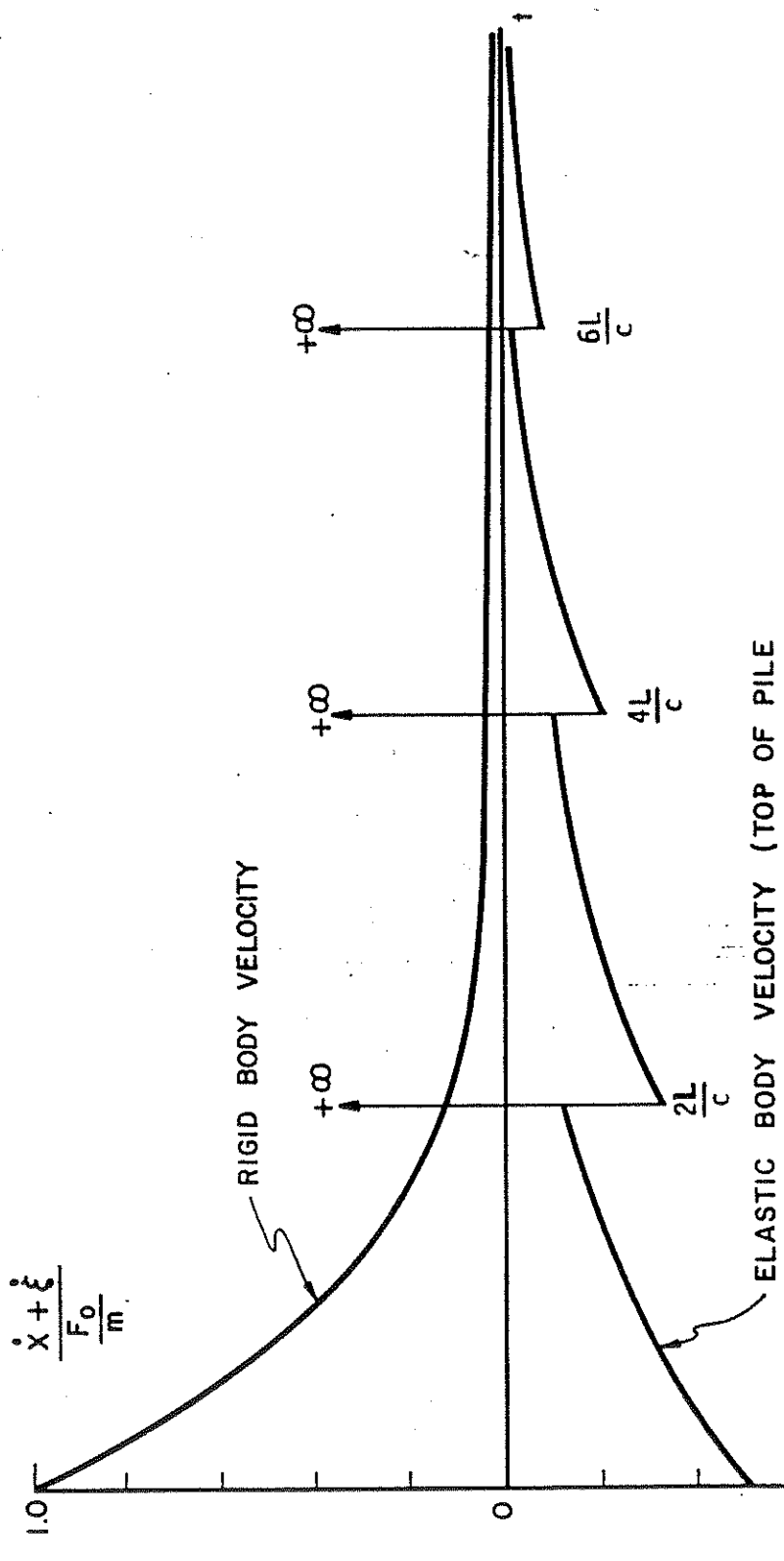


Figure 4. 8

Pile Velocity Responses  
to Instantaneous Pulse

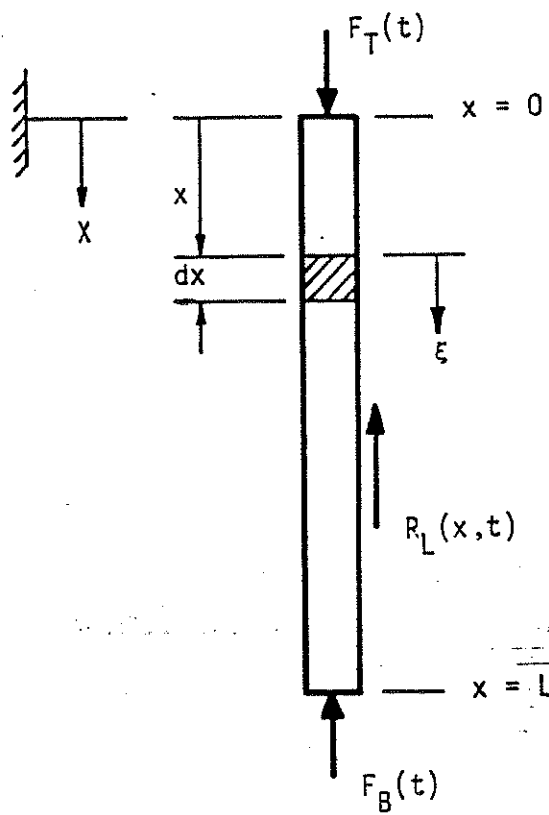


Figure 4.9 Theoretical Model of Pile with Active and Passive Forces

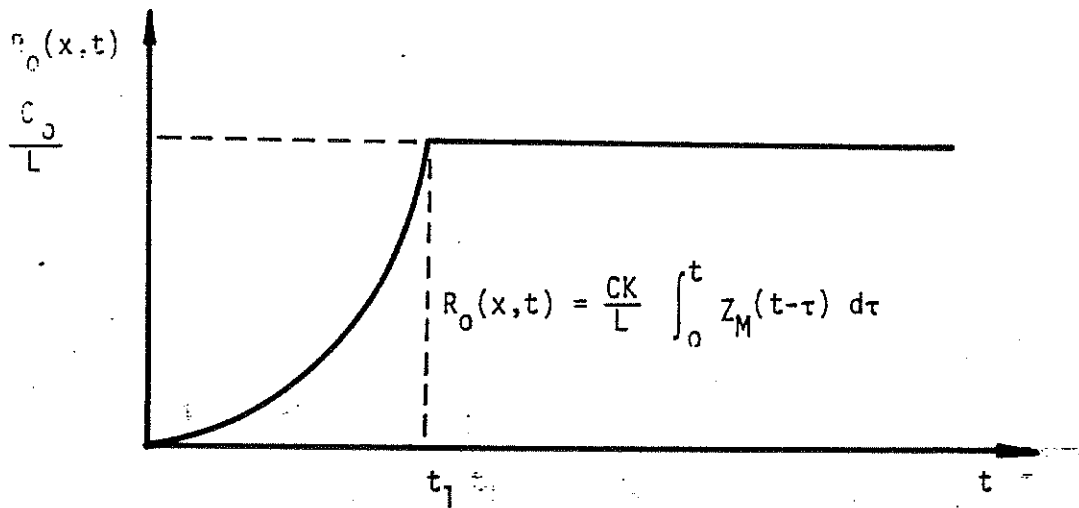


Figure 4.10 - Resistance Law Assumed for the Soil-Pile Interaction

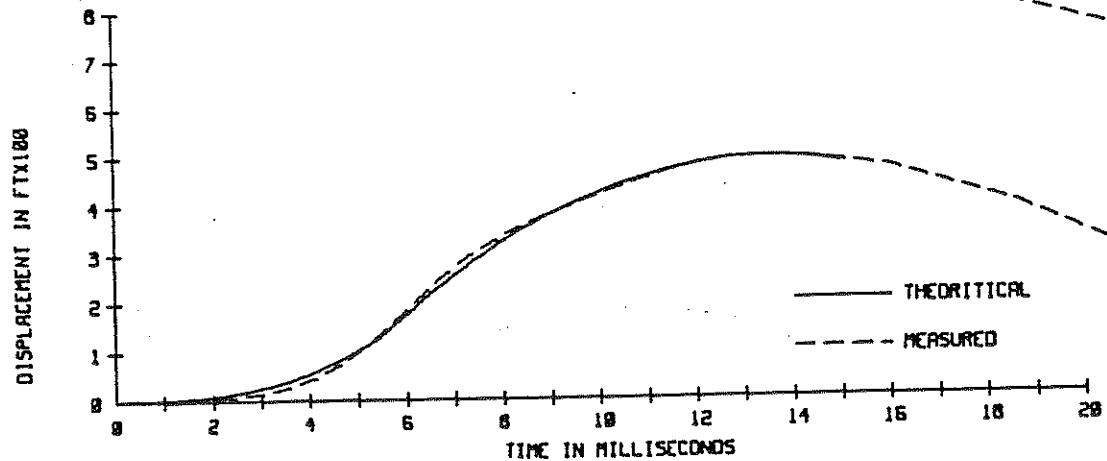
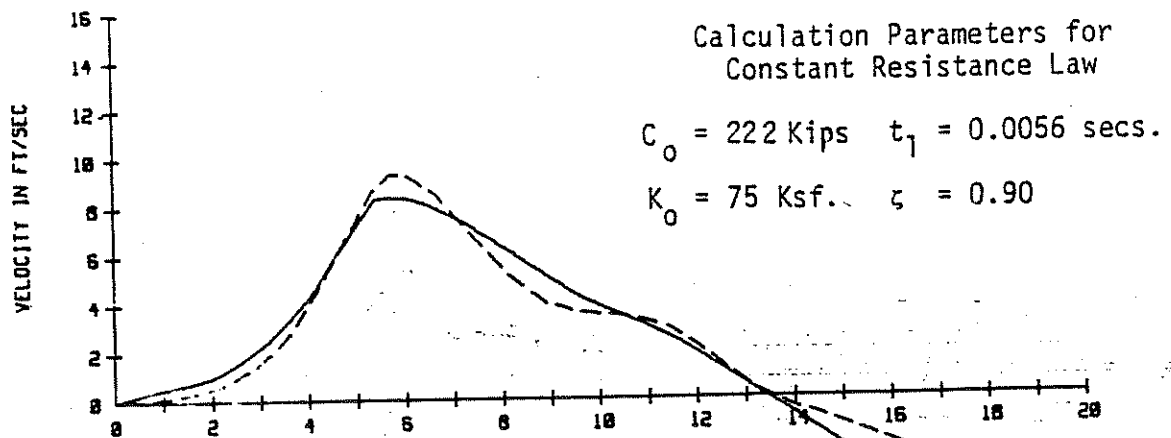
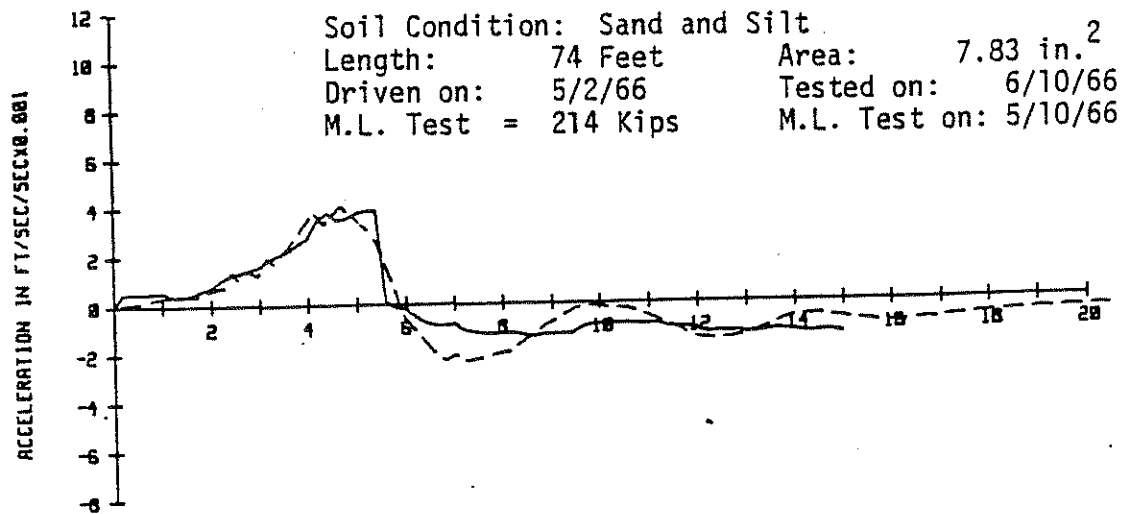


Figure 4.11 Matching Results of Full-Scale Pile 103 of Pier No. 2,  
 Blow No. 1A

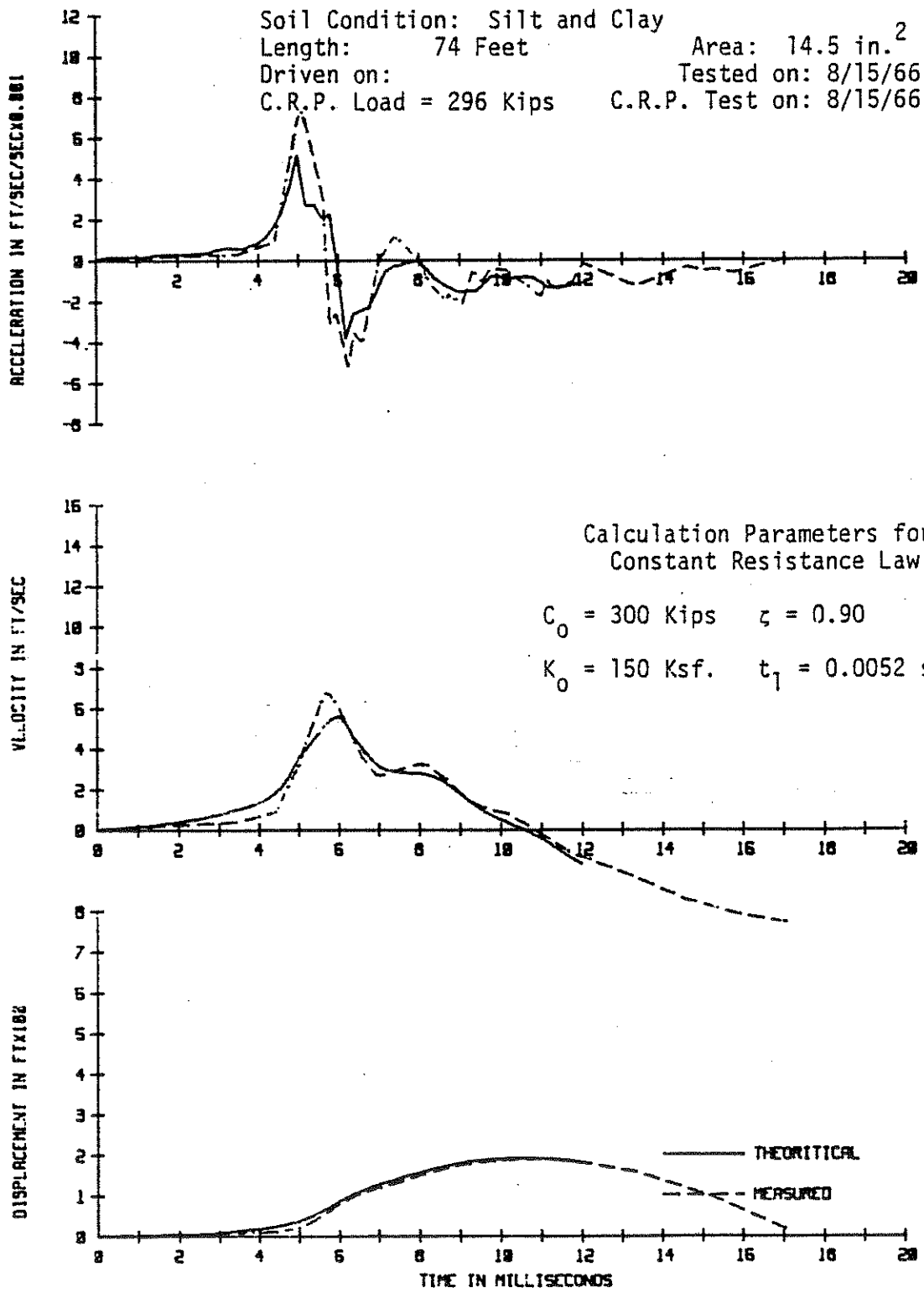


Figure 4.12 Matching Results of Full-Scale Pile 692 Youngstown, Ohio; Last Blow

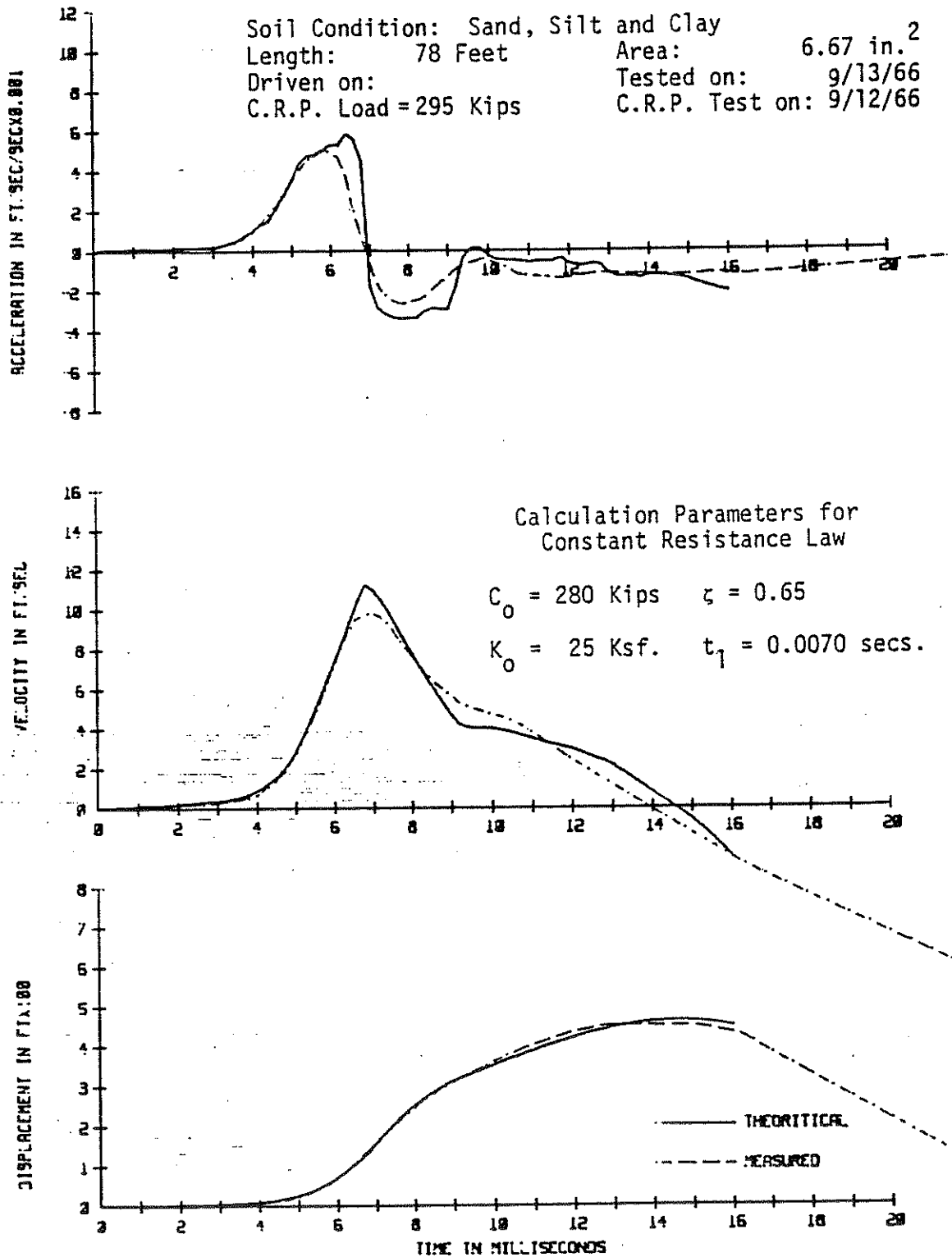


Figure 4.13 Matching Results of Full-Scale Pile 506 in Uhrichville, Ohio; Blow No. 6A

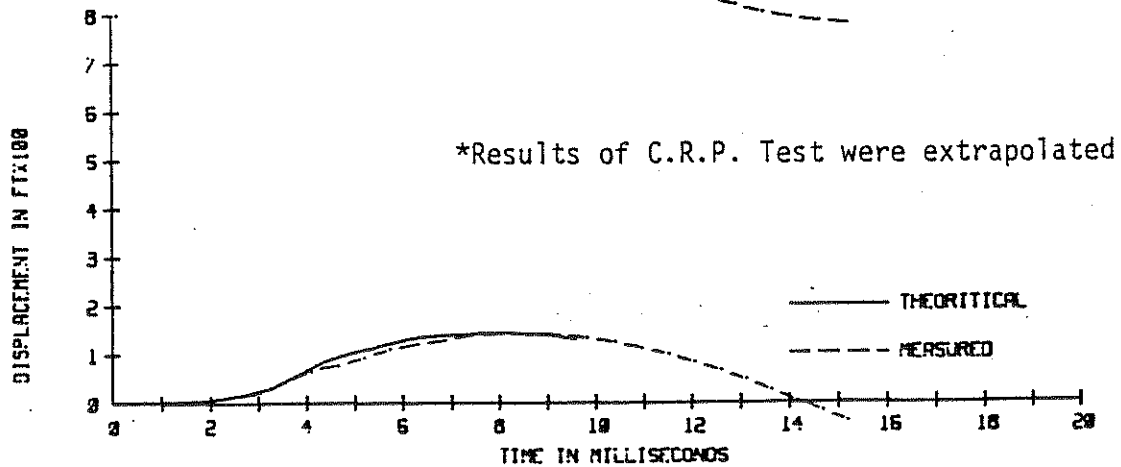
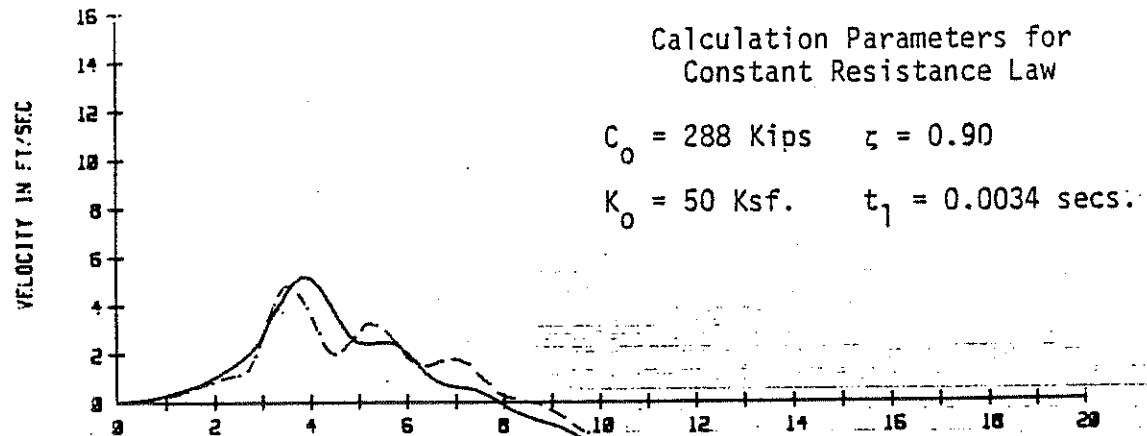
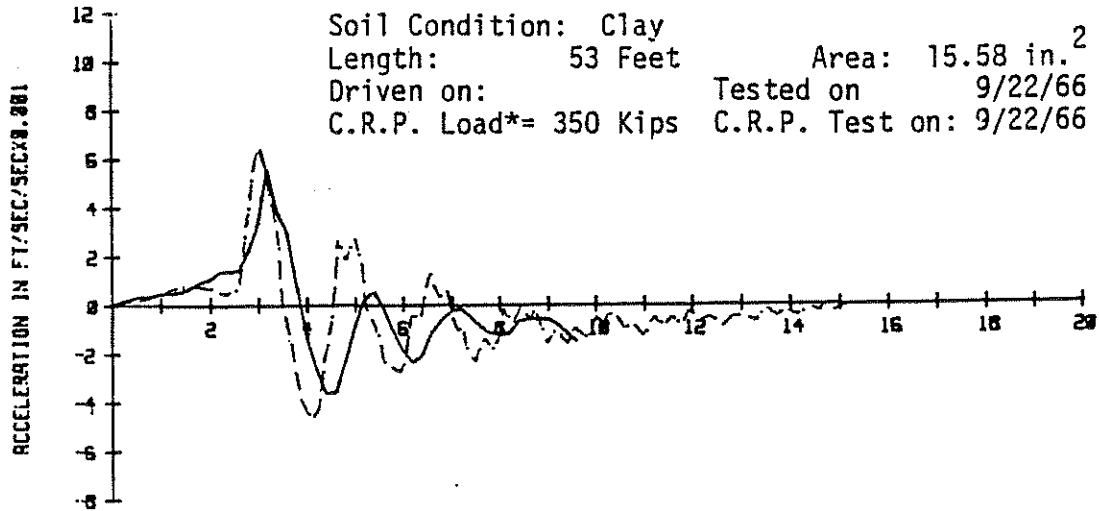


Figure 4.14 Matching Results of Full-Scale Pile in Toledo, Ohio;  
 Blow No. 23A

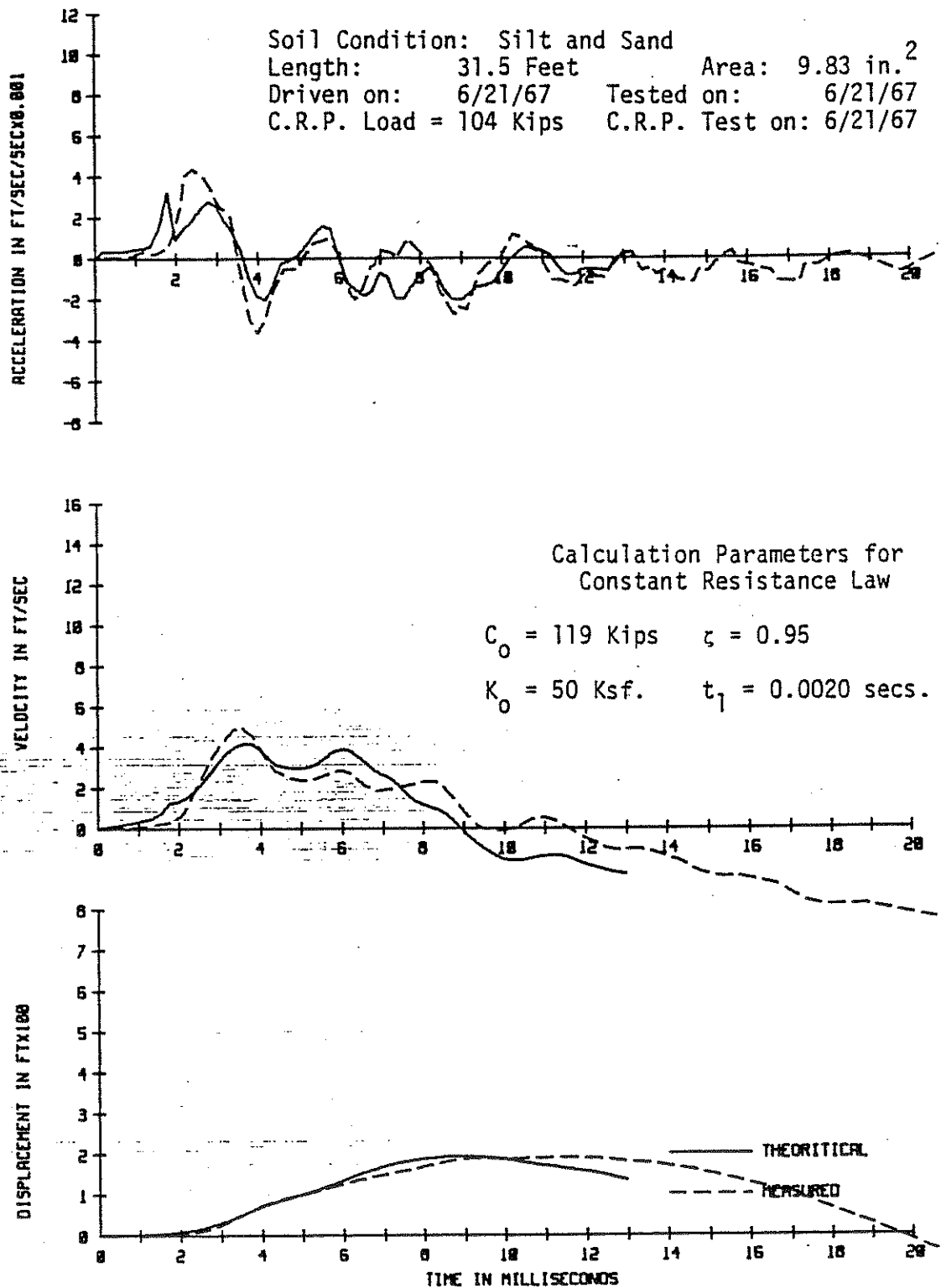


Figure 4.15 Matching Results of Full-Scale Pile F-30 in Akron, Ohio; Blow No. 13



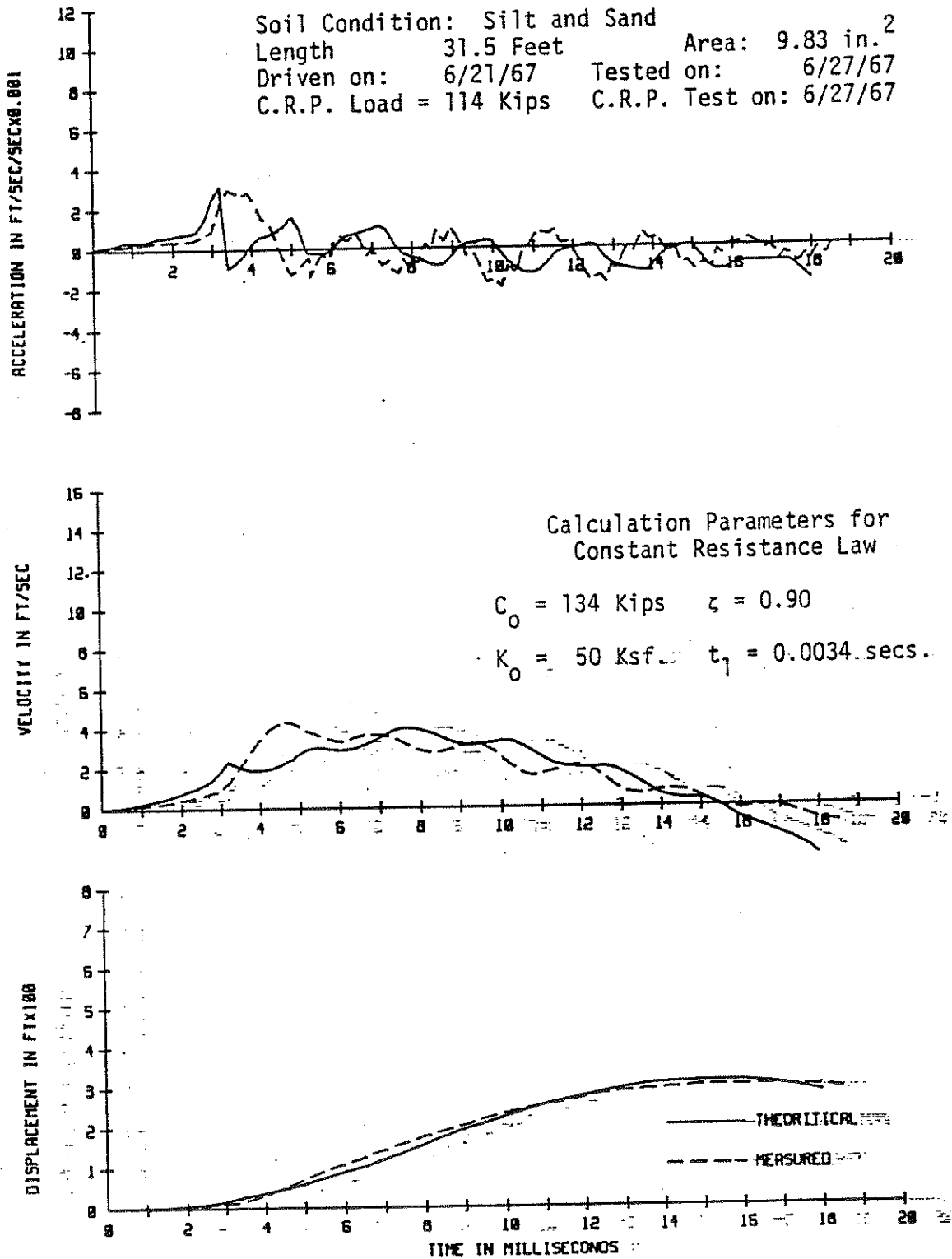


Figure 4.16 Matching Results of Full-Scale Pile F-30 in Akron, Ohio; Blow No. 1A

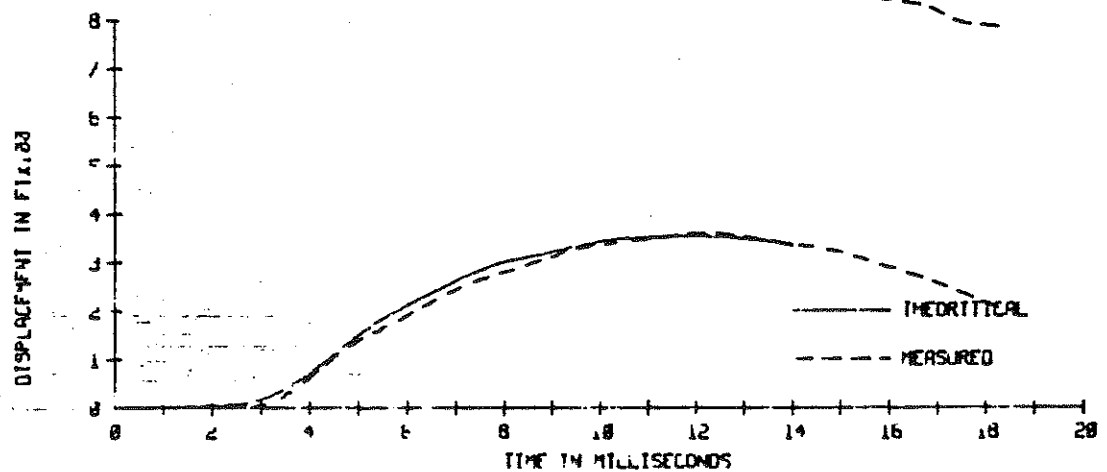
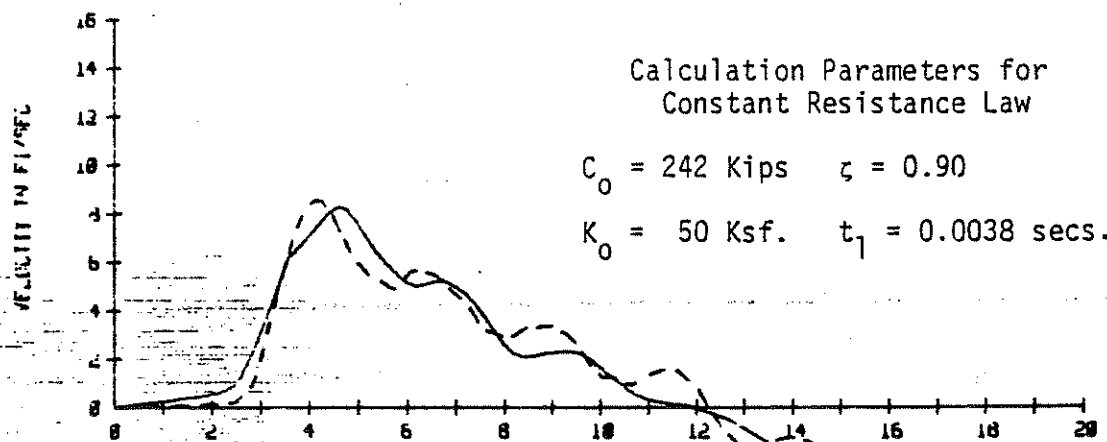
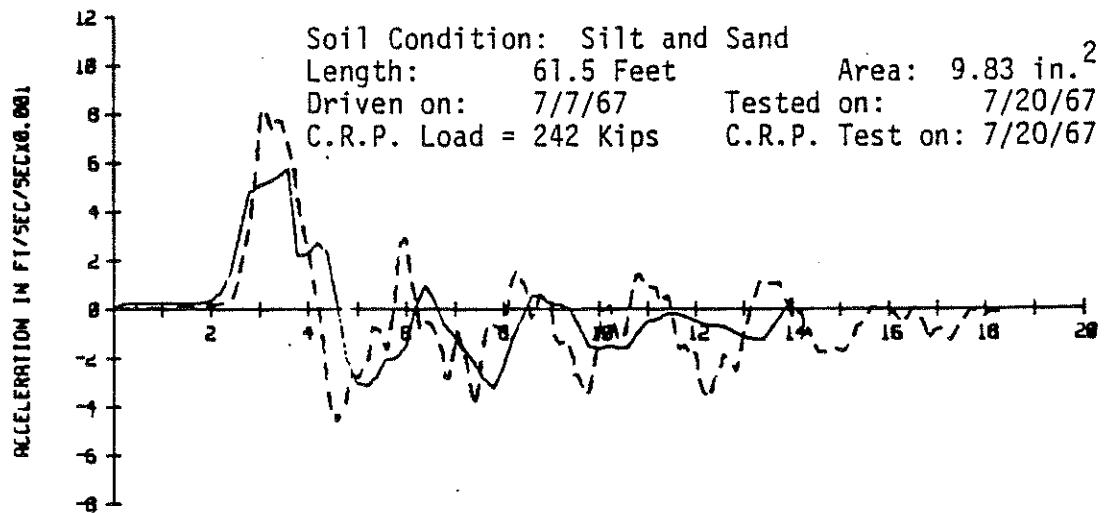


Figure 4.17 Matching Results of Full-Scale Pile F-60 in Akron, Ohio; Blow No. 26A

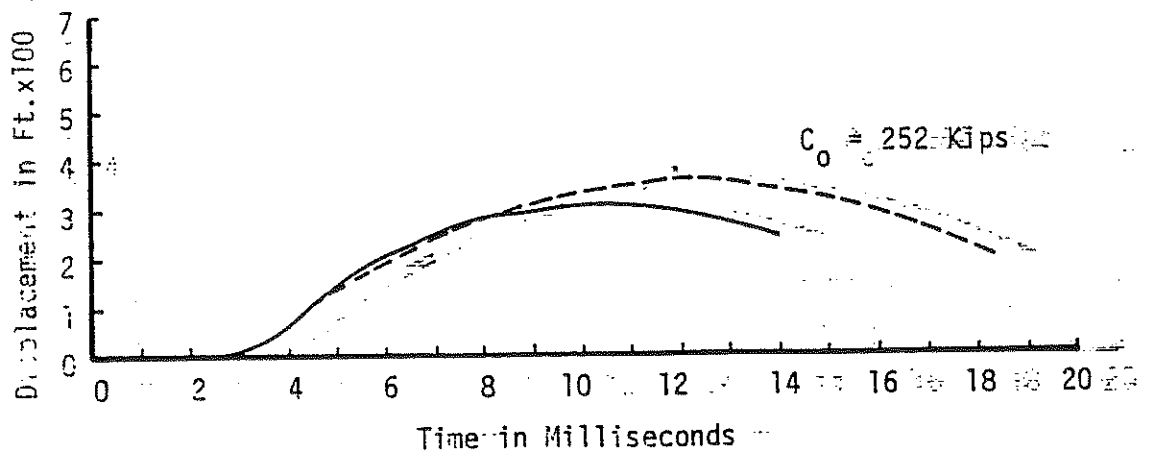
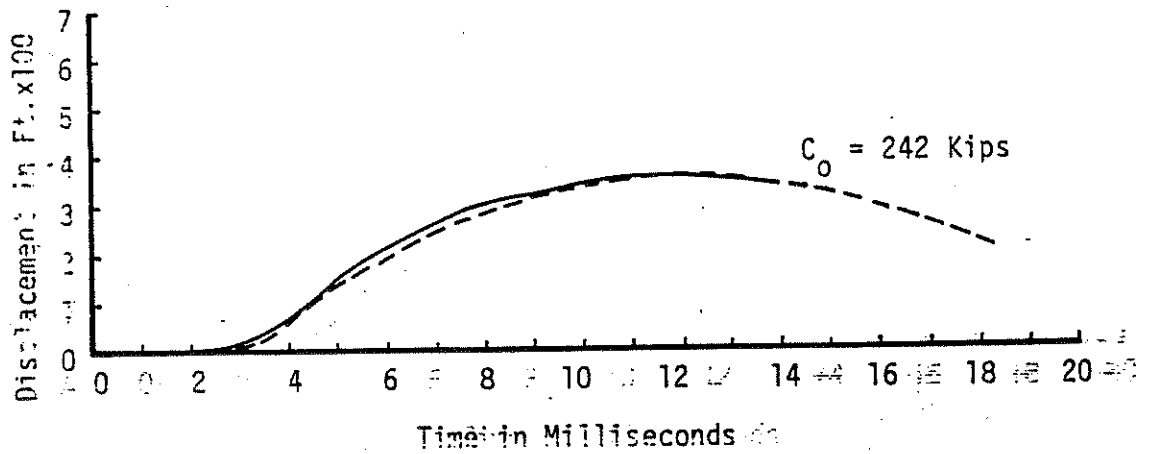
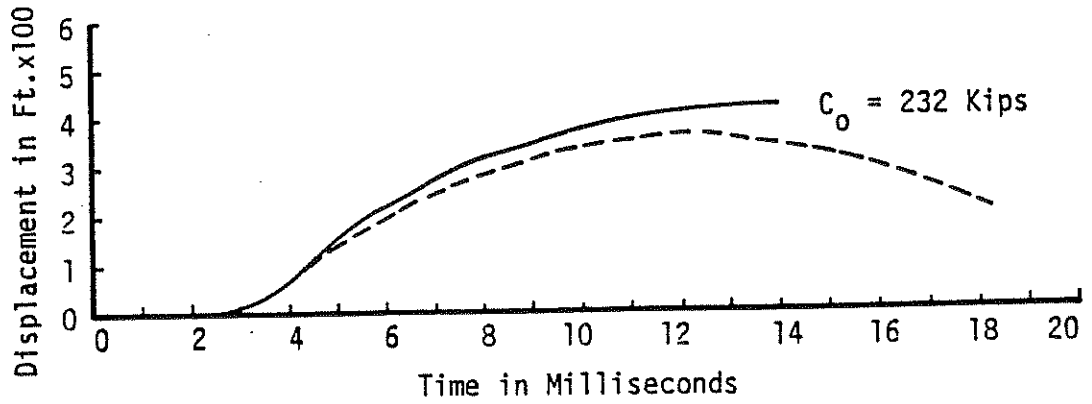


Figure 4.18 Sensitivity of Matching Scheme as a Function of  $C_0$  for Full-Scale Pile F-60, Blow 26A

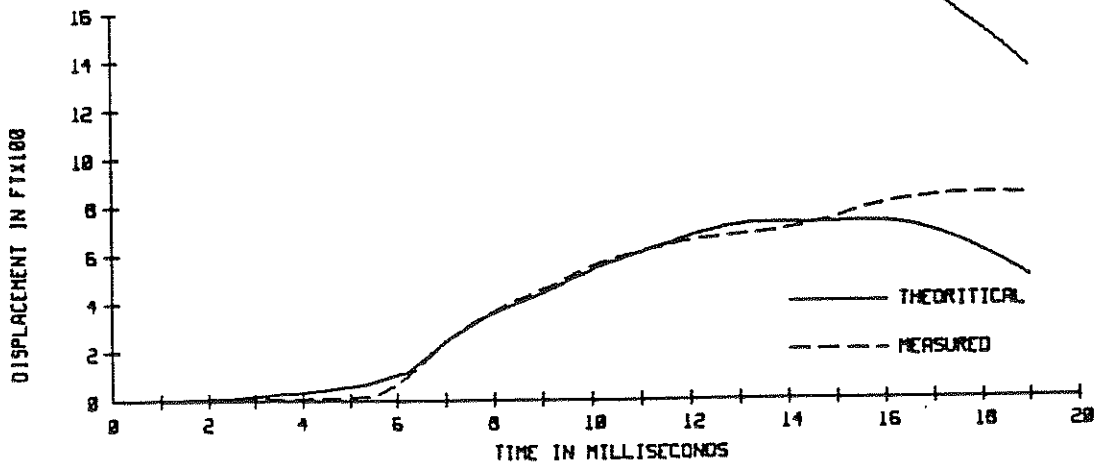
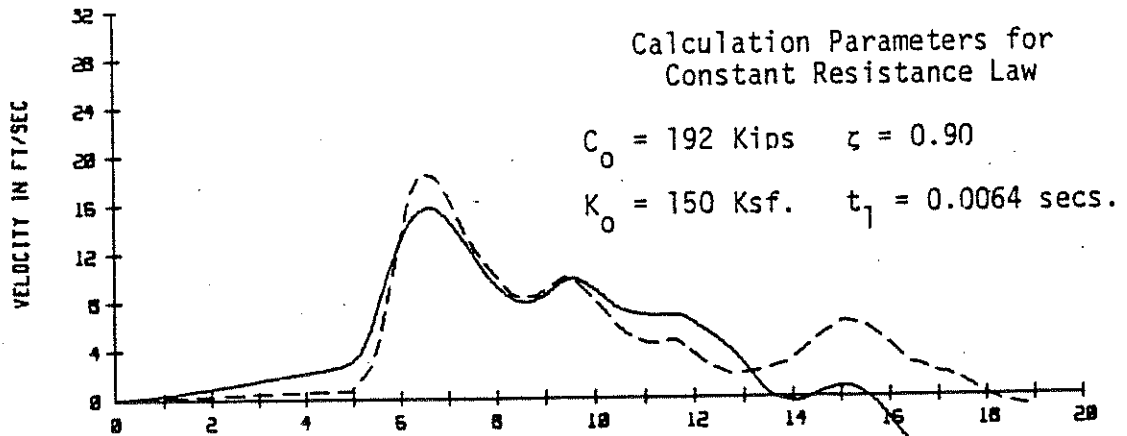
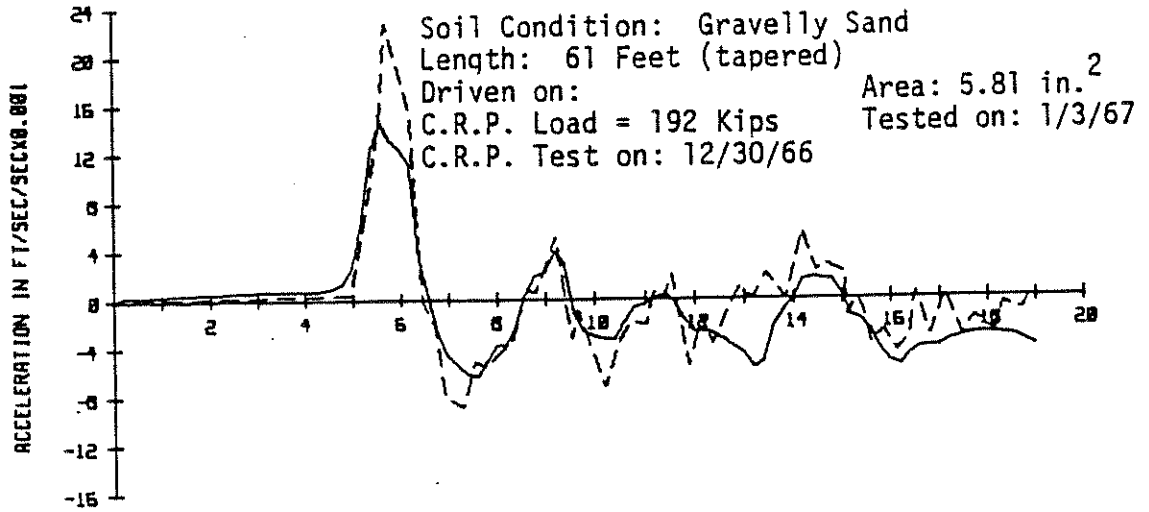


Figure 4.19 Matching Results of Full-Scale Pile C-1 in Canton, Ohio;  
 Blow No. 2A

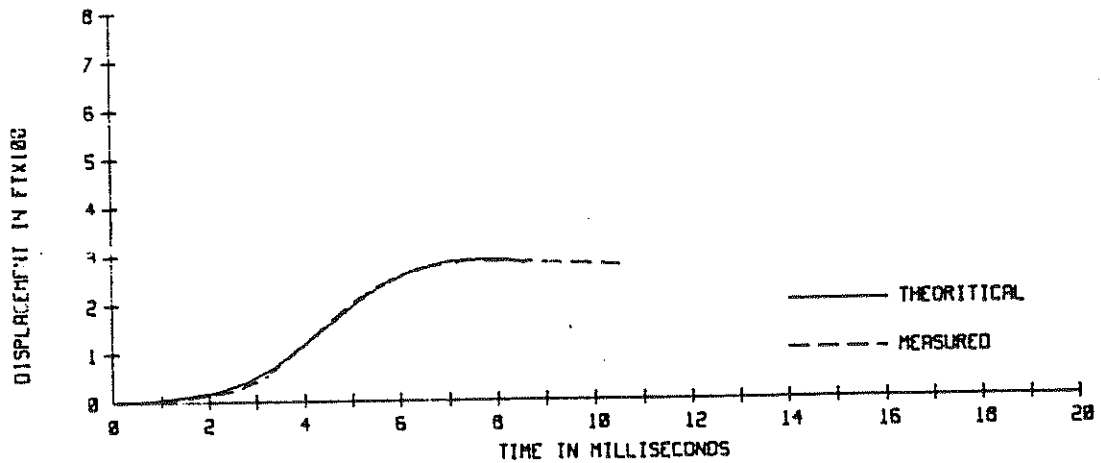
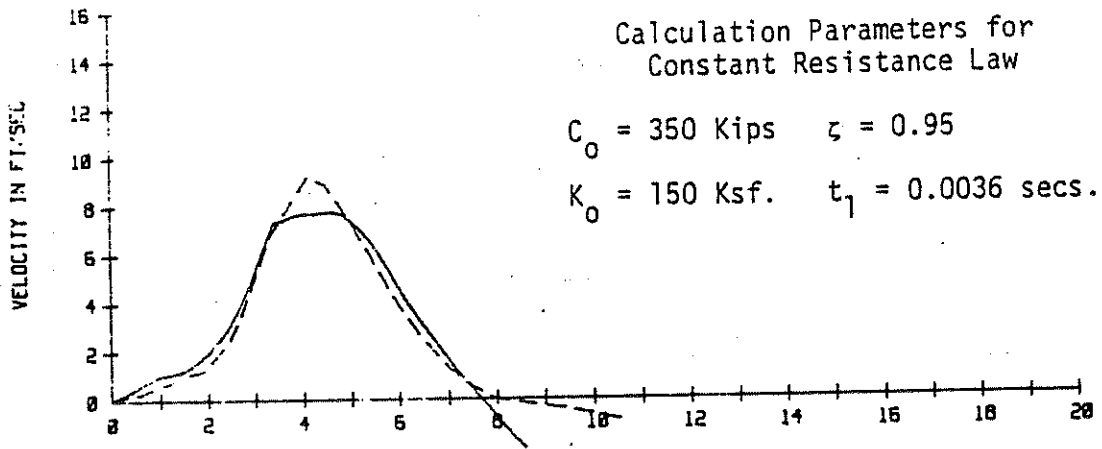
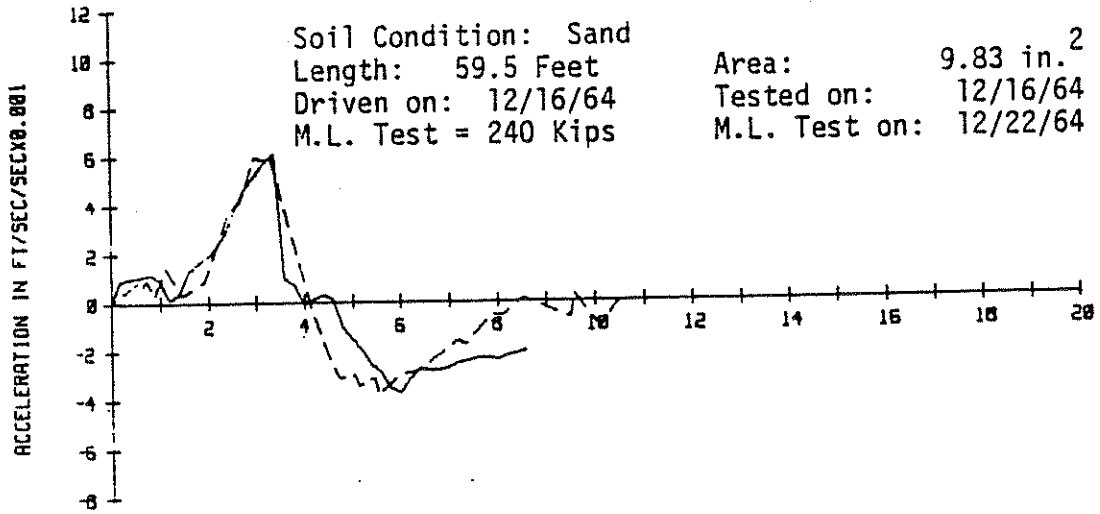


Figure 4 20 Matching Results of Full-Scale Pile No. 113 of North Pier, Last Blow

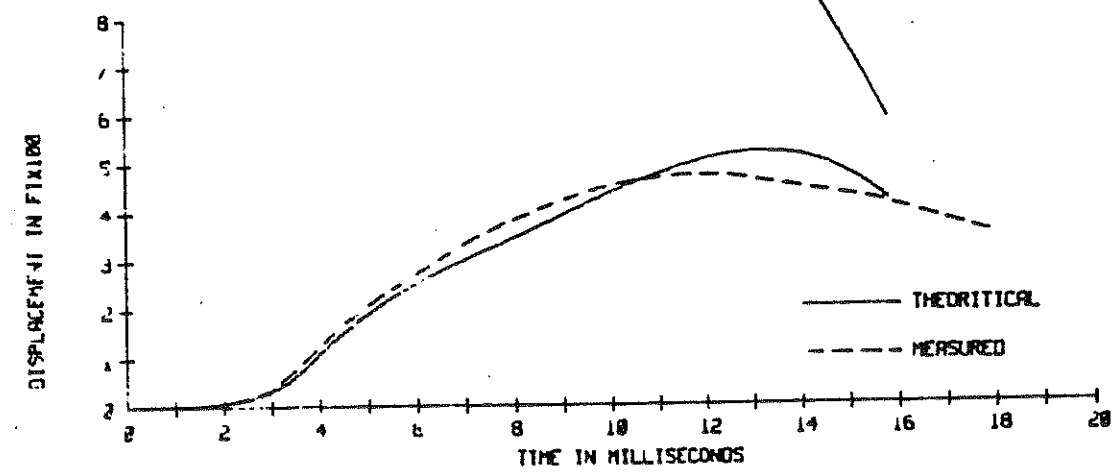
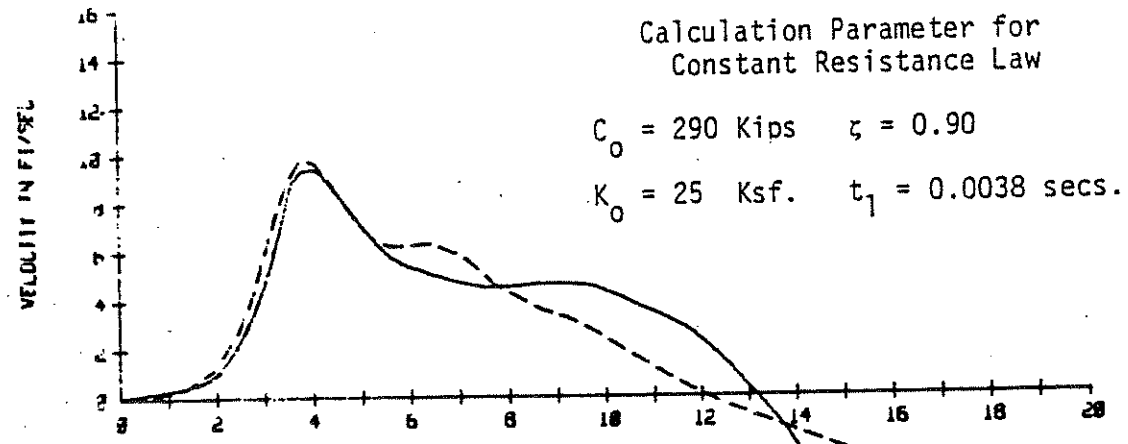
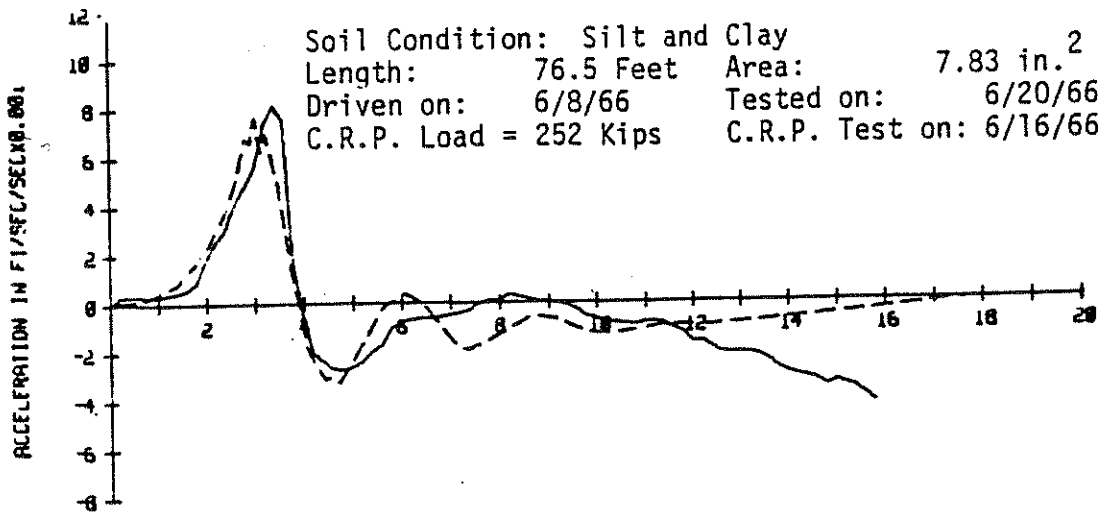


Figure 4.21 Matching Results of Full-Scale Pile A of Wall 91A, Blow No. 3A

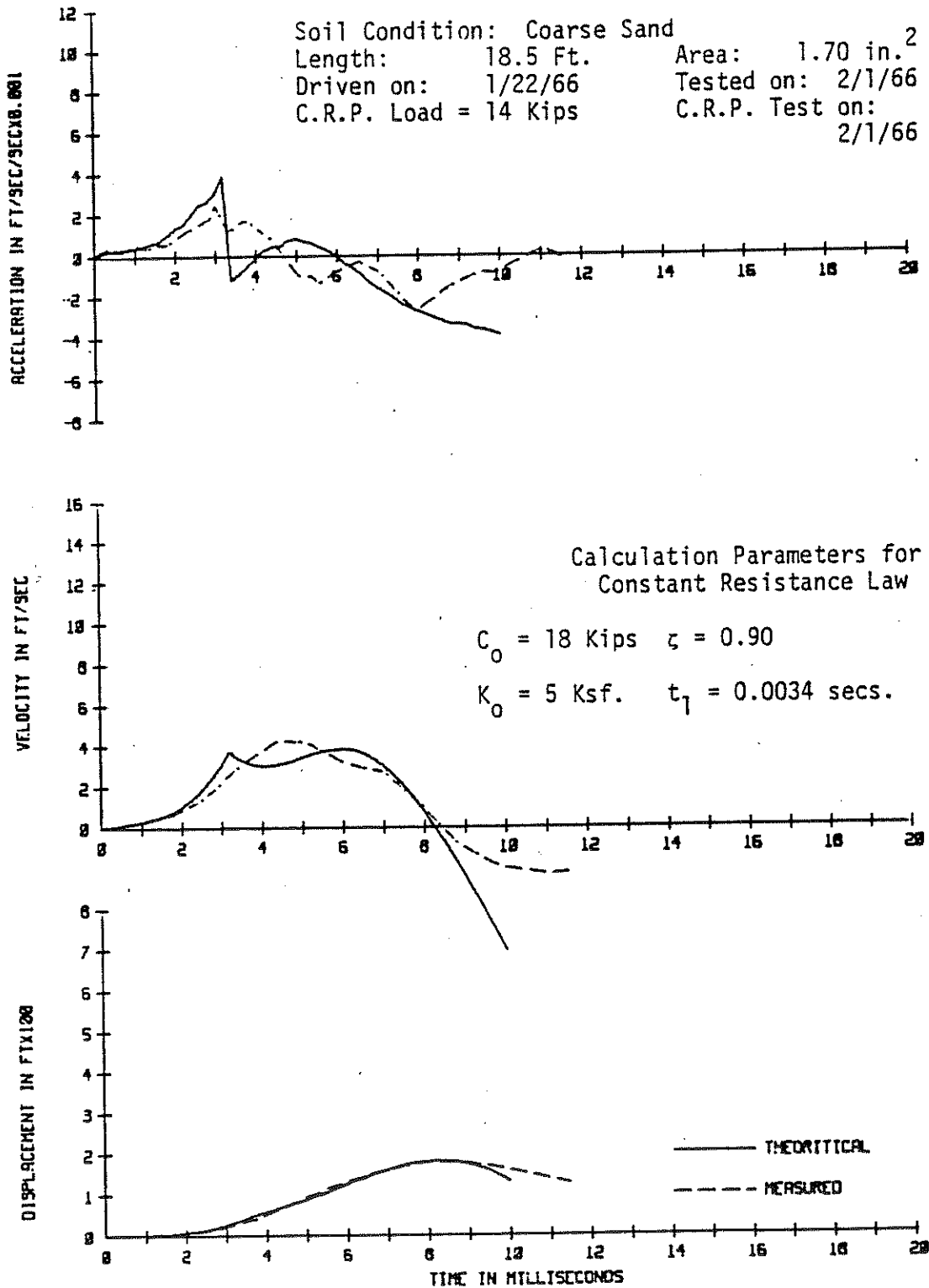


Figure 4.22 Matching Results of Reduced-Scale Pile 15-7, Blow #1A

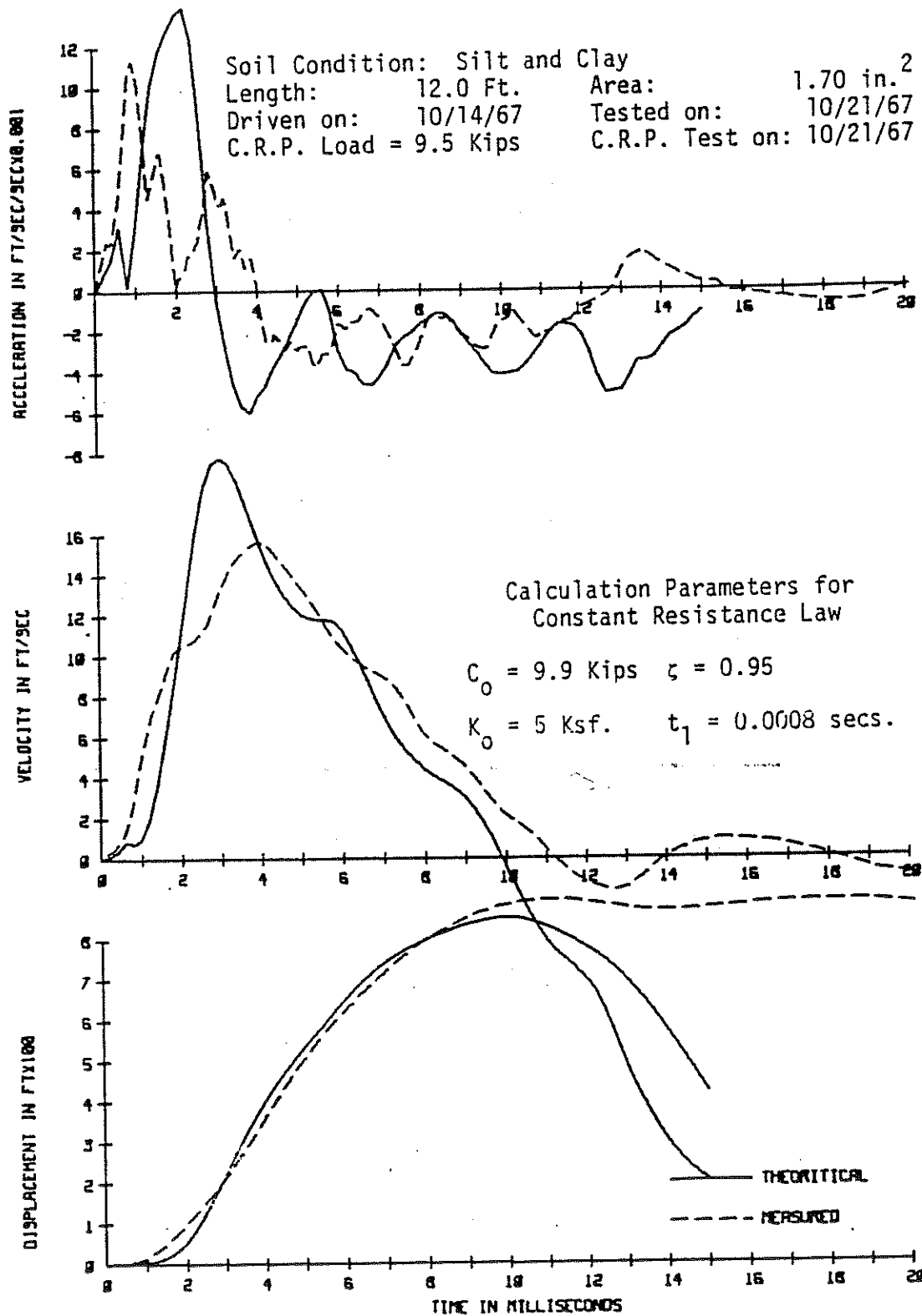


Figure 4.23 Matching Results of Reduced-Scale Pile 1-T-10, Blow #2A



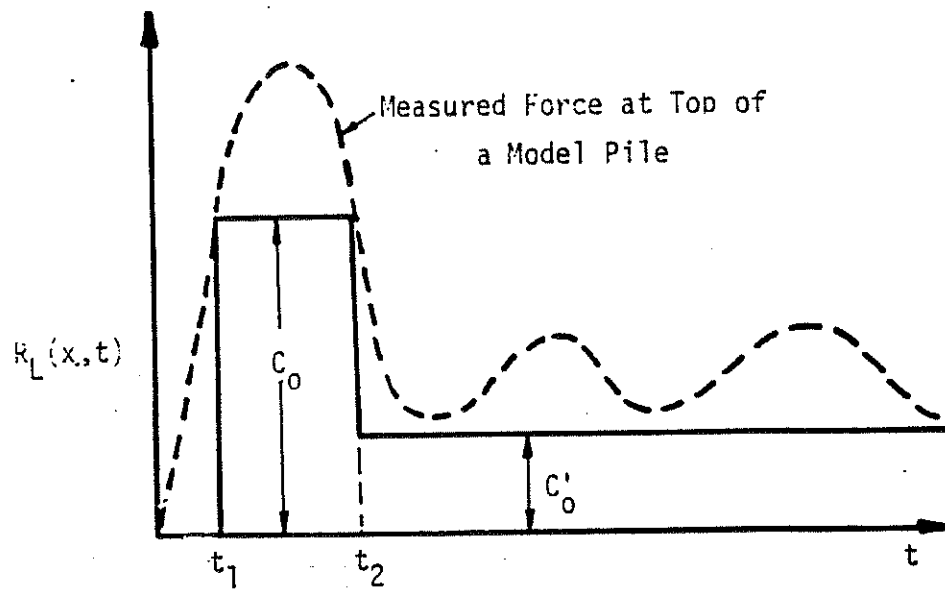


Figure 4.24 Resistance Law Proportional to Measured Top Force  $F_T(t)$

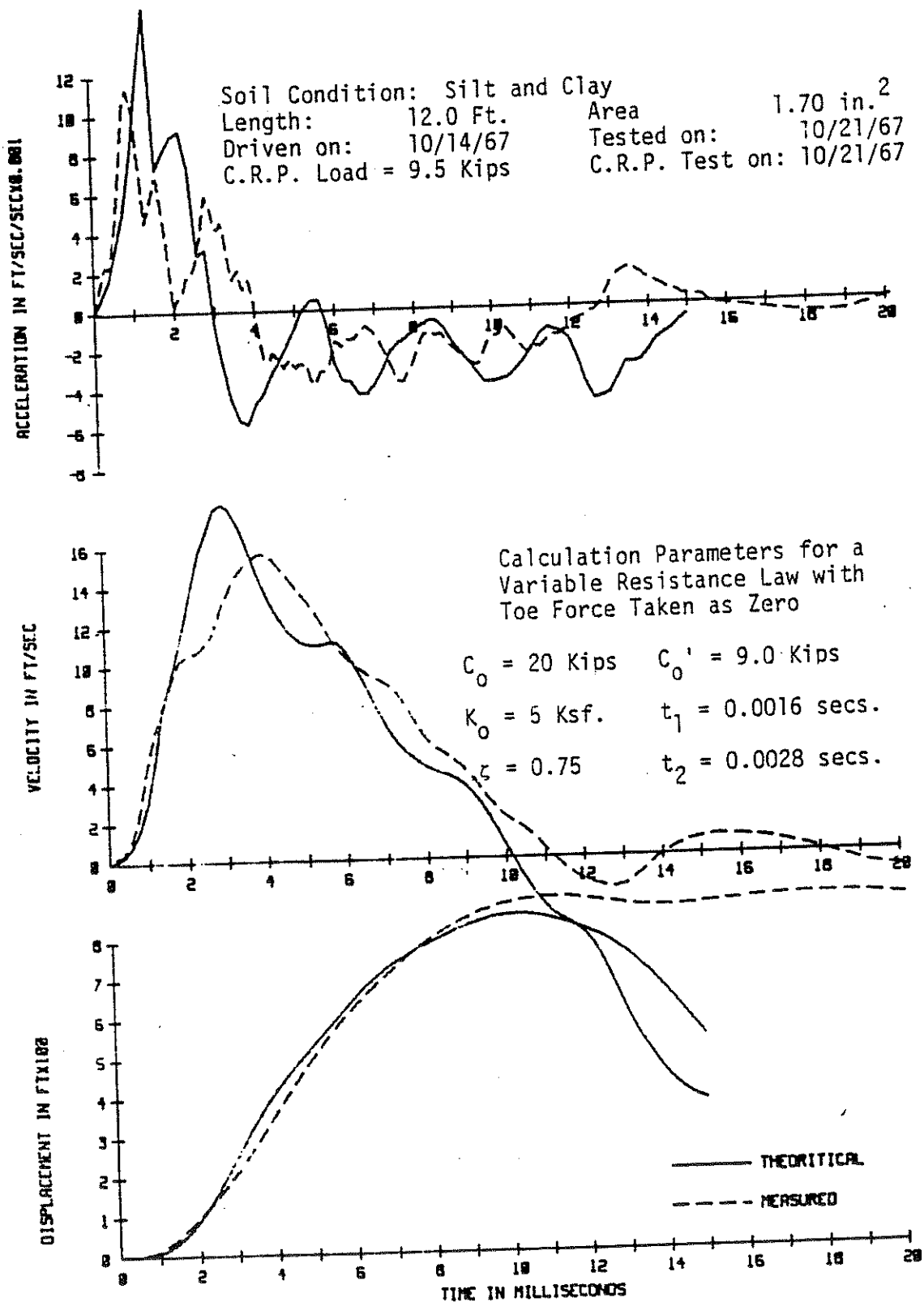


Figure 4 25 Matching Results of Reduced-Scale Pile No. 1-T-10 (Variable Resistance), Blow 2A

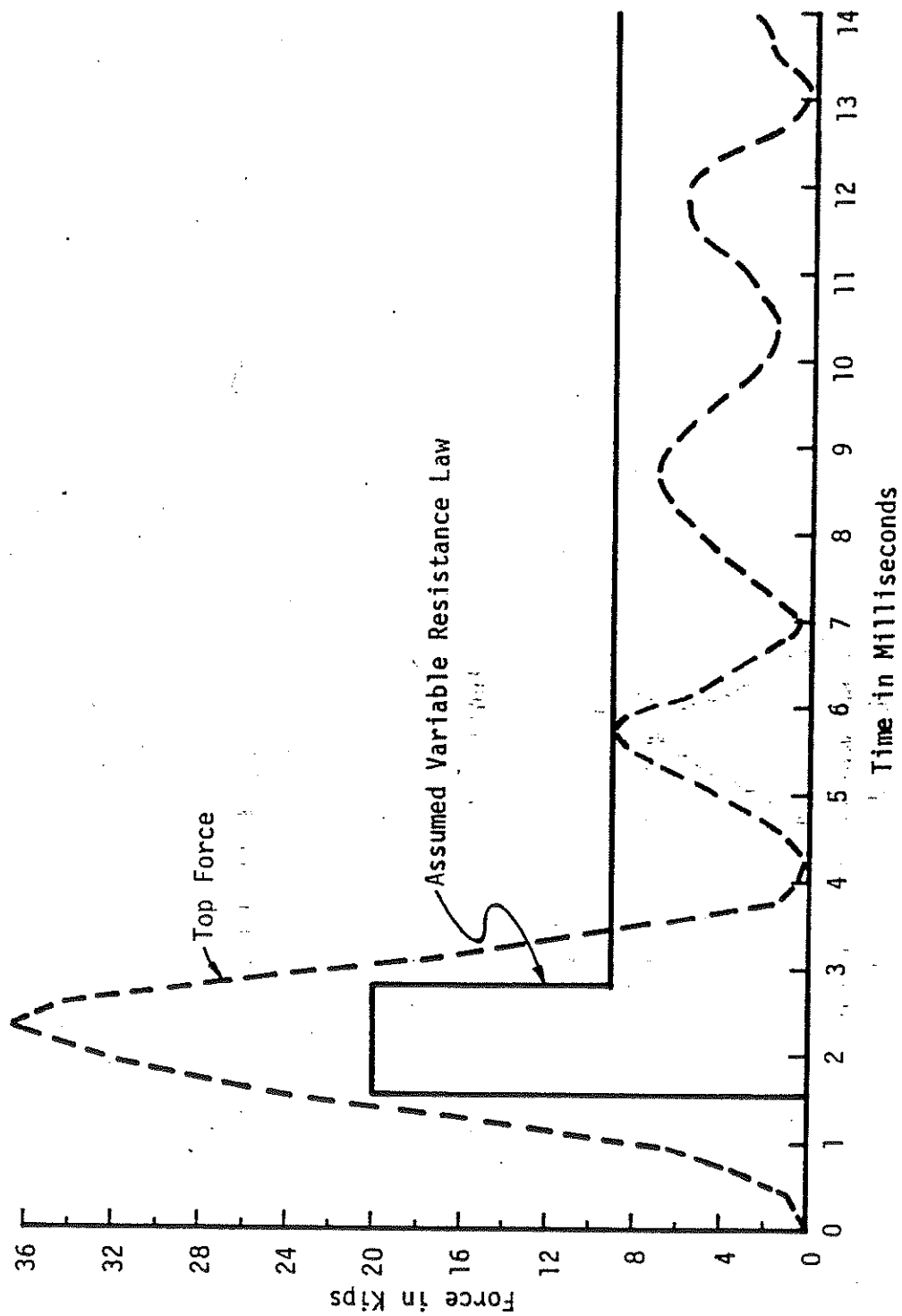


Figure 4.26 Assumed Variable Resistance Law for Model Pile 1-T-10, Blow 2A

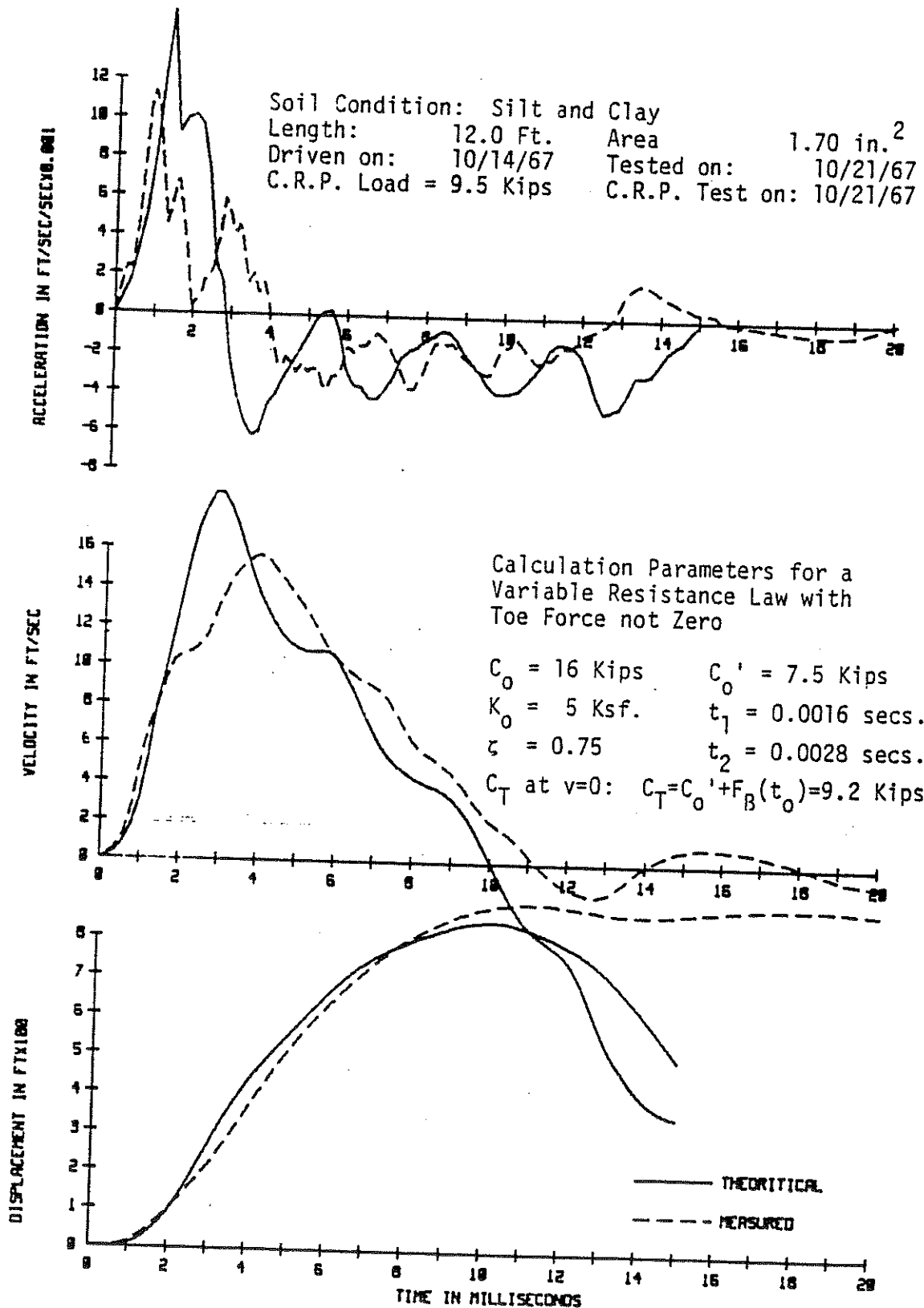


Figure 4.27 Matching Results of Reduced-Scale Pile 1-T-10 (Variable Resistance and Toe Force Included), Blow 2A

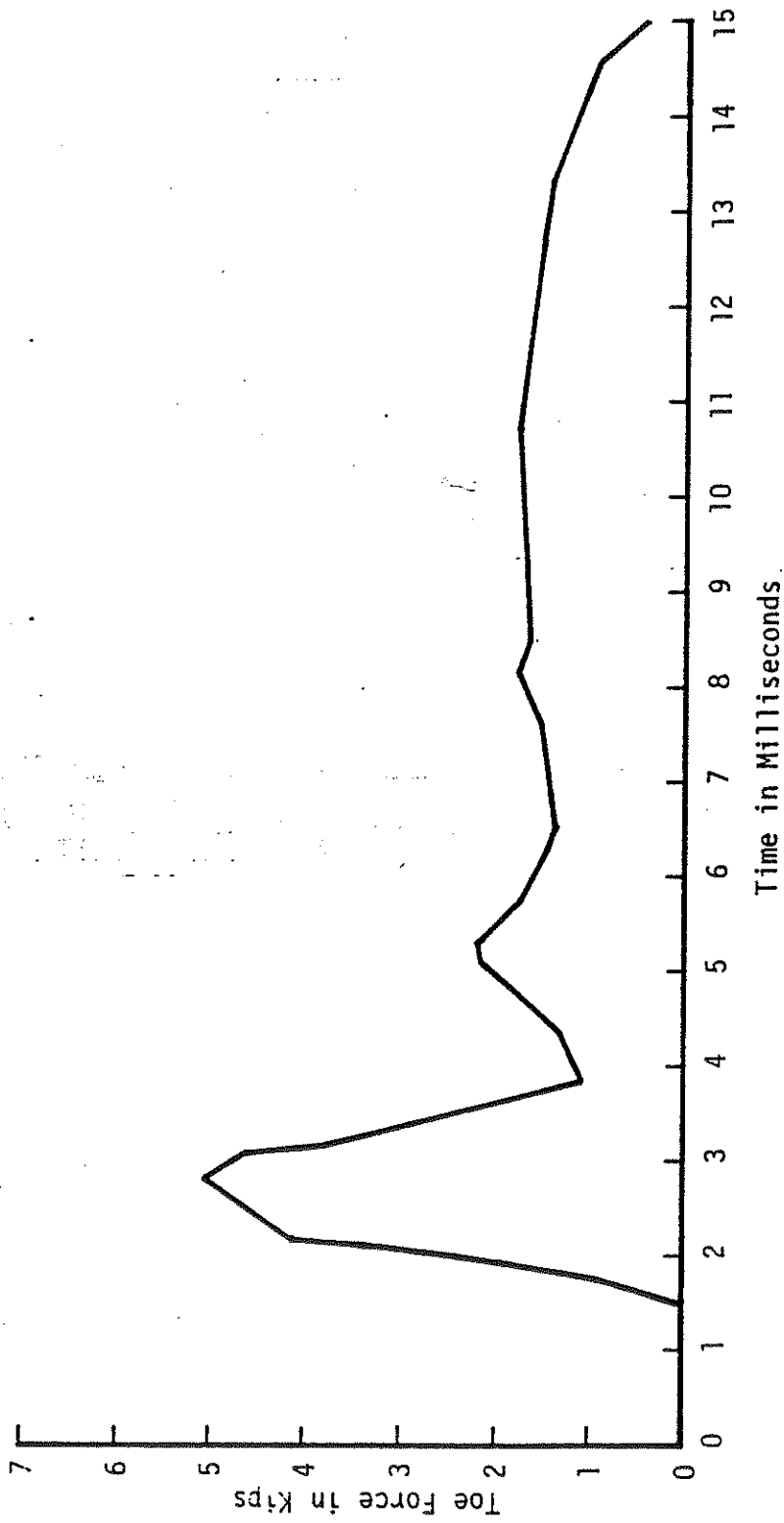
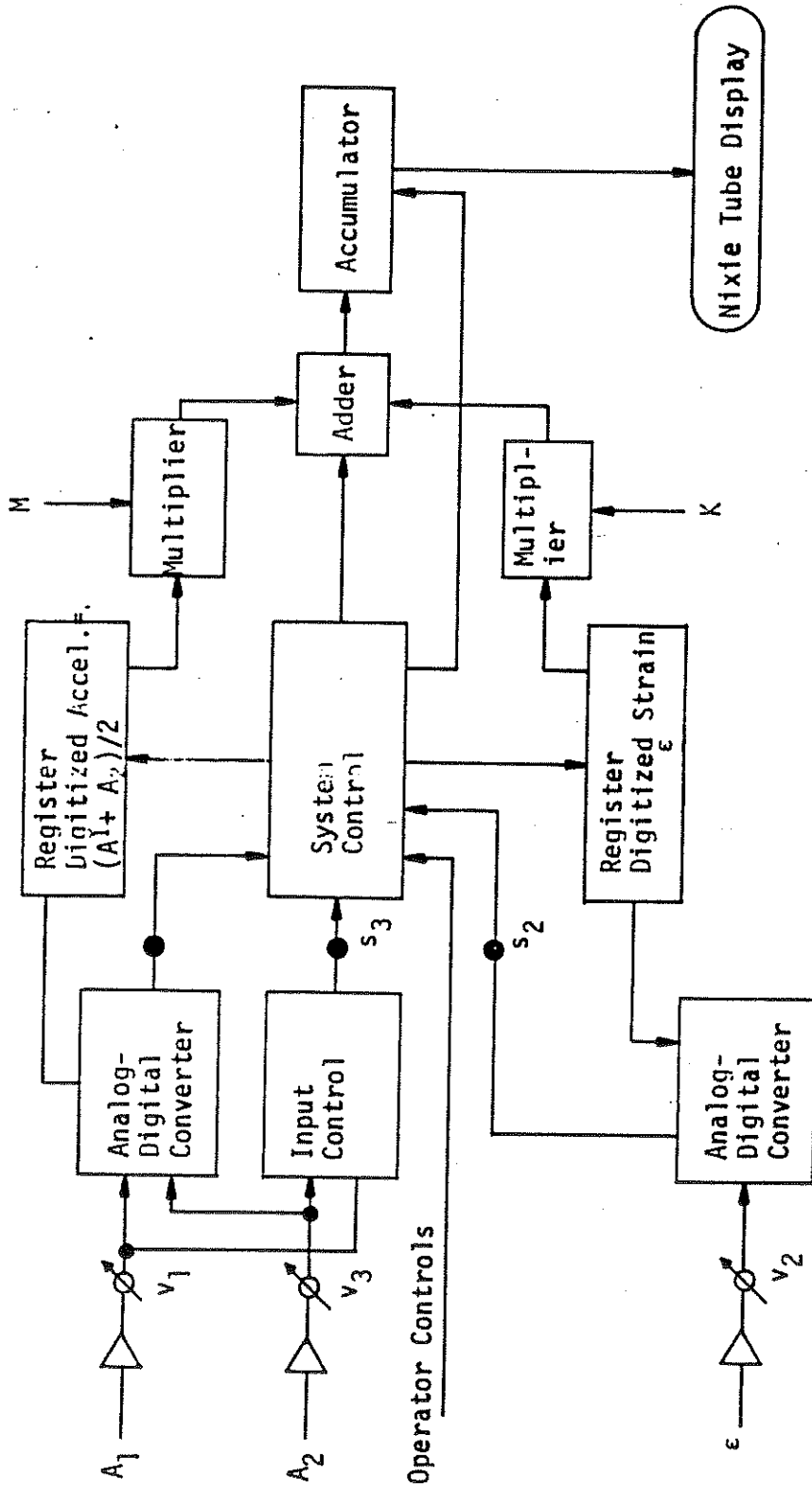


Figure 4.28 Toe Force of Reduced Scale Pile No. 1-T-10 Blow No. 1A



COMPUTER SYSTEM ORGANIZATION



-  Indicates gain control on operators console
-  Indicates on/off switch on operators console

Figure 5.1

Computer System Organization

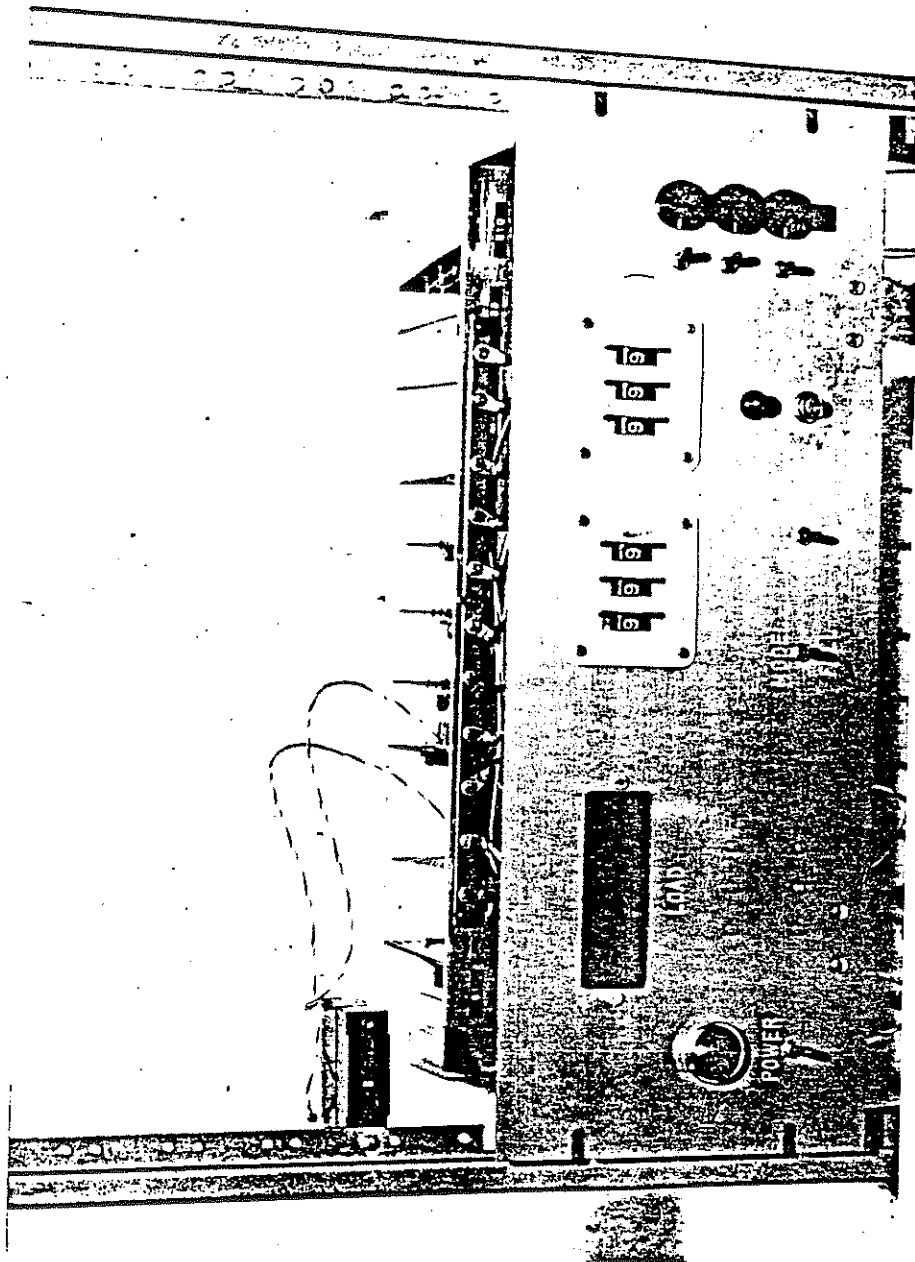


Figure 5.2

Operator Control Panel

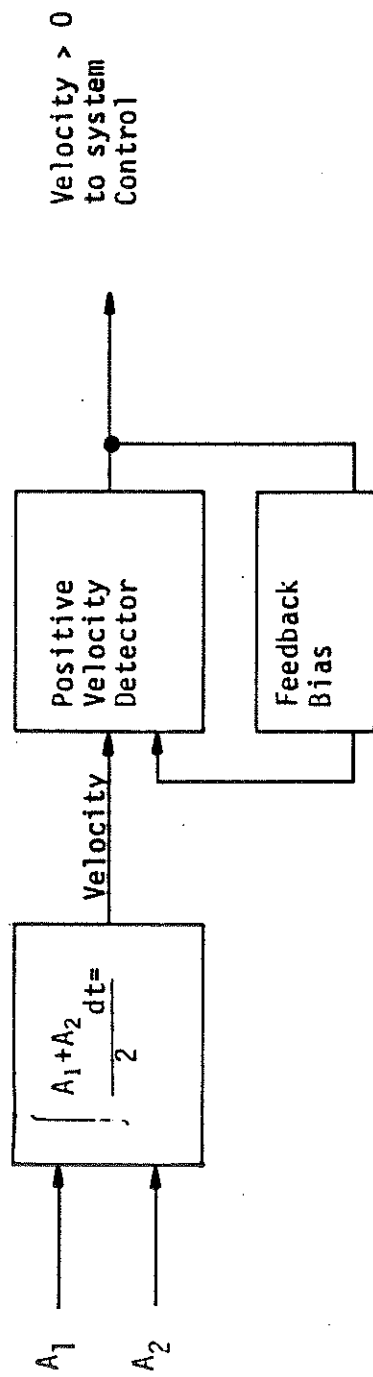


Figure 5.3  
Functional Components of Input Control



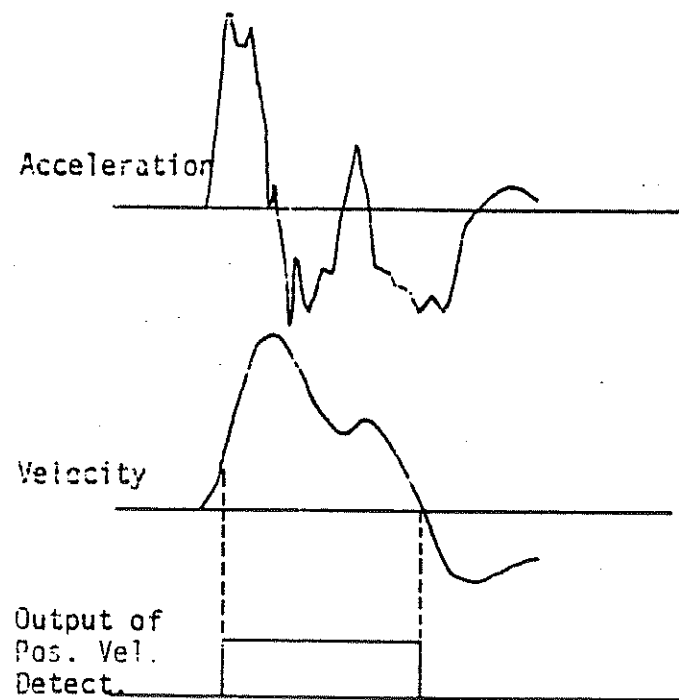
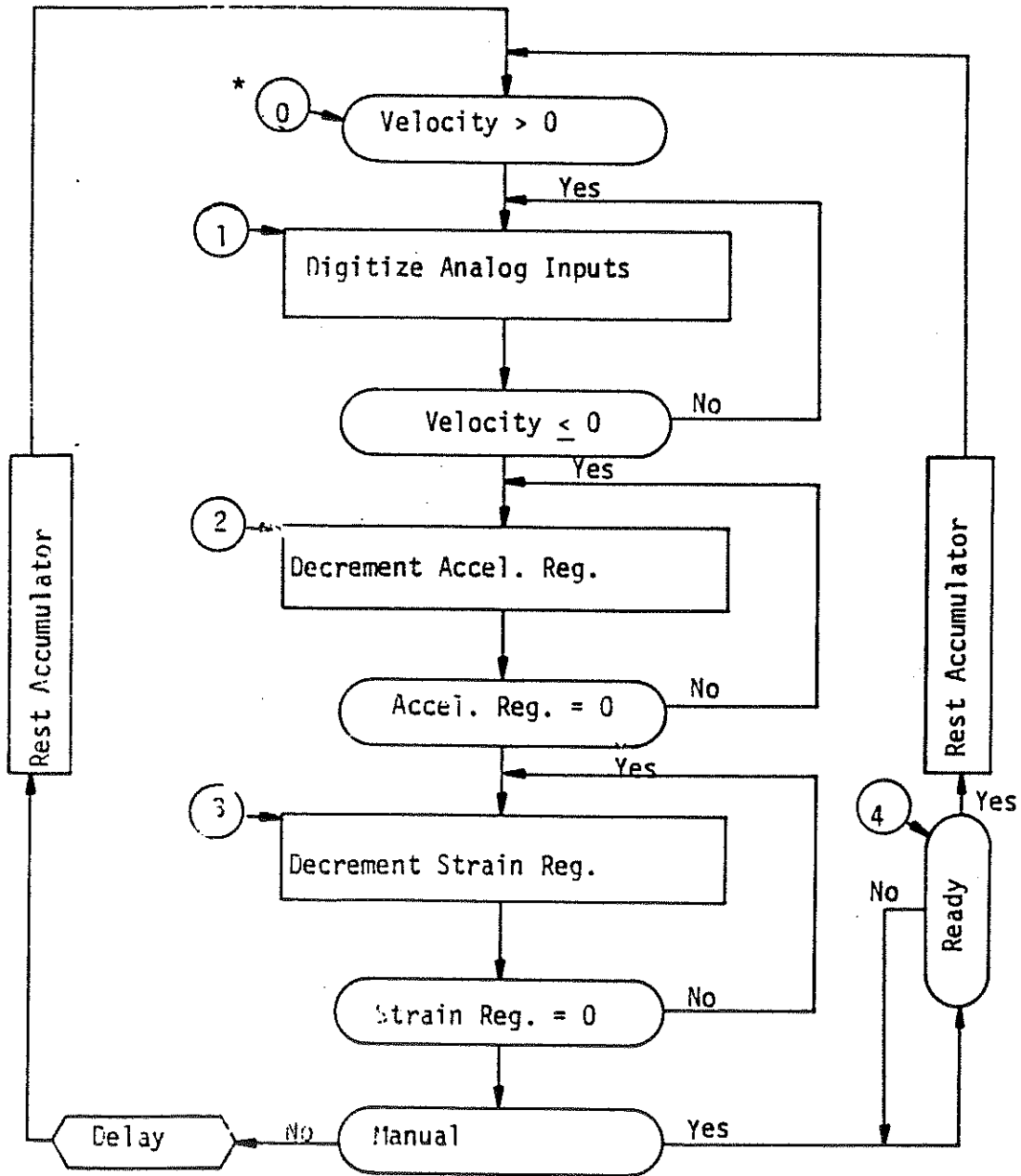


Figure 5.4  
Output Detector Function



\* Encircled numbers indicate control state numbers

Figure 5.5

Flow Chart